NATIONAL CENTER FOR EARTHQUAKE ENGINEERING RESEARCH
Headquartered at the State University of New York at Buffalo

ISSN 1088-3800

PB98-153406

# Seismic Fragility of Existing Conventional Reinforced Concrete Highway Bridges

by

Chris L. Mullen and Ahmet S. Cakmak
Princeton University
Department of Civil Engineering and Operations Research
Princeton, New Jersey 08544

Technical Report NCEER-97-0017



December 30, 1997

This research was conducted at Princeton University and was supported by the Federal Highway Administration under contract number DTFH61-92-C-00106.

# NOTICE

This report was prepared by Princeton University as a result of research sponsored by the National Center for Earthquake Engineering Research (NCEER) through a contract from the Federal Highway Administration. Neither NCEER, associates of NCEER, its sponsors, Princeton University, nor any person acting on their behalf:

a. makes any warranty, express or implied, with respect to the use of any information, apparatus, method, or process disclosed in this report or that such use may not infringe upon privately owned rights;
or

b. assumes any liabilities of whatsoever kind with respect to the use of, or the damage resulting from the use of, any information, apparatus, method, or process disclosed in this report.

Any opinions, findings, and conclusions or recommendations expressed in this publication are those of the author(s) and do not necessarily reflect the views of NCEER or the Federal Highway Administration.

NATIONAL CENTER FOR EARTHQUAKE ENGINEERING RESEARCH
Headquartered at the State University of New York at Buffalo

# Seismic Fragility of Existing Conventional Reinforced Concrete Highway Bridges

by

C.L. Mullen[1] and A.S. Cakmak[2]

Publication Date: December 30, 1997
Submittal Date: November 25, 1996

Technical Report NCEER-97-0017

NCEER Task Number 106-E-7.1.1

FHWA Contract Number DTFH61-92-C-00106

1 Assistant Professor, Department of Civil Engineeering, Unversity of Mississippi; former Graduate Student, Princeton University
2 Professor and Chairman, Department of Civil Engineering and Operations Research, Princeton University

NATIONAL CENTER FOR EARTHQUAKE ENGINEERING RESEARCH
State University of New York at Buffalo
Red Jacket Quadrangle, Buffalo, NY 14261

50272-101

| REPORT DOCUMENTATION PAGE | 1. REPORT NO. NCEER-97-0017 | 2. | 3. Recipient's Accession No. |
|---|---|---|---|
| 4. Title and Subtitle: Seismic Fragility of Existing Conventional Reinforced Concrete Highway Bridges | | | 5. Report Date: December 30, 1997<br>6. |
| 7. Author(s): Chris L. Mullen and Ahmet S. Cakmak | | | 8. Performing Organization Rept. No. |
| 9. Performing Organization Name and Address: Princeton University<br>Department of Civil Engineering and Operations Research<br>Princeton, NJ 08544 | | | 10. Project/Task/Work Unit No. 106-E-7.1.1<br>11. Contract(C) or Grant(G) No.<br>(C) FHWA Contract Number DTFH61-92-C-00106<br>(G) |
| 12. Sponsoring Organization Name and Address: National Center for Earthquake Engineering Research<br>State University of New York at Buffalo<br>Red Jacket Quadrangle<br>Buffalo, NY 14261 | | | 13. Type of Report & Period Covered: Technical report<br>14. |

15. Supplementary Notes: This research was conducted at Princeton University and was supported by the Federal Highway Administration under contract number DTFH61-92-C-00106

16. Abstract (Limit: 200 words) Seismic fragility is estimated for an existing conventional reinforced-concrete highway bridge using nonlinear-dynamic finite element analysis. The bridge selected for analysis is the Meloland Road Overcrossing located near El Centro, California. The fundamental response modes of the bridge affecting damage involve three-dimensional interaction between deck flexure/torsion and column flexure. A beam-column damage element is used which allows for such an interaction between the column element and the deck elements. The column element uses fiber modeling of the basic kinematic interaction between axial force and biaxal bending moments using one-dimensional nonlinear constitutive relations that require only a few basic stress and strain parameters. The damage element is first shown to predict the capacity and ductility of cantilever specimens without sensitivity to scale or geometry. The selected bridge is then analyzed using the damage elements. By tuning the elastic moduli for the deck plate elements to match measured frequencies for the bridge under a moderate seismic event, a fixed-base model is able to predict acceleration time history records for the event. A soil-structure interaction model is then developed from the fixed-base model by adding lumped spring and lumped mass effects of the foundations. Artificially generated random motions are input to the soil-structure model to predict damage response over a range of input intensities. A damage index analogous to interstory drift is computed and is shown to correlate well with peak ground acceleration of the simulated time histories. Fragility curves are computed on the basis of linear regression analysis of the simulated data.

17. Document Analysis a. Descriptors: Earthquake engineering. Fragility curves. Damage indices. Flexure. Reinforced concrete bridges. Finite element analysis. Nonlinear dynamic analysis. Nonlinear constitutive relationships. Box girder bridges. Highway bridges. Fiber models. Deck plate elements. Column elements.

b. Identifiers/Open-Ended Terms

c. COSATI Field/Group

| 18. Availability Statement | 19. Security Class (This Report) | 21. No. of Pages |
|---|---|---|
| Release unlimited | Unclassified | 121 |
| | 20. Security Class (This Page) Unclassified | 22. Price |

## PREFACE

The National Center for Earthquake Engineering Research (NCEER) was established in 1986 to develop and disseminate new knowledge about earthquakes, earthquake-resistant design and seismic hazard mitigation procedures to minimize loss of life and property. The emphasis of the Center is on eastern and central United States *structures*, and *lifelines* throughout the country that may be exposed to any level of earthquake hazard.

NCEER's research is conducted under one of four Projects: the Building Project, the Nonstructural Components Project, and the Lifelines Project, all three of which are principally supported by the National Science Foundation, and the Highway Project which is primarily sponsored by the Federal Highway Administration.

The research and implementation plan in years six through ten (1991-1996) for the Building, Nonstructural Components, and Lifelines Projects comprises four interdependent elements, as shown in the figure below. Element I, Basic Research, is carried out to support projects in the Applied Research area. Element II, Applied Research, is the major focus of work for years six through ten for these three projects. Demonstration Projects under Element III have been planned to support the Applied Research projects and include individual case studies and regional studies. Element IV, Implementation, will result from activity in the Applied Research projects, and from Demonstration Projects.

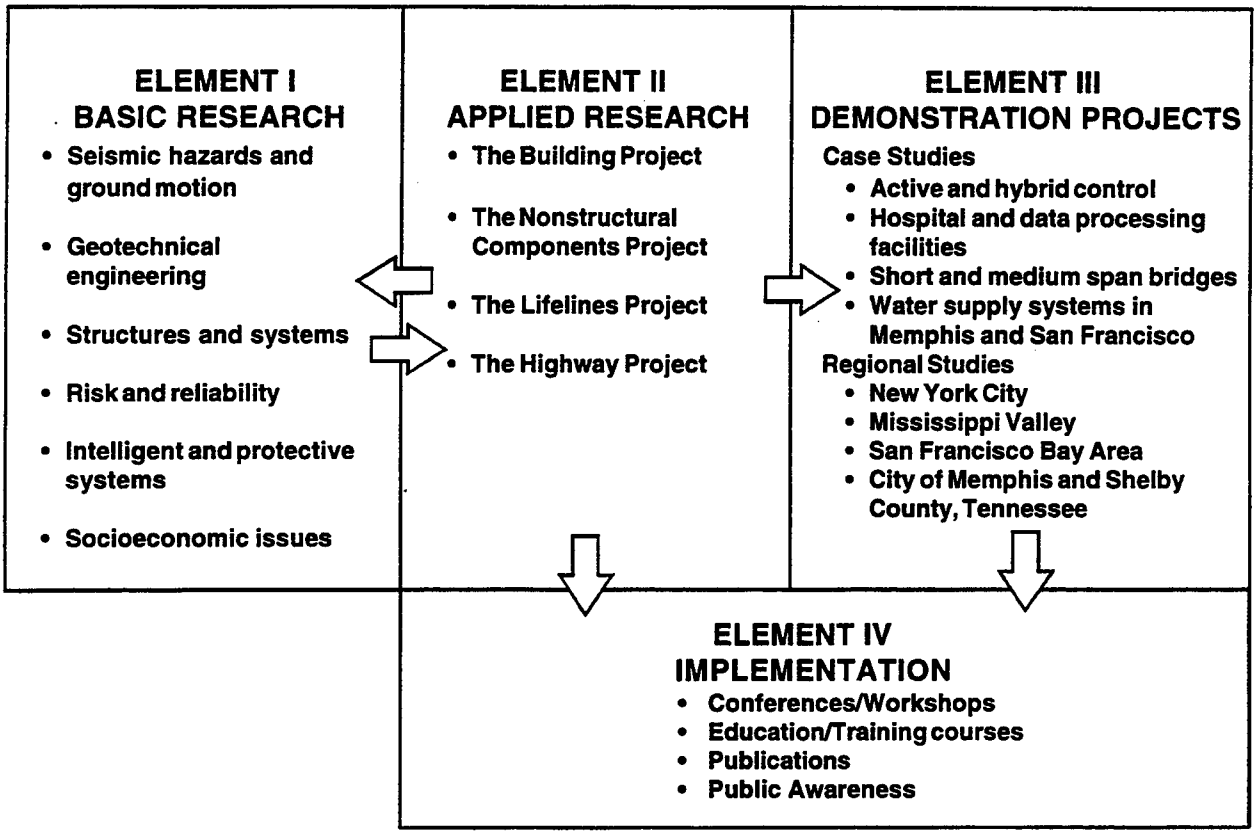

Research under the **Highway Project** develops retrofit and evaluation methodologies for existing bridges and other highway structures (including tunnels, retaining structures, slopes, culverts, and pavements), and develops improved seismic design criteria and procedures for bridges and other highway structures. Specifically, tasks are being conducted to: (1) assess the vulnerability of highway systems and structures; (2) develop concepts for retrofitting vulnerable highway structures and components; (3) develop improved design and analysis methodologies for bridges, tunnels, and retaining structures, with particular emphasis on soil-structure interaction mechanisms and their influence on structural response; and (4) review and improve seismic design and performance criteria for new highway systems and structures.

**Highway Project** research focuses on one of two distinct areas: the development of improved design criteria and philosophies for new or future highway construction, and the development of improved analysis and retrofitting methodologies for existing highway systems and structures. The research discussed in this report is a result of work conducted under the existing highway construction project, and was performed within Task 106-E-7.1.1, "Examination and Upgrading of ATC-13 and Development of Analytical Methods for Fragility Curve Derivation" of the project as shown in the flowchart on the following page.

*The overall objective of this task was to calibrate seismic damage states for existing bridges. The report establishes a framework for fragility analysis of typical short span continuous reinforced concrete highway bridges. A three-dimensional approach to modeling the damage response of reinforced concrete highway bridge columns was used, which included full-scale column behavior under simultaneous and time varying action of axial forces and biaxial bending moments. The key parameters of the proposed column damage element were calibrated as was soil-structure interaction effects. The calibrated model was then used to construct an intensity-damage relationship and family of fragility curves for the example bridge.*

*In developing the model, emphasis was placed on representing the three-dimensional interaction of the major subsystems, which include the column of the central pier, the deck and the foundation. The principal damage mode considered was flexural damage to the columns. The study was an attempt to develop an integrated fragility analysis procedure, and the overall methodology described herein can be used as the basis for developing a more reliable assessment of the fragility of typical highway bridges.*

## SEISMIC VULNERABILITY OF EXISTING HIGHWAY CONSTRUCTION
## FHWA Contract DTFH61-92-C-00106

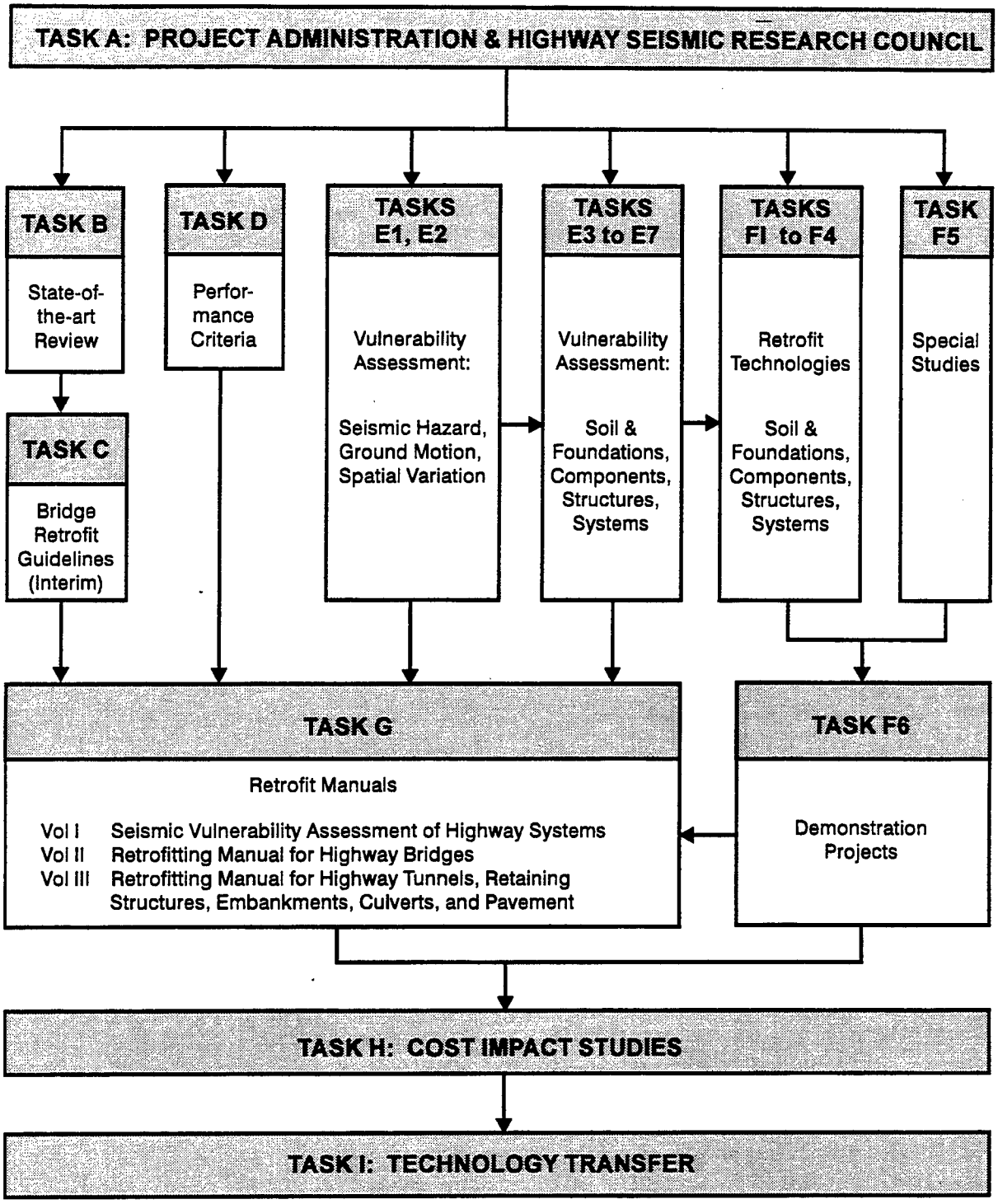

## ABSTRACT

Seismic fragility is estimated for an existing conventional reinforced-concrete highway bridge using nonlinear-dynamic finite element analysis. The bridge selected for analysis is the Meloland Road Overcrossing located near El Centro, California. It is representative of a large class of two-span continuous bridges in California and other locations in the United States. The column supporting the deck is assumed to govern the damage state for the entire bridge. The column is about 20 ft high and has an outside diameter of 5 ft. Flexure is assumed to be the critical damage mode for the column. The fundamental response modes of the bridge affecting this damage mode involve a three-dimensional interaction between deck flexure/torsion and column flexure. A beam-column damage element is used which allows for such an interaction between the column element and the plate elements used to representing the multi-cell hollow box girder deck. The column element uses a practical fiber modeling approach that models the basic kinematic interaction between axial force and biaxial bending moments using one-dimensional nonlinear constitutive relations that require only a few basic stress and strain parameters. Confinement effects are specified through the concrete parameters and an effective dimension for the confined zone. The constitutive relations consist of envelope curves and loading/unloading rules which permit time and load-path dependent modeling of key damage mechanisms including concrete cracking, concrete crushing, concrete spalling and reinforcing steel plasticity. The damage element is first shown to adequately predict the capacity and ductility of cantilever specimens tested by others without showing sensitivity to either scale or geometry effects. The selected bridge is then analyzed using the damage elements. By tuning the elastic moduli for the deck plate elements to match measured frequencies for the bridge under the moderate seismic event, a fixed-base model is able to predict acceleration time history records for the event. A soil-structure interaction model is developed from the fixed-base model by adding lumped spring and lumped mass effects of the foundations at the abutments. The predicted column base moments of the soil-structure interaction model are shown to be in excellent agreement with the fixed-base model considering the complexities of the foundation response. Artificially generated random motions are input to the soil-structure model to predict damage response over a range of input intensities. A damage index analogous to interstory drift is computed and is shown to correlate well with peak ground acceleration of the simulated time histories. Fragility curves are computed on the basis of linear regression analysis of the simulated data. The effect of span length on the curves is examined using the identical time histories applied to replicas of the bridge proportioned according to California Department of Transportation design guidelines.

## ACKNOWLEDGEMENTS

The report is based in part on the dissertation of the first author under the supervision of the second author. It also represents the final report of the Structural Fragility Task of the NCEER Highway Project, Task 106-E7.1.1 which spanned three years. The authors are very appreciative of the generous support the Federal Highway Administration has provided to this task during that time period.

The authors wish to thank the following project investigators who have provided invaluable assistance. Professor Ian Buckle of the State University of New York (SUNY) at Buffalo and the NCEER Highway Project Director identified the source of data for the Meloland Road Overcrossing (MRO). Ian Friedland, the Assistant Project Director, obtained the data from Mr. Stuart Werner of Dames and Moore, Inc., who has been under contract with the California Department of Transportation (CalTrans) to study the MRO. CalTrans Structures Manager Mr. James Gates provided design guidelines and typical span ranges for the MRO type of bridge in California. Mr. Pat Hipley, Caltrans engineer in charge of strong motion instrumentation of bridges, was very helpful in gaining access to drawings.

Thanks are also extended to Princeton University Professors Jean Prevost, who generously provided access and insights to the DYNAFLOW code, and George Deodatis, who provided insight into ground motion modeling and spatial variation issues. Professor Mustafa Erdik of the Earthquake Engineering Research Institute at Bogazici University in Istanbul, Turkey, provided valuable comments on the research findings and report. Professor Sashi Kunnath of the University of Central Florida shared his source code for IDARC during early stages of the project, and Dr. Roy Imbsen provided free use of his proprietary program, IAINEABS. Professor Nigel Priestley of the University of California at San Diego was kind enough to arrange for a tour of his bridge column retrofit testing facility and discussions with his research associates, Professor Gregory MacRae and Dr. Ronnie Yang. Drs. H.-S. Lew, Andrew Taylor, and William Stone provided research reports on the unique bridge column testing performed at the National Institute for Standards and Testing (NIST) and the column test database they have compiled.

It has been a pleasure to work with such an outstanding group of researchers and practitioners. They have demonstrated their genuine concern for the problems this task has attempted to address through their willingness to share both their time and resources in order to progress toward a solution.

# TABLE OF CONTENTS

# LIST OF ILLUSTRATIONS

# LIST OF TABLES

# SECTION 1
# INTRODUCTION

Recent major earthquake events in California and Japan have demonstrated the fragility of some of our basic types of highway bridges. It is the premise of this work that even today significant fragility remains not only in California but other moderately seismic regions of the United States as well. It is believed that a major deficiency in dealing with this problem exists in our inability to reliably predict damage response to seismic events and thus to rationally assign fragilities.

Seismic fragility prediction involves estimation of both demands and capacities on systems and components. The focus of this study is on prediction of damage in the most critical and fragile component as evidenced by observed cases in past seismic events, the columns supporting the deck superstructure. In particular, the focus is on columns of statically indeterminate structure systems where the demands and capacities are time-varying and depend on the load-path dependent stiffness and deformation levels. Thus, both the demands and the capacities depend on the current state of damage in the material within key regions of the element and on the time-variation of the applied loading.

For columns dominated by flexural deformations, the key region is near the column ends where sudden stiffness changes force development of plastic hinges that permit large rotations to occur at the hinge location. For columns with high depth-to-height ratios dominated by shear deformations, the key region may occur anywhere along the height. The primary goal of this work is to obtain improved engineering predictions of stiffness and deformation and thereby damage demand and capacity for flexure dominated damage modes in columns. The treatment of shear dominated damage modes is considered of equal importance for shorter columns but requires a higher level of modeling than will be attempted here.

Common design and analysis procedures for highway bridges have tended to ignore the 3D nature of response and its effect on both demand and capacity, primarily because of the complexity this introduces to the problem. Design codes deal mostly with 2D and even statically equivalent systems of forces. Testing programs and analysis tools devised alongside these programs have focused primarily on 2D frames and substructures. Unfortunately, such an attitude has fostered a false sense of security in the understanding of actual behavior and a complacency in the general approach to testing, analysis, and design.

Nonetheless, most bridge configurations, deformation patterns, and loading systems are inherently 3D, and observed damage from actual seismic events repeatedly indicates this fact. This fact is finally beginning to be recognized as evidenced by the major priority given to the testing, design, and construction of truly massive transfer or edge-beam girders in the recently retrofitted Interstate-280 freeway in San Francisco which developed a large number of cracks during the 1989 Loma Prieta earthquake.

In Section 2, a fully 3D approach is taken to modeling the damage response of reinforced-concrete (RC) highway bridge columns with attention paid to full-scale column behavior under the simultaneous and time-varying action of axial forces and biaxial bending moments. The basis of this approach is the assumed dominance in flexure mode response of a single stress and strain component acting normal to assumed plane cross-sections of the beam-column. Numerical integration procedures permit the computation of element stiffness using only a finite number of points located on two cross-sections within the element length. These points take on the common interpretation of flexural fibers.

The flexure damage response is then captured through the introduction of 1D stress-strain laws appropriate for the concrete and steel fibers. Rules consistent with available experimental evidence are defined which permit modeling of loading-unloading behavior during damage processes including gradual concrete crack opening-closing in tension and hardening/softening phases of crushing in compression.

The fiber modeling of these deformation processes which are inherently unstable in unreinforced concrete is therefore premised on the more stable composite action of the concrete and steel fibers on the cross-section as defined by the strain compatibility assumption. In this work, no relaxation of the compatibility assumption is made to accommodate either warping or bond slip.

The formulation discussed in Section 2 is consistent with basic principles of continuum mechanics and offers a unique approach to fiber modeling of reinforced concrete columns. Emphasis is placed on accuracy, efficiency, and simplicity as they apply to the practical modeling of the flexure damage mode in RC columns typically appearing in conventional highway bridges.

Section 3 calibrates the key parameters of the proposed column damage element in RC cantilever tests indicative of bridge pier geometries and loadings. Two sets of tests are considered, one having a circular cross-section and the other a square cross-section. The first set examines scale effects using a unique pair of specimens, and the second examines gross section geometry effects under biaxial bending moments caused by unusual loading along the diagonal of the section.

Section 4 calibrates the other parameters of the 3D bridge system on a relatively simple configuration of conventional RC highway bridge. The selected bridge is one for which response data are available for an extensive enough array capable of characterizing overall system modes. At the time this study was initiated, the most complete set of strong motion records available for a highway bridge structure of any configuration during a moderately severe seismic event was the Meloland Road Overcrossing (MRO) located 0.5 kilometer from a fault that ruptured near El Centro, California.

The MRO is one of the simplest and most common configurations in the United States. It is a straight, two-span continuous overpass with a RC multi-cell box-girder deck, a well-confined single circular column central pier, and integral well-detailed connections at the pier footing, pier cap, and deck abutments. The 1971 San Fernando earthquake focused retrofit designers attention on:

1) large transverse reinforcement spacing that inadequately confined concrete in columns in many structures designed prior to 1971, and

2) gaps that develop in deck joints and tend to increase transverse deformations and allow deck unseating at abutments and piers.

The MRO was designed prior to 1971 but nonetheless exhibited neither of these two major deficiencies.

Section 4 applies a simple procedure for tuning natural frequencies of simple bridge configurations. These frequencies may be used as the basis for characterizing global system damage. They are also important in predicting the dynamic response of the system to a given seismic event. The procedure is applied to the MRO making use of the results of system identification studies performed at the site by others. Two sets of frequencies were identified using different sets of instrument recordings. The first set included only instruments located on the deck superstructure. The second set included all those in the first set as well as several instruments located on the embankment. The second set thus encompasses a broader description of the structure system and identified lower frequencies indicating a softer system.

Tuning of the MRO damage model is performed first by defining a fixed base system matching the first set of frequencies. The free parameter that is adjusted is the elastic modulus of the linear plate elements used to model the deck. A second model is then constructed by adding discrete linear springs for the lumped effects of abutment and embankment stiffness and embankment mass at either ends of the superstructure. The second set of frequencies are then matched using engineering estimates of the lumped properties of the foundation.

Results of simulations are presented in Section 4 demonstrating the performance of the tuned structure model and column damage model in terms of deck transverse and rotation response prediction at the central pier location. These responses are critical for determining the column demand and capacity. The tuned fixed based model is used to predict the response to measured motions applied at abutment and footing locations. The tuned soil-structure interaction model is then analyzed to demonstrate the effect of the soil-structure interaction. This necessitates simulation of the motions at uninstrumented locations defining the boundary of the SSI model. This procedure highlights the importance of the embankments in driving the damage of the column for this type of short-span structure.

Finally, in Section 5 the calibrated SSI model is used to construct an intensity-damage relationship and family of fragility curves for the MRO. Random variation in key fiber model parameters controlling the column damage are considered for the measured input motion scaled to increasing intensities. In addition, random ground motions are generated using an ARMA model of the underlying stochastic process. The latter provides significant variation in the predicted damage response and thus dominates the estimated variance of the damage measure. A damage measure is selected which takes advantage of the capabilities of the fiber model in predicting the deformation capacity of the column. Limit

states are proposed which relate to material states which can be interpreted in terms of performance of the structure and may be computed easily using the fiber model. The effect of span on the computed fragility curves is examined using simulations of replica MRO structures of lengths 50, 75, 125, and 150 percent of the original. Each replica structure is subjected to the same set of input histories as the original.

# SECTION 2
# A 3D COLUMN DAMAGE ELEMENT FOR RC STRUCTURES

A column damage model should include the following features in order to meet the goals of this work:

1. Time/load-path dependent stiffness and flexure damage mechanisms in a 1D continuum, 2-noded finite element.
2. 3D kinematic interaction of deformations imparted by axial force and biaxial bending moments during flexural damage processes.
3. 3D 6-DOF/node force-displacement relations that are not subject to element scale or geometry effects.
4. Arbitrary steel and concrete material, cross-section geometry, and reinforcement detailing.
5. Compatibility with linear and nonlinear-dynamic 2D and 3D solid finite elements such as plates, shells, 3D-continuum, and 1D lumped springs/dashpots.

To the authors' knowledge, there does not at present exist an element which satisfies all of the above requirements. This lack of availability of a computational tool for research and design analysis motivated the development work discussed in this chapter. The general-purpose program, DYNAFLOW (Prevost,1997) developed at Princeton University has all of the elements listed above including nonlinear 3D beam-column and 3D-continuum elements. The original nonlinear 3D beam-column element formulation, BEAMNL, lacks the important features of arbitrary geometry and flexural damage mechanisms appropriate for reinforced concrete. The new formulation used here has been implemented as a new element, CONCRETE_BEAM (Prevost, 1997).

The following damage mechanisms are considered essential to the achievement of satisfactory performance of the element under realistic seismic loadings:

1. Concrete tensile cracking behavior.
2. Concrete softening and spalling behavior.
3. Confinement effects of transverse reinforcement on concrete strength and ductility.
4. Plasticity of longitudinal reinforcement up to fracture strains.

Existing computational tools and analytical formulations are available in the literature to model these effects using equivalent 1D stress-strain relations to represent complex 3D stress-strain responses. While some room for improvement is seen in the treatment of these responses under dynamic interaction of axial force and biaxial bending moments, no major modification of these modeling approaches was attempted for this project. Rather, the emphasis was placed on selection of simple formulations and practical modeling assumptions which will perform adequately in the analysis of 3D highway bridge systems not

just individual components tested in the laboratory.

The above objectives were decided upon after an extensive survey of the literature relating to analysis of highway bridge response and the purported capabilities of commercially-available general-purpose, proprietary special-purpose, and research-oriented computer programs. Table 2-I summarizes the primary limitations found for the major programs identified in this survey.

The principles of continuum mechanics dictate that the force-displacement relations are consequences of integration of stress and strain quantities over surfaces and volumes. In addition, time and load-path dependent damage mechanisms are governed by basic relations of dynamic equilibrium, stress-strain (constitutive laws), strain-displacement (kinematics), and compatibility (continuity). These relations should not be subject to scale or geometry effects.

The simplest and perhaps most direct means of incorporating the mechanisms mentioned above in a manner consistent with the continuum mechanics principles is a fiber approach. In this approach the coupling between normal and shear stress and strain components is neglected. Simple 1D normal normal stress-strain relations may then be defined which follow intuitive cracking and plastic deformation rules and permit modeling of softening and large strain behavior.

Appendix A provides the formulation of the basic equations governing the damage model to be adopted in subsequent analysis of a conventional RC highway bridge. The formulation starts from first principles of continuum mechanics and proceeds to an implementation of a fiber basis for computing nonlinear-dynamic interaction of axial force and biaxial bending. The stiffness method is adopted throughout and provides for all the features stated as desirable in the beginning of this section. Some practical considerations of importance to the computed results are presented below.

## 2.1 Practical Fiber Modeling of RC Sections

The objectives of this work necessitate a balance between accuracy, practicality, and efficiency. Modeling complete 3D structural systems requires that computational demands do not become excessive as a result of the beam-column element modeling. On the other hand, the full range of bridge column detailing found in practice should be addressed in the fiber property specification, keeping the set of user-defined parameters to a minimum number whose values are readily obtained from standard references or basic material tests and are not subject to scale or element geometry limitations.

To achieve the desired balance, the approach used in this work implements the following basic features:

1. Arbitrary user-defined piecewise-linear stress-strain envelope curves for each fiber material type. This eliminates dependence on any semi-empirical model and permits direct use of measured data.

**TABLE 2-I** Principle Limitations of Available Elements

| Program | Ref. | Comments |
|---|---|---|
| | NONLINEAR DYNAMIC STRUCTURES PACKAGES | |
| | | **General Purpose** |
| FENRIS | (Fyrileiv, 1993) | No concrete confinement<br>No concrete softening allowed<br>Poor concrete cyclic loading/cracking model<br>Limited reinforcement detailing |
| | | **Buildings** |
| IDARC | (Kunnath et al. 1994) | 2D elements only<br>Wall elements but no shells/3D continua<br>Moment-curvature based |
| DRAIN3D | (Powell et al. 1993) | Wall elements but no shells/3D continua |
| | | **Bridges** |
| IAINEABS | (IAI-NEABS 1993) | No plates/shells or 3D continua<br>Moment-curvature based |
| | 3D FIBER MODELS IN LITERATURE | |
| | | **Limitations Common to All** |
| | | Restrictive concrete confinement model<br>Restrictive steel stress-strain relations<br>Not verified on full-scale tests<br>Not verified on 3D systems |
| | | **University of California at Berkeley** |
| ANSR | (Zeris et al. 1991) | Mixed flexibility-stiffness method with<br>ad hoc element state-determination<br>Not implemented with shells/3D continua |
| BEAMCOL/ FEAP | (Taucer et al. 1991) | Mixed flexibility-stiffness method with<br>complex element state-determination<br>Not implemented with shells/3D continua |
| | | **Imperial College, London** |
| ADAPTIC | (Madas et al. 1992) | Not implemented with shells/3D continua |
| | | **State University of New York at Buffalo** |
| UB-COLA | (Chang et al. 1994) | Not implemented for dynamic analysis<br>Not implemented as a finite element<br>Numerous ad hoc hysteretic rules<br>Verified on 2D one-member tests |

2. Multiple user-specified envelope curves for concrete and steel fibers with the number of curves conceptually unlimited but currently set at one steel and two concrete curves for conventional reinforced concrete applications. This permits specification of localized behavior on the section especially those introduced by confinement.

3. Cyclic concrete loading-unloading rules based on a fixed compression envelope curve and a tension envelope curve that shifts depending on the permanent compressive plastic strain.

4. A plasticity-based kinematic hardening multi-yield-level loading-unloading rule for steel with identical initial envelope curves for compression and tension.

5. A one- or two-parameter characterization of the size of the effectively confined concrete region which separates confined from unconfined concrete fibers.

*Cyclic Concrete Fiber Modeling*

Measured stress-strain test data extracted from a variety of sources has been presented by Chang (Chang and Mander, 1994) and supports the use of the envelope curve as a basis for cyclic loading-unloading behavior of the concrete in both compression and tension.

The envelope curve in compression acts as a backbone rigidly fixed in stress-strain space. Since the envelope curve does not change with load history, passive confinement effects are not modeled. Such effects appear to be relatively small in the work presented by Madas (Madas and Elnashai, 1992).

Softening behavior is permitted and is necessary to capture the concrete response at large strains where the ductility capacity of the member is typically developed. Such softening violates Drucker's postulate for stable materials (see e.g. Chen and Han, 1988), but may be considered acceptable in the present context as long as the element and system remain stable. In the present numerical formulation, such stability is established by the convergence of the residual force computation at the global level.

In the CONCRETE_BEAM option, any paired set of stress-strain data can be accepted as the specification of the envelopes for concrete in compression. For the verification and application analyses performed in this work, however, a limited set of key values shown schematically in figure 2-1a have been selected as parameters of the modeling. In particular, the curves are separated into ascending (hardening) and descending (softening) branches.

The ascending branch for the envelope curve of both confined and unconfined concrete in compression is taken to be the simple parabola expressed by the Saenz formula (Saenz, 1964). A total of five points at equal strain increments are used to express this parabola up to and including the peak. For confined concrete, define $\sigma_0 = \sigma_0^{cc}$ and $\epsilon_0 = \epsilon_0^{cc}$, and, for unconfined concrete, $\sigma_0 = \sigma_0^{c}$ and $\epsilon_0 = \epsilon_0^{c}$. Then,

$$\frac{\sigma}{\sigma_0} = \frac{\epsilon}{\epsilon_0} \cdot (2 - \frac{\epsilon}{\epsilon_0}) \tag{2.1}$$

The values of $\sigma_0^c$ and $\epsilon_0^c$ are available in standard references (see e.g. Wang and Salmon,

1985). The value of $k = \sigma_0^{cc}/\sigma_0^c$ is considered a free parameter in this work, with $1 \leq k \leq 2$, and $k = \epsilon_0^{cc}/\epsilon_0^c$.

Three key points are considered as free parameters for characterizing the descending branch for compression. These points are defined as follows.

$\sigma_{3\cdot\epsilon_0}$ = Stress at strain, $\epsilon = 3 \cdot \epsilon_0$
$\epsilon_{.2\sigma_0}$ = Strain at stress, $\epsilon = .2 \cdot \sigma_0$
$\epsilon_u$ = Ultimate strain such that compressive stress, $\sigma = 0$

Tension is permitted in this work as it does not overly complicate the analysis and is more realistic conceptually and physically. In order to avoid unnecessarily high numbers of iterations for convergence, however, the envelope curve for tension is taken as bilinear with linear softening from the peak tensile stress, $\sigma_o^t$, down to a cracking strain, $\epsilon_u^t$, of the order of the strain at peak compressive stress. Unlike the compression envelope curve, the strain coordinates defining this curve are allowed to shift during the loading history.

Chang (Chang and Mander, 1994) indicated that no tests have been performed which cycle between tension and compression envelope curves. Thus, any reasonable approach seems justified.

Figure 2-2 shows schematically the treatment of cyclic concrete loading and unloading in the presence of tensile cracking adopted in this work. In figure 2-2a, the cycling begins with an excursion into tensile stresses which causes complete cracking and loss of tensile capacity followed by reloading into compression stresses which begins at a zero strain. In figure 2-2b, the cycling begins with an excursion into compressile stresses which produces a plastic residual strain, $\epsilon_p$, upon complete unloading. Without prior cycling in tension, the loading proceeds as in the case of figure 2-2a except that the tension envelope is now shifted by an amount equal to $\epsilon_p$. Subsequent reloading then occurs when $\epsilon_p$ is reached during a negative strain increment. Unloading from either the tension or compression envelope is assumed to be purely elastic. From the data presented in Chang (Chang and Mander, 1994) this appears justified for well-confined concrete.

*Cyclic Reinforcing Steel Fiber Modeling*

Measured stress-strain data presented in Chang (Chang and Mander, 1994) support the use of a kinematic hardening plasticity-type evolution law (see e. g. Chen and Han, 1988). In this work, a trilinear curve is chosen which is adjusted in stress-strain space according to the progression of the back stress, $\alpha$. The key parameters become the three points defining this curve as shown schematically in figure 2-1b. The first point is determined from the typical monotonic curve reported in standard references such as (see e.g. Wang and Salmon, 1985). The initial hardening slope is extrapolated backward toward the initial elastic curve. The intersection defines the initial estimate of the first stress value, $\sigma_y^*$. This estimate results in a 10-20 percent decrease in the value of the plateau value typically reported as the yield strength, $\sigma_y$. The initial elastic modulus, $E_s$, is reduced by 25 percent in order to better represent the nonlinear cyclic stress-strain curve which the measured data exhibit. Together, the reduced modulus, $E_s^*$, and the first yield stress

a) Concrete Fibers

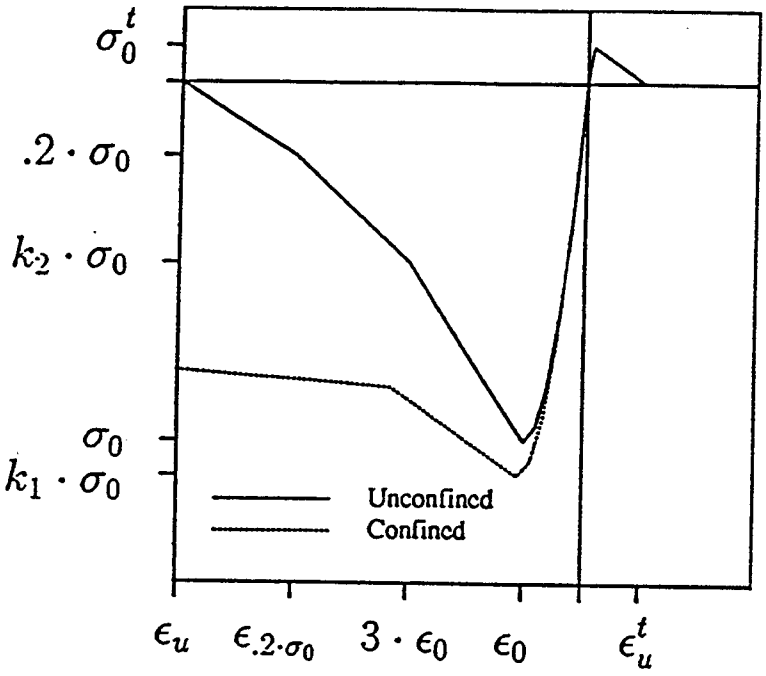


b) Steel Fibers

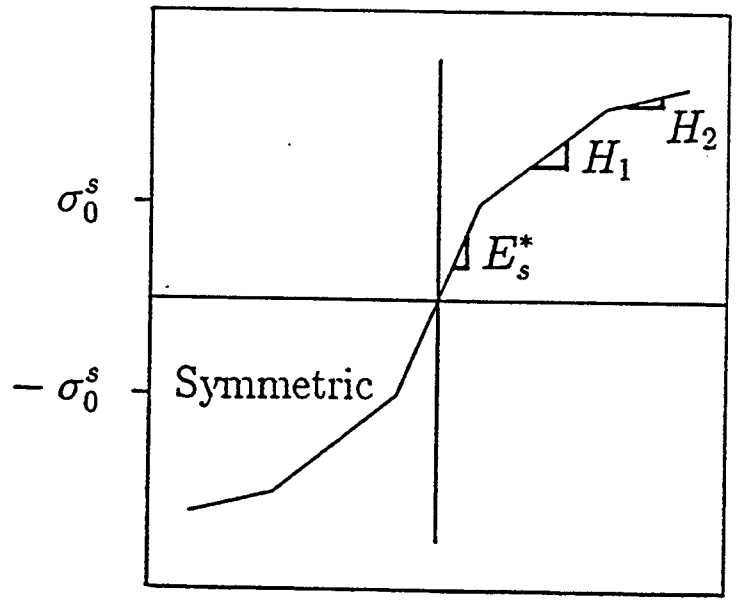


**FIGURE 2-1 Monotonic Fiber Material Curves**

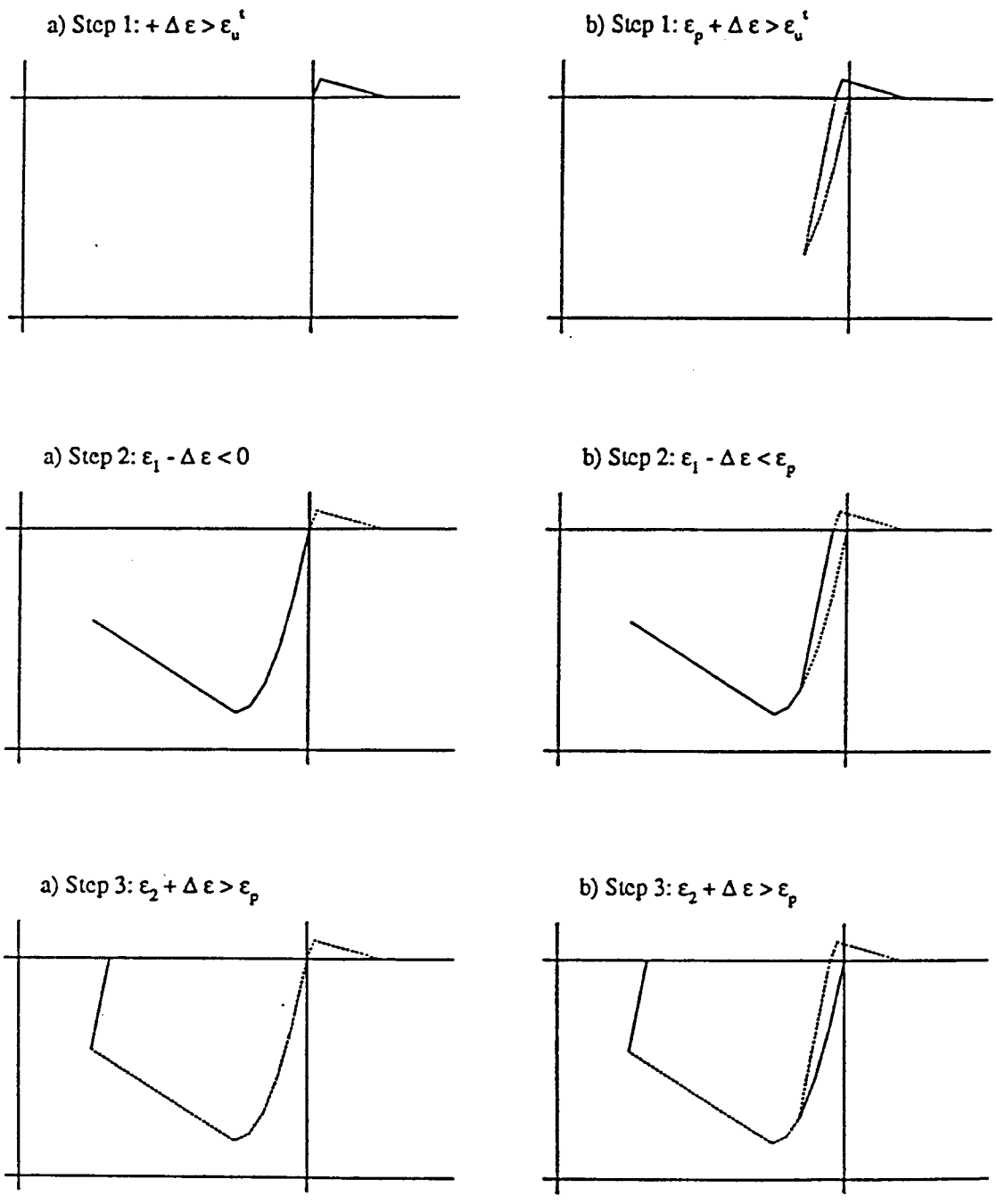


**FIGURE 2-2 Cyclic Concrete Material Loading-Unloading**

define the first point on the curve. The remaining two points are taken to best represent the monotonic curve up to the peak value which tends to occur at a strain fairly close to the monotonic fracture strain.

*Effective Confinement Parameter*

The arbitrary shape of the fiber domain (see App. A, figure A-3) permits flexibility in the arrangement of fiber meshes for concrete and steel. In this work, this leads to a single parameter defining effective confinement regions for simple cross-section shapes. Figure 2-3 identifies these regions schematically for the columns to be examined in the next section. The choice of the parameter remains user-defined in this work in that the user defines the fiber layout and assigns to each fiber the geometric properties and the appropriate envelope curves. A simple mesh generator subroutine, FIBXS, was written to automate this task for circular and rectangular sections, given a basic set of input parameters. The fiber meshes generated for the columns to be examined in the next section are shown in figure 2-4 which identifies each fiber centroidal location by a square symbol.

A purely geometric basis for selecting the effective confinement shape parameter is given by Mander (Mander, Priestley, and Park, 1988) which assumes a parabolic shape for the vertical loss of effective confinement between transverse bars and, in the case of cross-ties, the horizontal loss between longitudinal bars. The experimental justification of such an approach is provided by Mander only for cases of concentric compressive axial load. In this work, the following expressions were adopted as the initial basis for estimating the single-parameter representations.

For a circular section with a circular spiral of transverse reinforcing bars, the following relation is obtained using the geometric arguments given by Mander (Mander, Priestley, and Park, 1988). Define,

| | |
|---|---|
| $s$ | = longitudinal pitch of spiral bar centers |
| $d_{st}$ | = nominal diameter of spiral bars |
| $d_s$ | = projected diameter between spiral bar centers |

Then,

$$d_e = d_s \cdot (1 - \alpha)^{\frac{1}{2}} \tag{2.2}$$

where

$$\alpha = \frac{s - d_{st}}{2 \cdot d_s}$$

Similarly, for a square section with cross-ties between all interior longitudinal reinforcing bars which are assumed equally spaced around the perimeter, the following is obtained. Define,

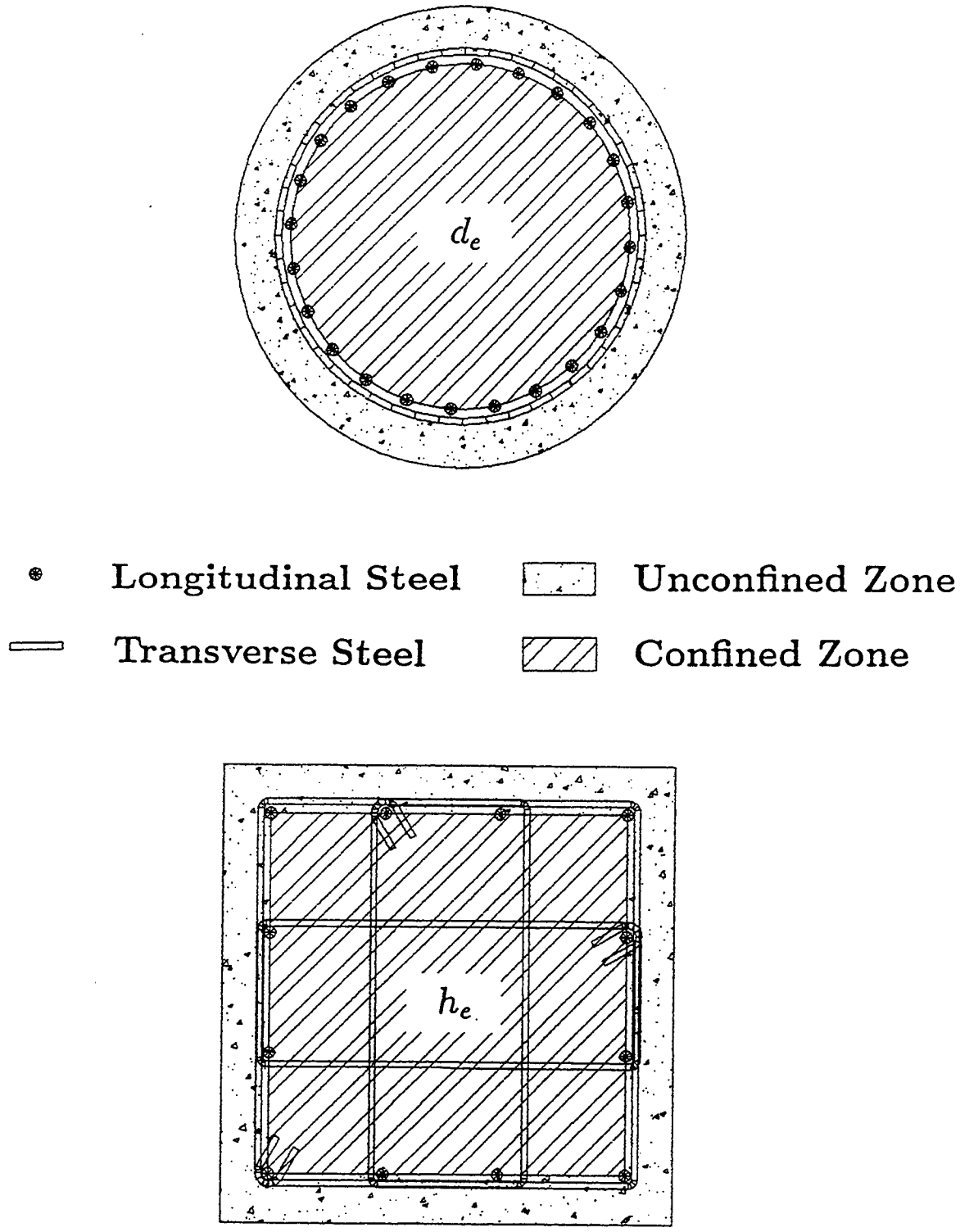


**FIGURE 2-3 Effective Confinement Zones for Simple Shapes**

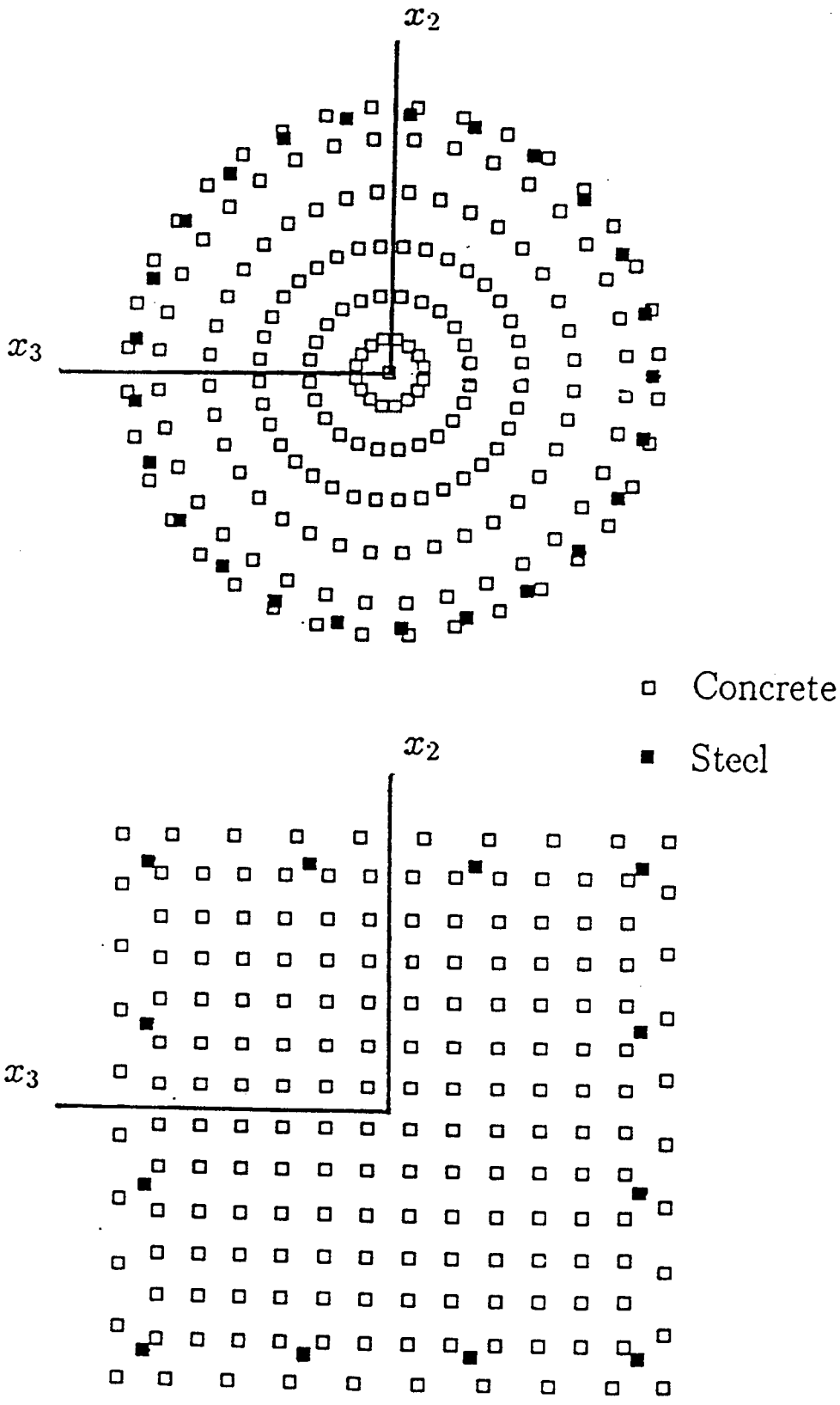


**FIGURE 2-4 Fiber Meshes for Simple Shapes**

| | |
|---|---|
| $s$ | = longitudinal spacing between hoop bar centers |
| $w$ | = transverse spacing between longitudinal bar centers |
| $n+1$ | = number of longitudinal bars on each face |
| $d_{st}$ | = nominal diameter of transverse bars |
| $d_{sl}$ | = nominal diameter of longitudinal bars |
| $h_s$ | = length between hoop bar centers |

Then,

$$h_e = h_s \cdot (1-\alpha) \cdot (1 - \frac{2}{3} \cdot n \cdot \beta^2)^{\frac{1}{2}} \tag{2.3}$$

where

$$\alpha = \frac{s - d_{st}}{2 \cdot h_s}$$

$$\beta = \frac{w - d_{sl}}{h_s}$$

For the purposes of characterizing the estimated values of the above effective confinement parameters, the following quantities are defined for circular and square shapes, respectively:

| | |
|---|---|
| $d_c$ | = projected diameter between longitudinal bar centers |
| $h_c$ | = length between longitudinal bar centers on opposite faces |

These quantities are easy to visualize from a section view on an as-built drawing and may be easily computed as follows:

$$\begin{aligned} d_c &= d - d_{st} - d_{sl} \\ h_c &= h - d_{st} - d_{sl} \end{aligned} \tag{2.4}$$

# SECTION 3
# CYCLIC DAMAGE CALIBRATION FOR RC COLUMNS

Application of the fiber modeling to existing structures has two main needs. The modeling should predict force and ductility demands on the column in reasonable agreement with physical testing without sensitivity to:
1. Scale of the specimen, e.g. L or *d*.
2. Geometry of the cross-section, e.g. circular or rectangular.
The problem of scale is important because of the lack of data available at full-scale. Geometry is important because of the variety of geometries that exist in practice.

Two experiments on RC beam-columns have been selected to demonstrate the model's basic performance with respect to these modeling needs. Both experiments were designed with seismic retrofit assessment of highway bridges as the basic application of the research.

The first experiment was performed at the National Institute for Standards and Technology (NIST) in Gaithersburg, Maryland, (Stone and Cheok, 1989). It involved quasi-static cyclic destructive tests on cantilever columns having a circular, spirally reinforced section. Of interest here are the so-called Flexure pair of specimens, one of which was a full-scale replica of a bridge pier and the other a 1:6 scale model. The dimensions were selected as representative of California design practice in cases where flexure failure would dominate.

The pair of NIST Flexure specimens provides the only direct test of scale relationships for bridge columns known to the authors. Of particular importance to this work is the fact that the circular cross-sectional dimensions and material strengths are almost identical to those of the MRO pier. The full-scale flexure test thus provides a good estimate of the basic set of fiber modeling parameters to be used for the MRO pier.

The second experiment was performed at the University of Canterbury in New Zealand (NZ) (Zahn, Park, and Priestley, 1989). It involved quasi-static cyclic destructive tests on double- cantilever columns of square section and scale comparable to the 1:6-scale NIST specimen. Loading was applied along the diagonal of the cross-section thus developing equal magnitude biaxial moments to develop in combination with a constant axial force. For this reason, the test will hereafter be designated the NZ Biaxial Flexure test. Since interaction is developed such that a sharp corner provides the extreme fibers for flexure, this is considered a severe test of the modeling performance with respect to geometry.

## 3.1 Full Scale Flexure Test on Circular Bridge Column

The gross cross-section and reinforcement detailing for the full-scale NIST Flexure specimen and the 1:6 scale NIST Specimen N6 are shown in figure 2-3. The geometric properties are summarized in the first two columns of table 3-I. All dimensions are based on the published data, (Taylor and Stone, 1993) and (Stone and Cheok, 1989). All quantities in table 3-I are defined in Section 2. The aspect ratio, L/d= 6, for both specimens

clearly indicates the predominance of flexure over shear deformations.

**TABLE 3-I Geometric Property Data**

| Parameter | Circular Section NIST Flexure Columns 1:6 Scale | Full-Scale | MRO Pier | Parameter | Square Section NZ Col. | Units |
|---|---|---|---|---|---|---|
| **Gross Section** | | | | | | |
| L | 1.50 | 9.14 | 6.36 | L | 1.60 | m |
| $d$ | 0.25 | 1.52 | 1.52 | $h$ | 0.40 | m |
| A= $\pi d^2/4$ | .049 | 1.82 | 1.82 | A= $\pi h^2/4$ | 0.16 | $m^2$ |
| I= $\pi d^4/64$ | .192 | 265. | 265. | I= $\pi h^4/64$ | 2.13 | $m^4$ |
| **Confinement** | | | | | | |
| s | .014 | .089 | .127 | s | .084 | m |
| | | | | w | .113 | m |
| | | | | n | 3 | |
| $d_{st}$ | .0027 | .016 | .016 | $d_{st}$ | .010 | m |
| $d_s$ | .23 | 1.41 | 1.36 | $h_s$ | .364 | m |
| $\alpha$ | .025 | .026 | .041 | $\alpha$ | .102 | |
| | | | | $\beta$ | .266 | |
| $d_e$ | .227 | 1.39 | 1.33 | $h_e$ | .303 | m |
| $d_{sl}$ | .007 | .043 | .057 | $d_{sl}$ | .016 | m |
| $d_c$ | .22 | 1.35 | 1.28 | $h_c$ | .338 | m |
| $d_e/d_c$ | 1.03 | 1.03 | 1.03 | $h_e/h_c$ ($h_e^*/h_c$) | 0.90 (1.03) | |

Figure 2-4 shows the fiber mesh used to model the two NIST specimens. Because of the scaled relationship, the fiber layout is identical for both specimens. Only the coordinate values are different. The design of the mesh in the longitudinal direction has been based on studies of an ideal elastoplastic cantilever. These studies revealed that no additional improvement in stiffness estimation was to be obtained when a finer mesh was used. By grading the mesh to have a short element nearest the plastic hinge, it is possible to capture high curvature gradients that occur there. The mesh design is not based on assumed linear response in any of the elements. Each element has the same formulation, thus no apriori or effective plastic hinge length is assumed or built-in to the computation.

The key point values/parameters used to define the material curves are summarized in the first two columns of table 3-II and are plotted in figure 3-1. The maximum strain plotted corresponds roughly to the highest value predicted by the fiber model analysis for

the tests. The basis for selecting the values/parameters in table 3-II is described in Section 2. In this case, however, some parameters were measured experimentally, so data from (Stone and Cheok, 1989) were substituted for data from standard references. Peak and post-peak parameters for confined concrete were selected assuming moderate confinement effects as indicated by the confinement parameters estimated by the experimenters.

The cantilever test arrangement and displacement-control loading sequence described in (Stone and Cheok, 1989) are depicted in figure 3-2. The element discretization along the member length is shown in figure 3-2a and the target ductility levels to be achieved during cycling are plotted in figure 3-2b.

**TABLE 3-II Material Property Data**

| Parameter | Circular Section NIST Flexure Columns 1:6 Scale | Circular Section NIST Flexure Columns Full-Scale | MRO Pier | Square Section NZ Col. | Units |
|---|---|---|---|---|---|
| **Concrete** | | | | | |
| $\nu_c$ | .17 | .17 | .17 | .17 | |
| *Compression* | | | | | |
| $f'_c$ | 23.3 | 35.9 | 35.9 | 36.2 | MPa |
| $E_c$ | 23.1 | 28.3 | 28.3 | 30. | GPa |
| $k_1$ | 1.1 | 1.1 | 1.1 | 1.8 | |
| $k_2^c$ | 0.3 | 0.5 | 0.3 | 0.5 | |
| $k_2^{cc}$ | 0.85 | 0.85 | 0.5 | 0.95 | |
| $\epsilon^c(.2 \cdot \sigma_o)$ | .01 | .01 | .02 | .02 | |
| $\epsilon^{cc}(.2 \cdot \sigma_o)$ | .04 | .04 | .06 | .2 | |
| $\epsilon_u^c$ | .02 | .02 | .03 | .04 | |
| $\epsilon_u^{cc}$ | .2 | .2 | .15 | .4 | |
| *Tension* | | | | | |
| $\sigma_o^t$ | | | | 2.1 | MPa |
| $\epsilon_o^t$ | .0001 | .0001 | .0001 | .0001 | |
| $\epsilon_u^t$ | .002 | .002 | .002 | .002 | |
| **Steel** | | | | | |
| $\nu_s$ | .33 | .33 | .33 | .33 | |
| $f_y$ | 446. | 475. | 312. | 318. | MPa |
| $E_s$ | 204. | 189. | 189. | 189. | GPa |
| $H_1$ | 3.45 | 3.45 | 2.76 | 5.17 | GPa |
| $H_2$ | 1.38 | 1.38 | 1.38 | 1.38 | GPa |
| $\epsilon_1^s$ | .0025 | .0025 | .0019 | .0026 | |
| $\epsilon_2^s$ | .025 | .025 | .056 | .033 | |

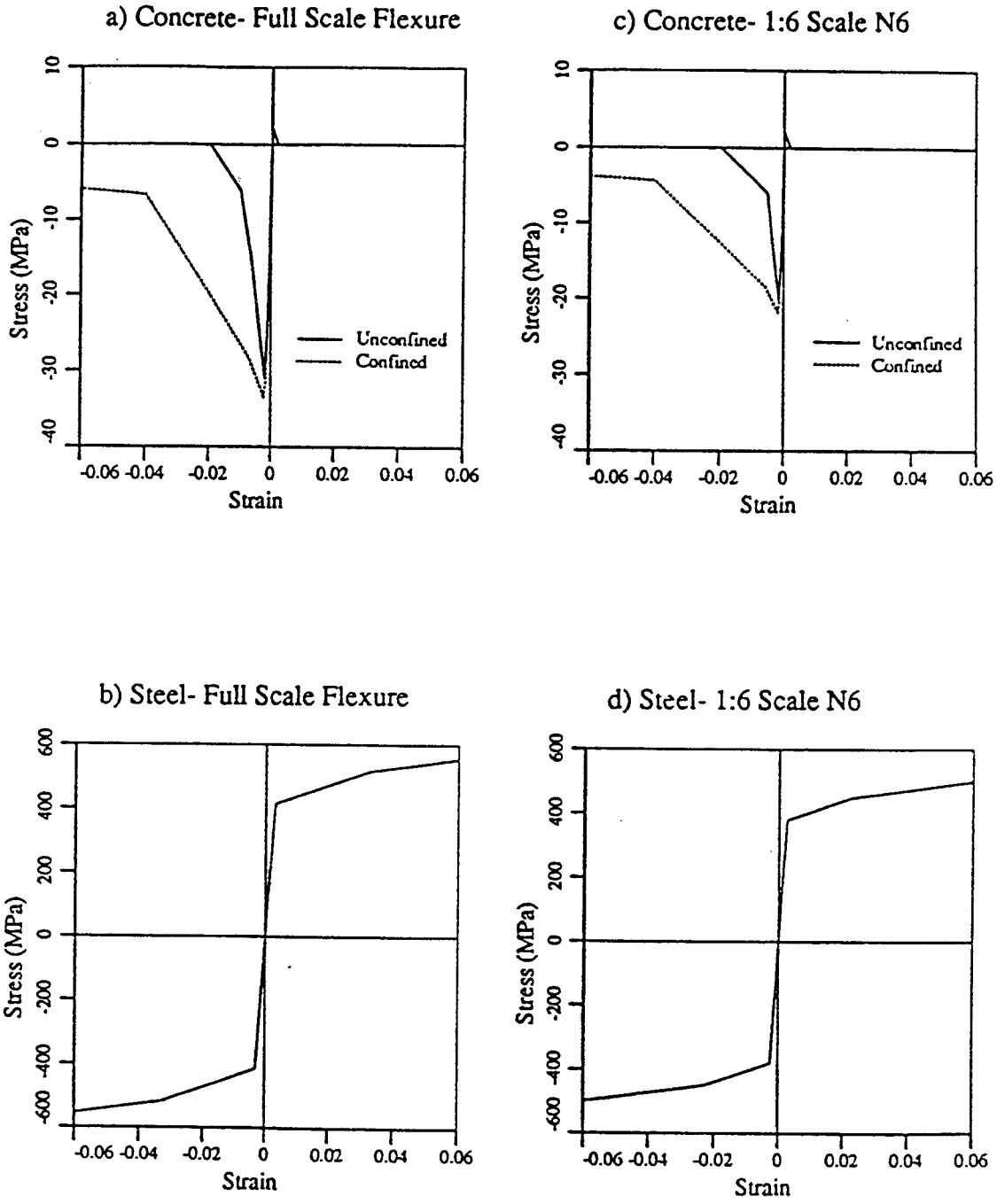


**FIGURE 3-1 NIST Flexure Tests: Material Curves**

The cyclic load-deformation curves for the two specimens are shown in figure 3-3 along with the fiber model predictions. All results are normalized with respect to the maximum load or deformation of the respective test specimen. The fiber model appears to follow the full-scale model response well up to a target ductility level, $\mu = 3$, or up to the end of the fifth full cycle. Based upon strain gage measurements on the longitudinal steel reinforcement (Stone and Cheok, 1989) and the fiber model predictions, it is clear that the unconfined concrete has already gone well into post-peak behavior at this point and the outer steel fibers reach tensile strains close to 1 percent. At a target ductility level, $\mu = 4$, 10 cycles are applied and beyond this the strength degrades more rapidly. Presumably, a low-cycle fatigue damage in which a fatigue crack grows in the presence of plastically deforming material occurs after this point. At the target ductility level, $\mu = 6$, some steel bars fracture and rapid degradation ensues. It appears from figure 3-3 that the fiber model does not degrade as rapidly as the test specimens at these large ductilities.

In the small-scale specimen, the degradation of the test specimen N6 at the target ductility level, $\mu = 4$, and beyond is much more severe than that of the full-scale specimen. This is a scale effect associated with the concrete used which in this case incorporated pea-gravel as aggegrate (Stone and Cheok, 1989). Another specimen designated N3 was tested at the 1:6 scale and found to have even more pronounced degradation. In the latter case so-called micro-concrete was used (Stone and Cheok, 1989). This specimen was not considered here because there is virtually no correspondence between the 1:6 scale and full-scale results.

In order to focus on the meaningful response prior to the point where the experimental scale effect detracts from the comparison of 1:6 scale and full-scale specimens, the results of the first three cycles, up to a target ductility, $\mu = 2$, have been isolated in figure 3-4. From these plots, the basic correspondence of the maximum and cyclic response appear acceptable at both scales, in the authors' view, for the purposes of this work.

For comparison, the widely distributed 2D program IDARC (Kunnath, Reinhorn, and Lobo, 1992), labeled IDARC2D here to distinguish it from IDARC-3D (Kunnath and Reinhorn, 1989), was used to model these two tests. IDARC2D first estimates the maximum plastic moment capacity using a 2D fiber model. The load-path dependent response, however, is computed based on moment-curvature relations which are governed principally by three hysteretic parameters that control the shape of the moment-curvature loops. The parameter, $HC$, controls the cyclic reduction of stiffness, $HDE$ the cyclic reduction of peak strength based on ductility attained, and $HS$ the pinching of loops associated with slip or crack-closing.

For this comparison, choices of these parameters were made to provide the best correspondence with the small-scale test (see fig. 3-5a). This was found to be given by:

$$HC = 9 \quad HBD = .07 \quad HS = .5$$

These values were then used to model the full-scale test (see fig. 3-5b)

The prediction of maximum response appears to be acceptable at both small and full scales, but this just confirms the validity of the fiber model approach which was used in

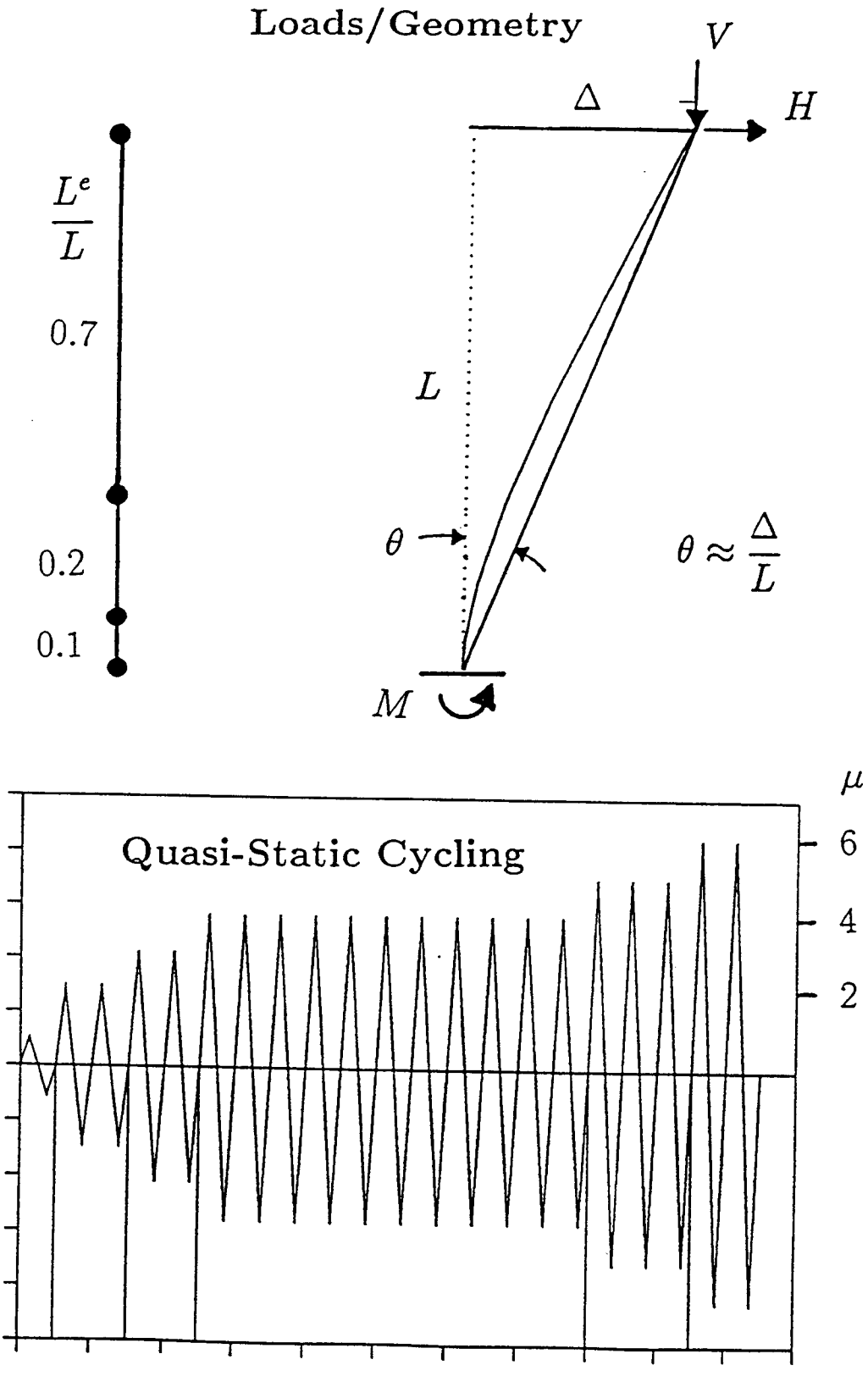


**FIGURE 3-2 NIST Flexure Tests: Loading and Geometry**

a) NIST Full-Scale Flexure

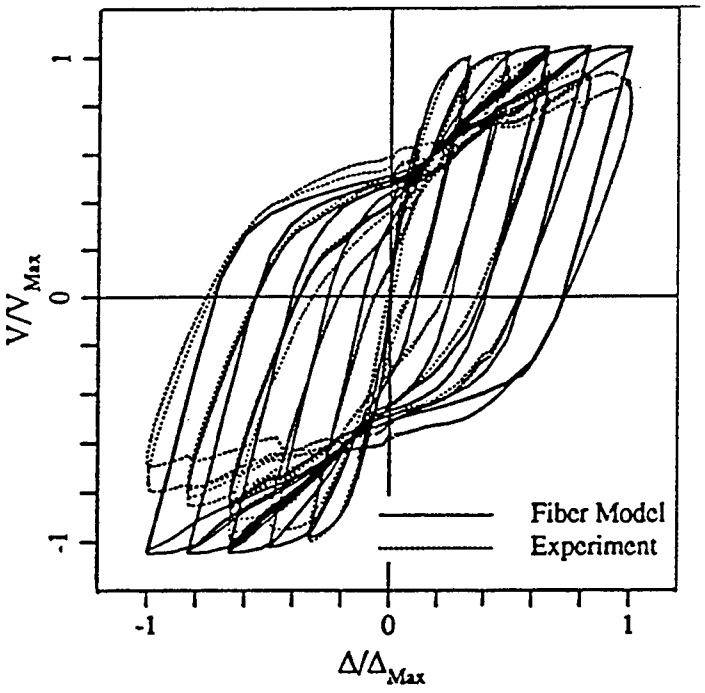


b) NIST 1:6-Scale N6

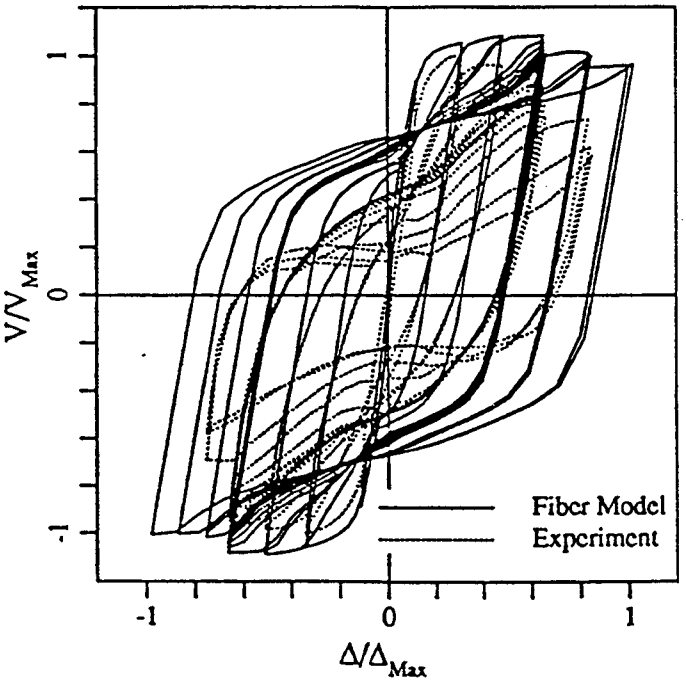


**FIGURE 3-3 NIST Flexure Tests: Load-Displacement Cycles**

a) NIST Full-Scale Flexure

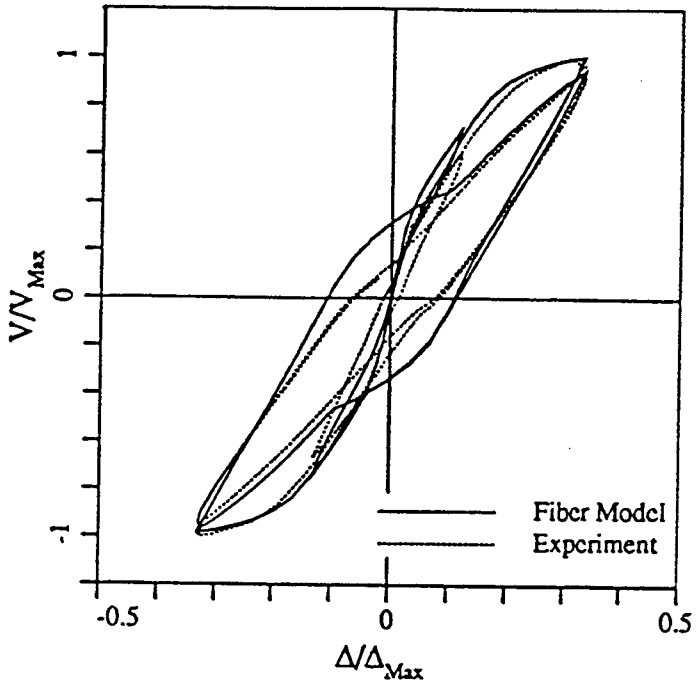


b) NIST 1:6-Scale N6

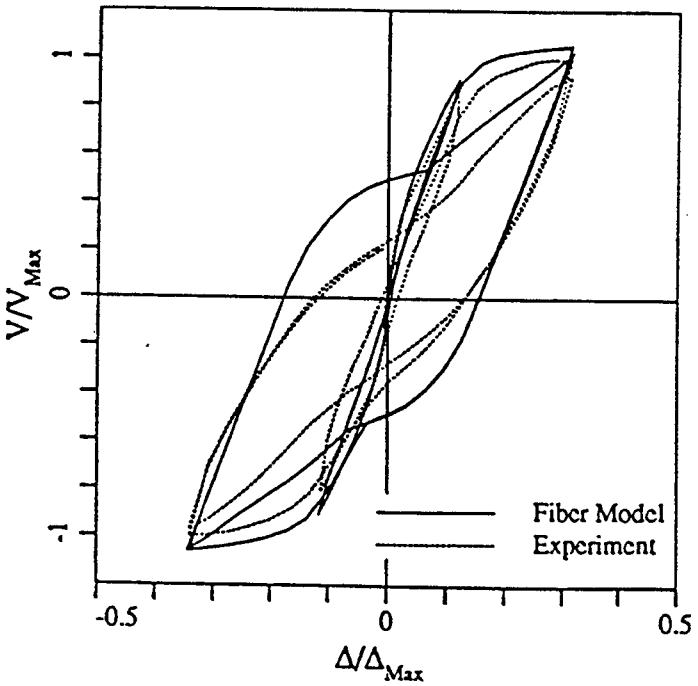


**FIGURE 3-4 NIST Flexure Tests: Cycles up to $\mu = 2$**

a) NIST Full-Scale Flexure Specimen

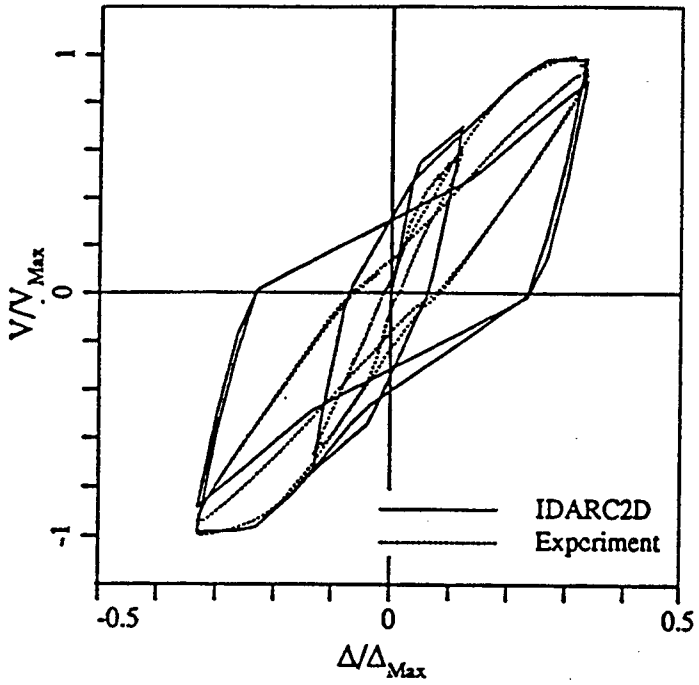


b) NIST 1:6-Scale Specimen N6

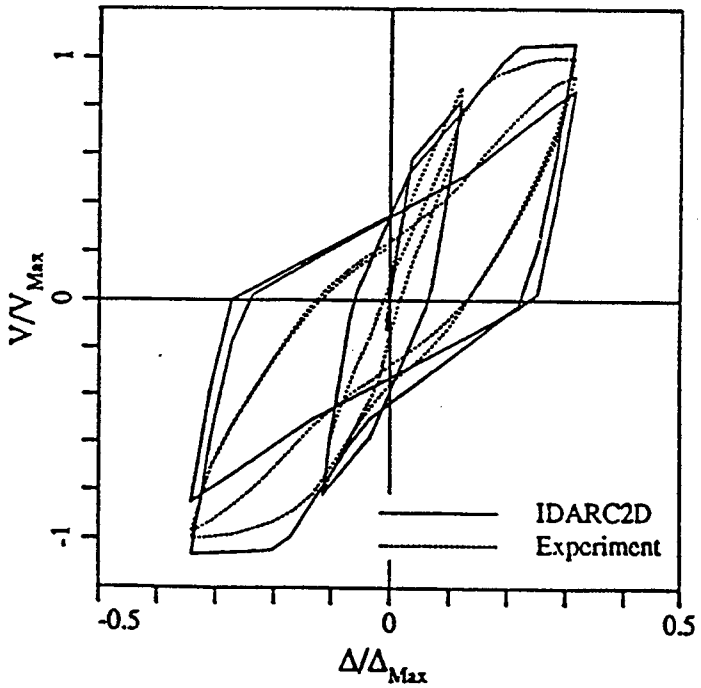


**FIGURE 3-5 NIST Flexure Tests: IDARC2D Predictions**

both cases. The cyclic response is not considered acceptable, however, significantly overestimating the unloading stiffness as evidenced by the large permanent plastic deformation obtained upon complete unloading. It was not possible to improve the correspondence without losing acceptable prediction of the maximum response. The overestimation of unloading stiffness appears to worsen slightly as the prediction moves from small to full scale.

Finally, it is noted that while the IDARC2D model has become widely accepted for frame analysis, it is incapable of performing a 3D analysis with biaxial moment interaction. The primary reason for this is the lack of correspondence of the above hysteretic parameters with the mechanics of the problem. Even in this essentially 2D example, however, the proposed fiber model performs as well as the fiber model used in the widely distributed routine with regard to maximum response, while performing better with regard to overall cyclic response.

### 3.2 Biaxial Flexure Test on Square Bridge Column

The gross cross-section and reinforcement detailing for the NZ biaxial flexure specimen, Unit 1, are shown in figure 2-6 also. The geometric properties are summarized in the next to last column of table 3-I. All dimensions are based on the data published in (Zahn, Park, and Priestley, 1989). All parameters in table 3-I relevant to square sections are defined in the Section 2. The aspect ratio, L/$h$= 4, is still sufficiently large to indicate dominance of flexural over shear deformations.

Figure 2-4 also shows the fiber mesh used to model the NZ biaxial flexure specimen, Unit 1. The key point values/parameters used to define the material curves are listed in the next to last column in table 3-II and are plotted in figure 3-6 to the same scale as in figure 3-1 for comparison. The maximum strain plotted corresponds roughly to the highest value predicted by the fiber model analysis for the tests. The basis for selecting the values/parameters in table 3-IV is described in Section 2. As for the NIST specimens, some parameters were measured experimentally, so data from (Zahn, Park, and Priestley, 1989) were substituted for data from standard references.

Peak and post-peak parameters for confined concrete were selected assuming significant confinement effects as indicated might be appropriate by the experimenters. In table 3-IV two values are given for the effective confinement parameter. The lower value corresponds to the value estimated using (2.2). In order to obtain a better prediction of the experimental results, however, the asterisked value was used. It is noted that the normalized value, $h_e/h_c$, is coincidentally the same as that used in the modeling of the NIST tests.

The loading configuration was essentially the same as that used for the NIST specimen except that a double-cantilever arrangement was used to obtain the boundary conditions and load components. The displacement-control cycle sequence was the similar to the NIST tests, except that only 2 cycles were applied at each increased ductility level until the test was stopped.

a) Concrete- Unit 1

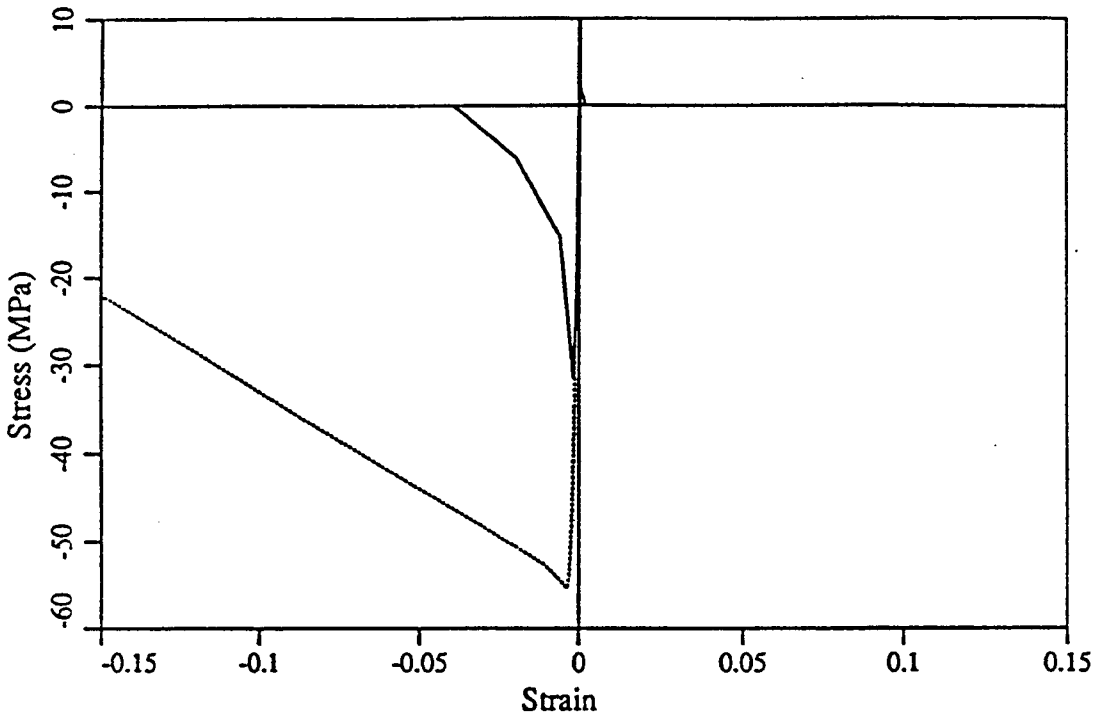


b) Steel- Unit 1

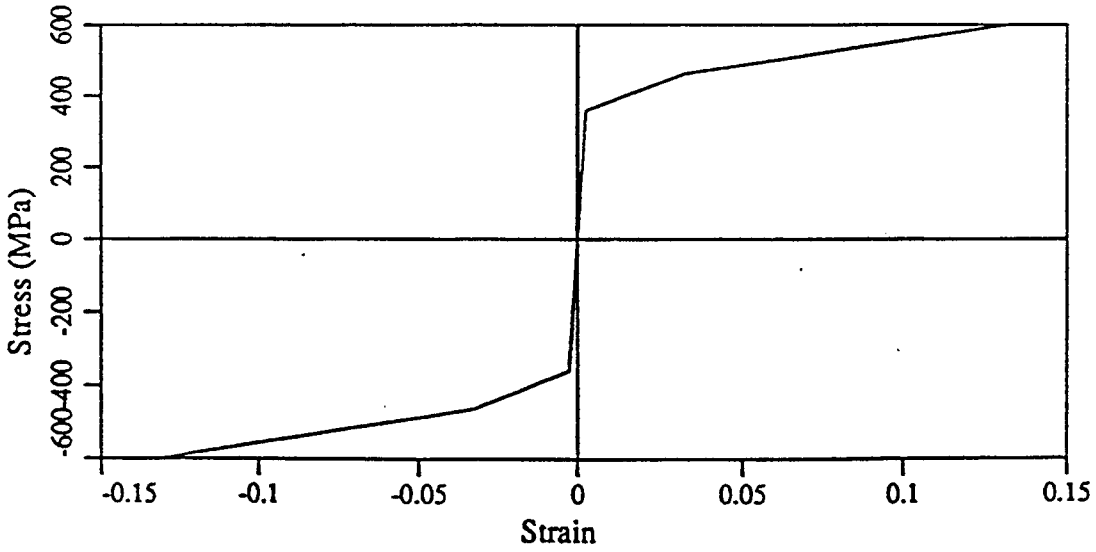


**FIGURE 3-6 NZ Biaxial Flexure Test: Material Curves**

The cyclic load-deformation curves for the two specimens are shown in figure 3-7 along with the fiber model predictions. All results are normalized with respect to the maximum load or deformation of the respective test specimen. In this case, the maximum deformation corresponded to a ductility level, $\mu = 14$. The fiber model appears to follow the full-scale model response well throughout the full test until the point where a longitudinal bar fractured and significant degradation ensued. After the second bar fracture, the test was apparently stopped.

This test serves to demonstrate the wide variety of gross cross-section and reinforcement detailing which the fiber model may be used to investigate successfully. It should be noted, however, that a broad range of confinement may be achieved as a result of the specimen geometry and reinforcement and detailing. The present database does not appear sufficient to fully investigate the relationship between these geometric parameters and the effective confinement parameters, however.

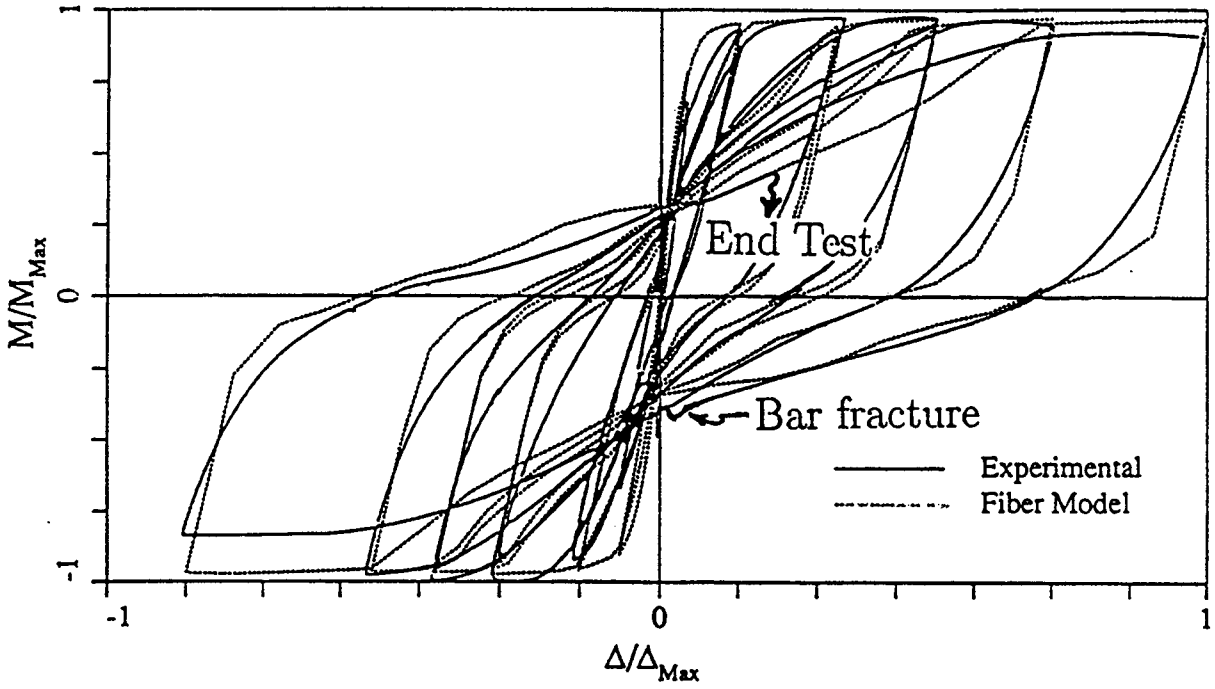


**FIGURE 3-7 NZ Biaxial Flexure Test: Load-Displacement Cycles**

# SECTION 4
# SEISMIC RESPONSE CALIBRATION FOR A RC BRIDGE

A full 3D highway bridge system involves a complex interaction of many different types of elements, the columns representing just one albeit critical type. The main objective of this work is not just the prediction of damage in column elements in isolation but the damage in the full bridge system which includes both the superstructure or deck elements and the foundation elements.

This section provides a case study of a simple RC bridge to illustrate both the performance of the column damage model under seismic loading as well as the modeling of the overall 3D dynamic response of the bridge system. The authors are not aware of any attempt by the developers of fiber models mentioned in Section 2.0 to compare predicted dynamic response directly to measured dynamic response of a highway bridge superstructure to seismic excitation at intensities causing significant nonlinear response.

The Meloland Road Overcrossing (MRO), located in El Centro, California, has been selected for the case study of seismic response of a bridge system, primarily, because it has:

1. One of the simplest and yet most common forms in both California and elsewhere in the United States.
2. An instrument array capable of capturing fundamental vibration modes of this simple system.
3. One of the few sets of records available for the response to a moderately intense ($M_L$= 6.4) seismic event at close proximity.

Other features which make the MRO a suitable choice for analyzing column damage in a bridge system are that it has:

1. A single column acting as the only intermediate pier and thus a focal damage location.
2. No intermediate deck hinges or expansion joints complicating response.
3. Integral connections between column and deck and between deck and abutments eliminating likely alternative damage locations.
4. A considerable discussion of measured and computed response in the literature covering various excitation intensity levels including: ambient. low-level forced, and moderate seismic.

Figure 4-1 shows schematically the plan, elevation, and isometric views of the MRO, and figure 4-2 shows the significant geometric and reinforcement details as they appear in the as-built drawings for the bridge ("As built", 1971). The MRO is seen to be a

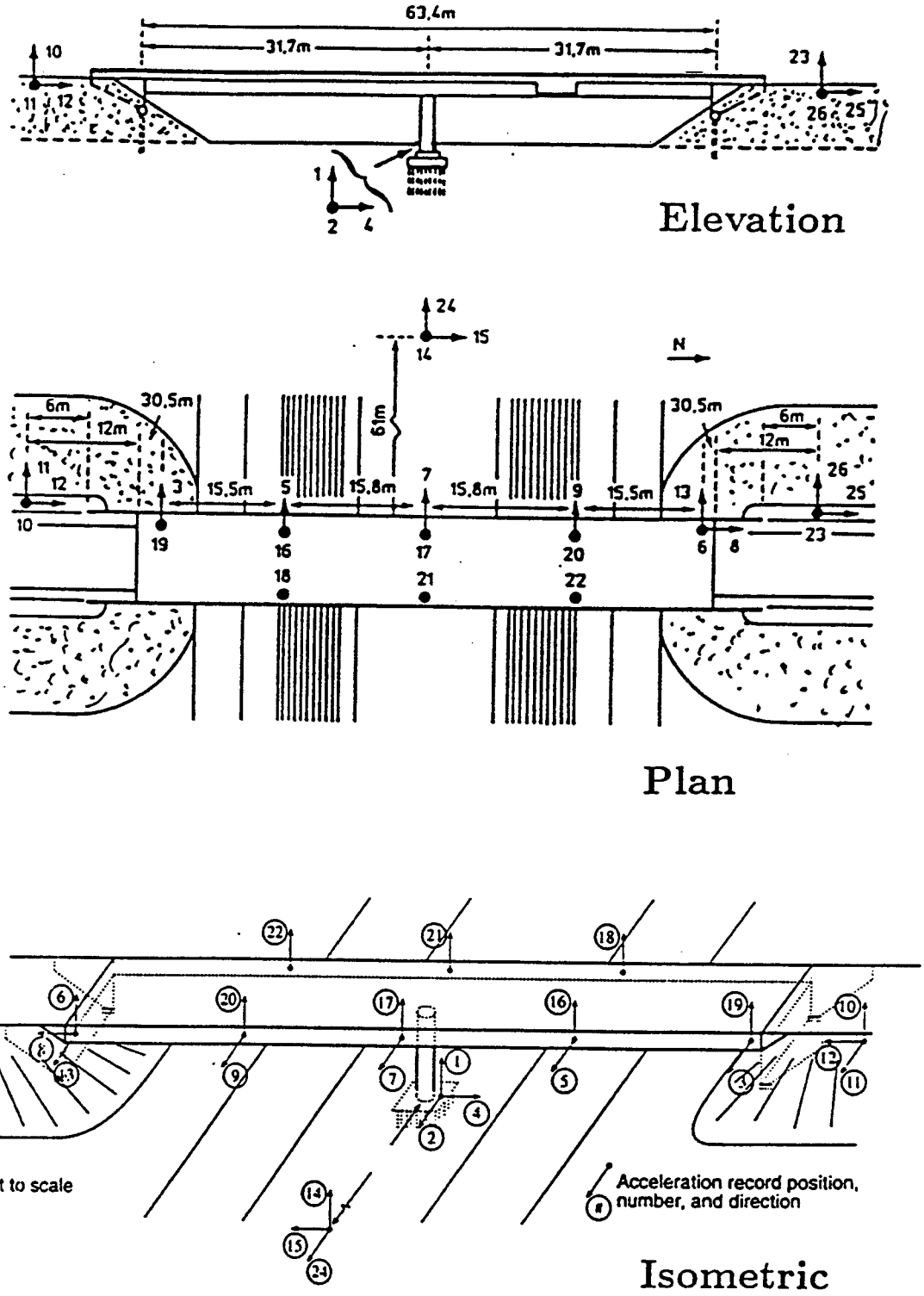


**FIGURE 4-1 MRO Overall Geometry and Strong Motion Instrument Array**

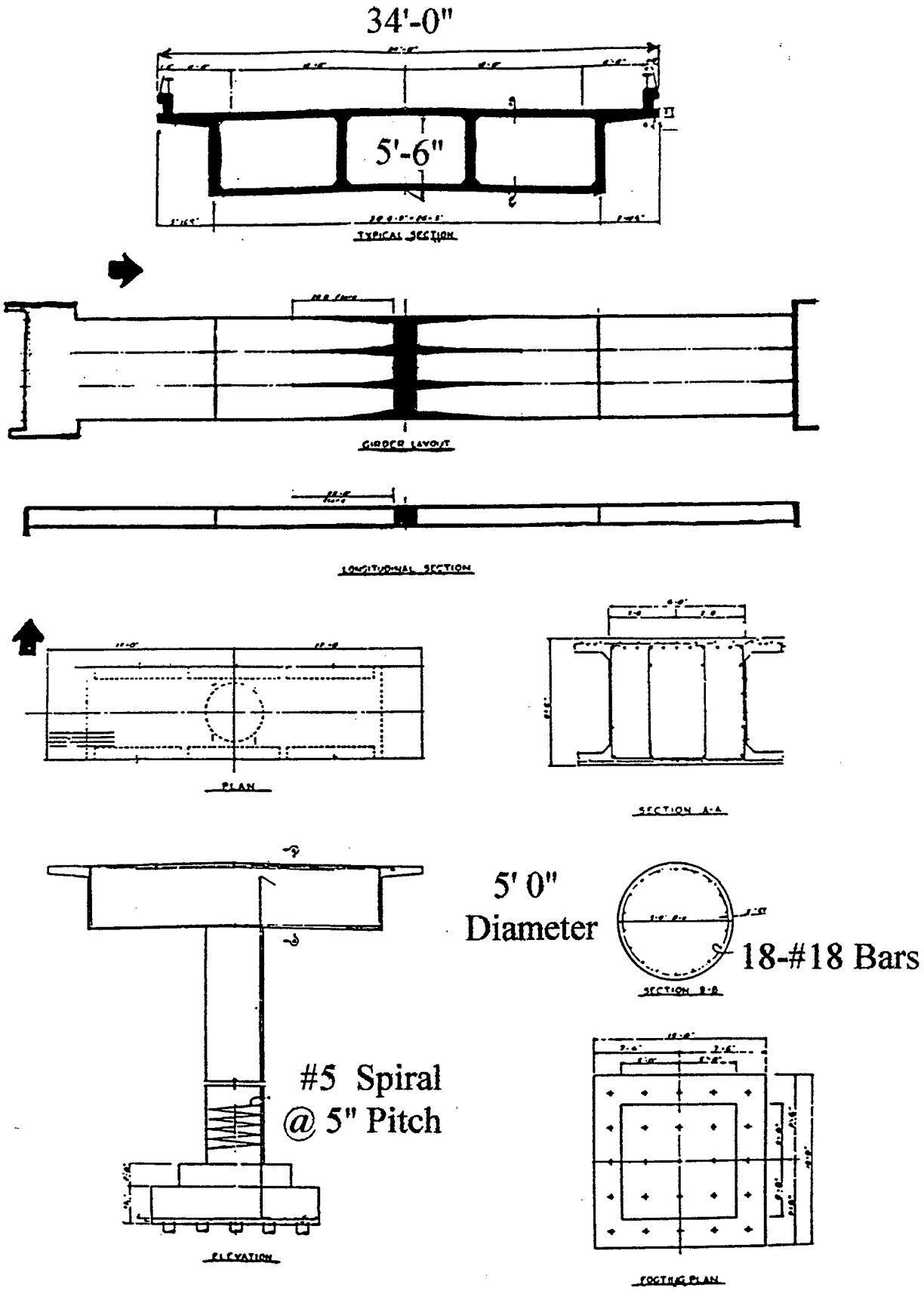


**FIGURE 4-2 MRO Deck and Central Pier Construction Details**

reinforced concrete (RC) two-span-continuous overpass with a single-column bent at the deck midlength. The deck is a three-cell box-girder which is integral with the solid RC pier cap located in the center and integral with the RC abutment walls at the ends. RC diaphragms are present at each deck quarter-length to stiffen the box sections. The box-girder webs are uniform thickness throughout the length except for flare sections that thicken as they approach the pier cap.

The longitudinal and transverse reinforcement for the central pier column is identified in figure 4-2. The close pitch of the transverse reinforcement is relatively unusual for the date of construction. It may be recalled that many of the failures that occurred during the 1971 San Fernando earthquake were attributed to inadequate transverse reinforcement which called only for No. 4 bars at 12 inch pitch.

Figure 4-1 also shows the strong motion accelerograph array that was in place at the time the 1979 Imperial Valley (IV79) earthquake occurred. The instrumentation array was originally installed as part of the California Strong Motion Instrumentation Program (CSMIP) as described by (Shakal, Ragsdale, and Sherburne, 1984).

The most intense motions which the array has recorded to present are the ones excited by the IV79 event. Frequency analysis of these records is discussed in (Werner, Beck, and Levine, 1987) and in (Bard, 1990). These records are still believed by the authors to be the most complete representation of 3D response to a moderate level event despite the occurrence of stronger events in the past few years and the expansion of CSMIP monitoring efforts since 1979.

Figure 4-3 shows the vertical and transverse horizontal accelerations (No. 14 and 24, respectively, in fig. 4-1) recorded at the instrument located 61 m (200 ft) from the central pier footing in the roadway median during the 1979 Imperial Valley earthquake. This instrument is considered as a free-field instrument in (Werner, Beck, and Levine, 1987). A moderate peak ground acceleration, PGA= 0.30 g, was observed at No. 24, and the peak deck response accelerations of 0.51 g was observed at No. 7. The bridge was virtually undamaged by the event even though the epicenter was only 16 km away and the causative fault was less than 1 km away. The transverse record indicates a single large cycle of response which will be seen to contribute the most to damage of the column. The power spectrum of this record shows that this cycle has an unusually low frequency content with two strong peaks well below 1 Hz.

The response to the 1979 Imperial Valley event was analyzed in (Werner, Beck, and Levine, 1987) and later in (Werner, Crouse, Katafygiotis, and Beck, 1993) using multiple-input, multiple output (MIMO) linear system identification procedures. In (Werner, Beck, and Levine, 1987), classical normal mode system damping, frequencies, and modal participation factors were identified. In (Werner, Crouse, Katafygiotis, and Beck, 1993) linear beam element model properties were identified. The frequencies obtained in (Werner, Beck, and Levine, 1987) serve as the target values for the DYNAFLOW modeling. The data and calculations in (Werner, Crouse, Katafygiotis, and Beck, 1993) serve as a reference set of results, but their primary use is for measured material properties and computed effective properties for deck flexural rigidities and for embankment transverse mass/stiffness. The

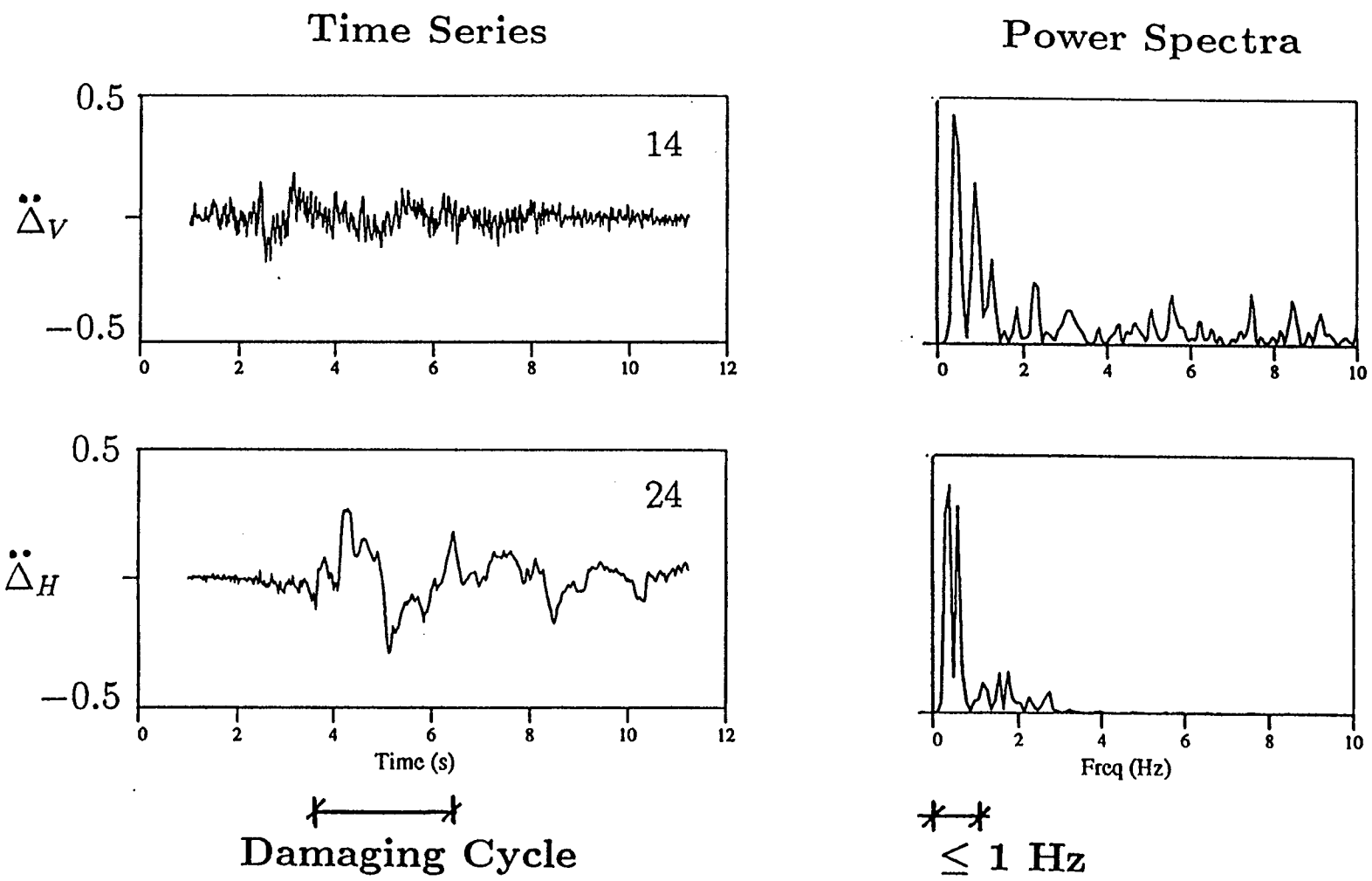


**FIGURE 4.3 IV79 Ground Motion Records 61 m from Central Pier**

material data are used directly in the fiber modeling and the property estimates serve as initial guides for the use in the DYNAFLOW modeling of the deck and foundation elements.

In (Werner, Beck, and Levine, 1987), two systems are identified which are designated Case 1 and Case 2. Case 1 uses motions at the abutments and the central pier footing as input motions and thus identifies a fixed base system. Case 2 uses motions at the embankments and the central pier footing as input motions and thus identifies a broader system with a limited amount of soil-structure interaction. The basic modal information identified are summarized in table 4-I.

**TABLE 4-I MRO Modal Data Identified from Seismic Records**
(Werner, Beck, and Levine, 1987)

| Mode No. | Freq. f (Hz) | Damp. $\xi$ | Mode Shape Description (Deck Behavior) |
|---|---|---|---|
| CASE 1 | | | |
| 1. | 3.72 | .066 | Torsion + Symmetric Transverse Bending |
| 2. | 4.74 | .066 | Symmetric Vertical Bending |
| CASE 2 | | | |
| 1. | 2.47 | .072 | Torsion + Symmetric Transverse Bending |
| 2. | 3.26 | .078 | Torsion + Symmetric Transverse Bending |
| 3. | 4.56 | .058 | Symmetric Vertical Bending |

In the next sections, the calibration of two DYNAFLOW models is discussed. The models correspond in effect to the two cases described above and will be designated the FIXED and SSI models, respectively. The FIXED model serves as the best estimate of response to the recorded seismic motions. The SSI model serves as the best predictive model for use with simulated motions. The need for the SSI model arises because the motion at the abutments involves propagation through the embankment soil which must be accounted for either in the structure model or the earthquake motion simulation model. The approach taken here is to incorporate the embankment effects in the structure model.

## 4.1 Fixed Base Model

The fixed base or FIXED model attempts to represent the mass and elastic stiffness distribution of the deck carefully using linear plate elements whose thickness is maintained in accord with the as-built drawings. The authors are of the opinion that this approach provides a more accurate representation of translational/rotatory inertia and flexural/torsional stiffness than the more common approach which lumps these properties using 3D beam elements. For example, in the latter approach, distortions of the box girder cross-section and membrane effects in the walls of the webs and flanges are neglected. Also, in the former approach, it is possible to visualize the torsional response and the interaction

of torsional and flexural deformation modes and to assess relative stiffness effects. This is not possible in the latter approach.

The mesh of plate elements used for the decks of both the FIXED and SSI models is shown in figure 4-4. Node point locations are selected to permit connectivity of the web elements with the two abutment end walls, the two intermediate diaphragms, and the pier cap. Four additional sets of node point locations are provided to allow changes in the thicknesses of the deck web elements adjacent to the abutments and the pier cap (see fig. 4-2). While the mesh may be viewed as coarse and the aspect ratio high for the purpose of computing stresses, it is stiffness that is of primary interest here.

Damage in the deck elements is not anticipated in this structure because of the integral connections and lack of any hinges. The plate material is, therefore, assumed to be linear, homogeneous, and isotropic with Young's modulus, $E$, taken to be some percentage of the Young's modulus for the concrete, $E_c$. The initial estimates of these percentages has been made so as to be consistent with estimates given in (Werner, Beck, and Levine, 1987) of cracked cross-section properties for a lumped beam model of the deck. The final selection serves as a free parameter for tuning the FIXED model to the CASE 1 frequencies.

The modeling of the column has been fundamentally guided by the fiber model developed for the NIST full-scale flexure specimen. The concrete fiber mesh shown in figure 4-4 is similar to the NIST specimen which has the same outside diameter and spiral transverse reinforcement. The effective confinement zone is slightly different, however, because of differences in the reinforcement detailing. The third column in table 3-I summarizes the geometric properties for the MRO central pier which may be compared to those for the NIST flexure and NZ column specimens. The L/$d$ ratio is seen to be smaller than the NIST specimen but about the same as the NZ specimen. The material properties are summarized in the third column of table 3-II along with those for the NIST flexure and NZ column specimens. The material curves are plotted in figure 4-5 to the same scale as figure 3-1. The same concrete behavior is observed except a slightly more conservative post-peak behavior is assumed. The steel is a lower grade than in the NIST specimen and thus has a lower yield strength.

An eigenvalue analysis was performed using the subspace iteration method available in DYNAFLOW (Prevost, 1996) to determine natural modes, natural frequencies, and modal participation factors. Table 4-II gives the results of the eigenvalue analysis for the FIXED model, and figure 4-6 shows the fundamental transverse and vertical mode shapes for the FIXED model. The agreement with frequencies in table 4-I is seen to be excellent and required little modification of the deck free parameter from the initial estimate.

A time history analysis was then performed using the tuned FIXED model with the mesh and properties described above. The recorded IV79 transverse (Nos. 6, 19, and 1) and vertical (Nos. 13, 3, and 2) motions were applied as inputs to the two abutments and the central pier footing. The longitudinal records were insufficient to represent the rotational motion at the abutments and were not used. The analysis consequently focuses on the transverse response which contributes the most to both the fundamental vibration mode and to the column flexural damage (see fig. 4-6). All 6-DOF of the nodes at the

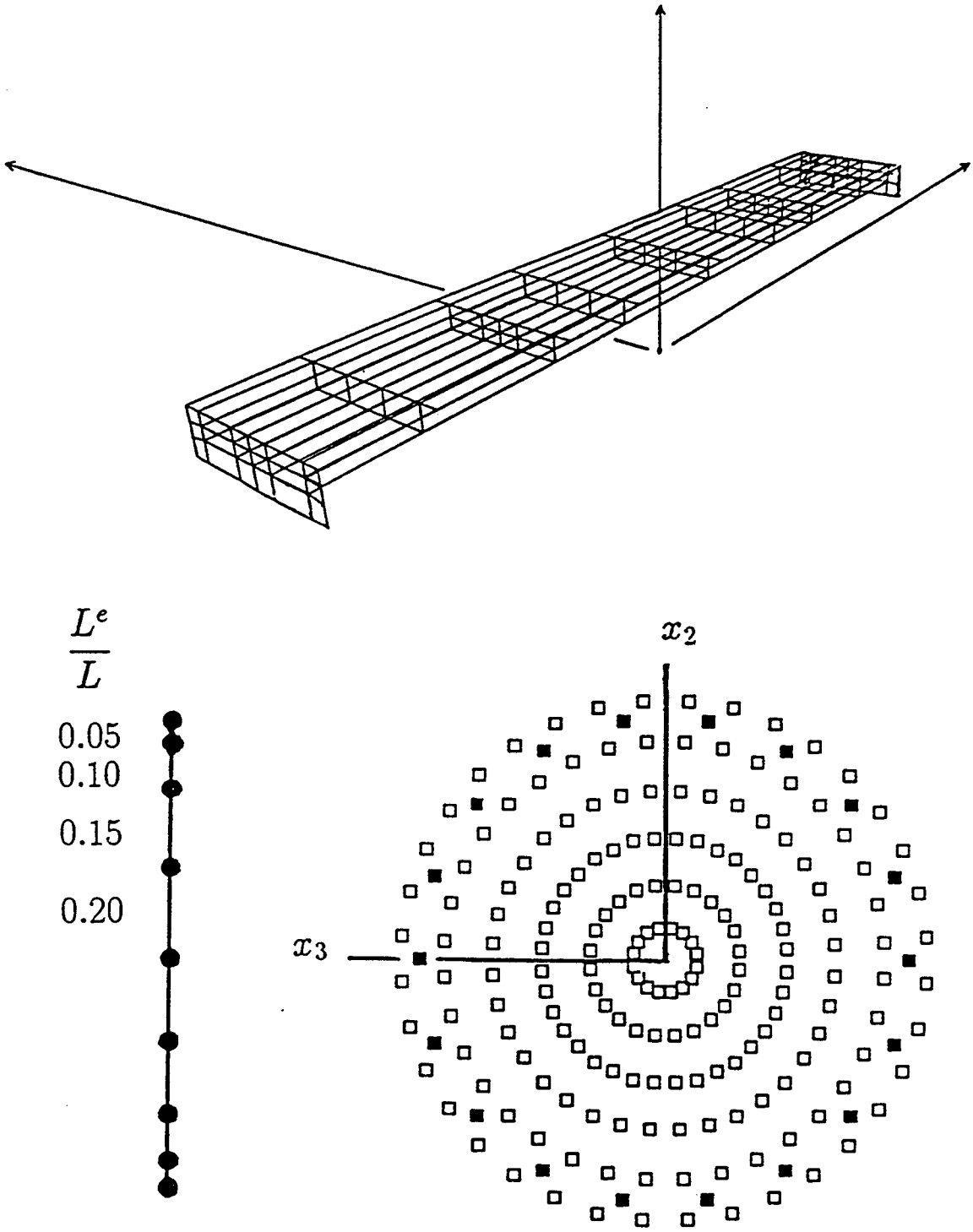


**FIGURE 4-4 DYNAFLOW fixed base model of MRO**

a) Concrete- MRO Central Pier

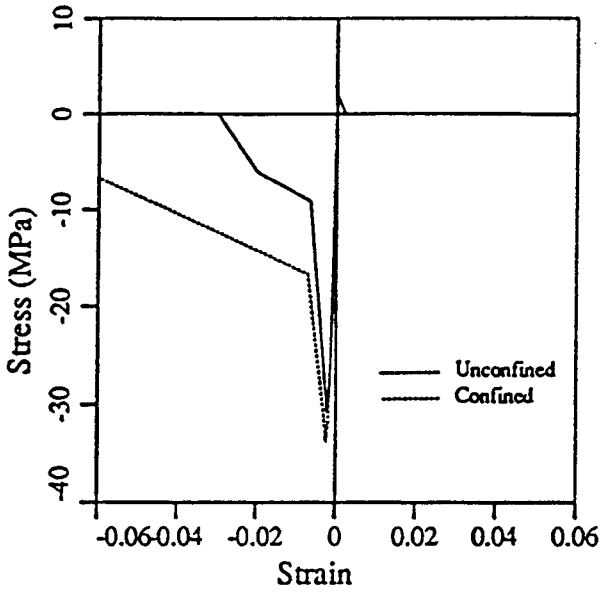


b) Steel- MRO Central Pier

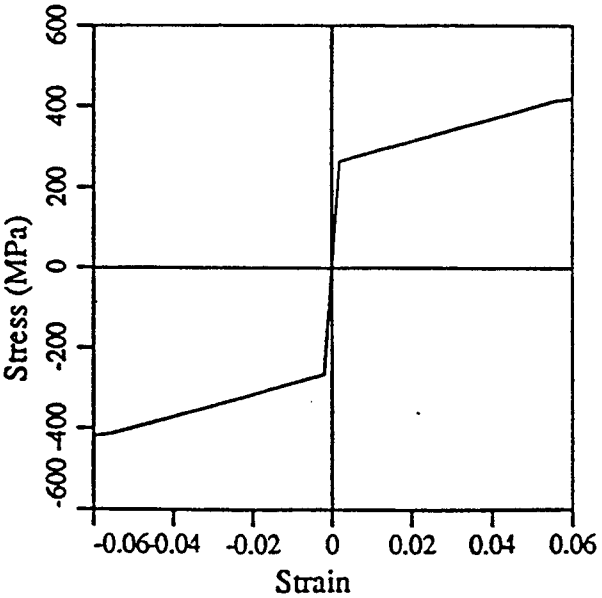


**FIGURE 4-5 MRO Central Pier Column: Material Curves**

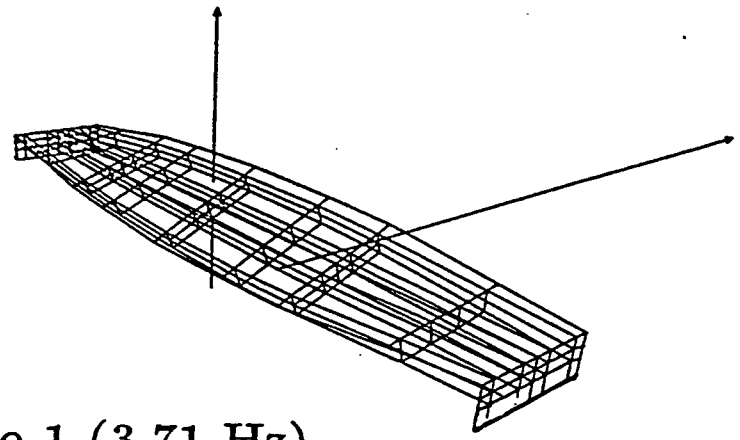

Mode 1 (3.71 Hz)

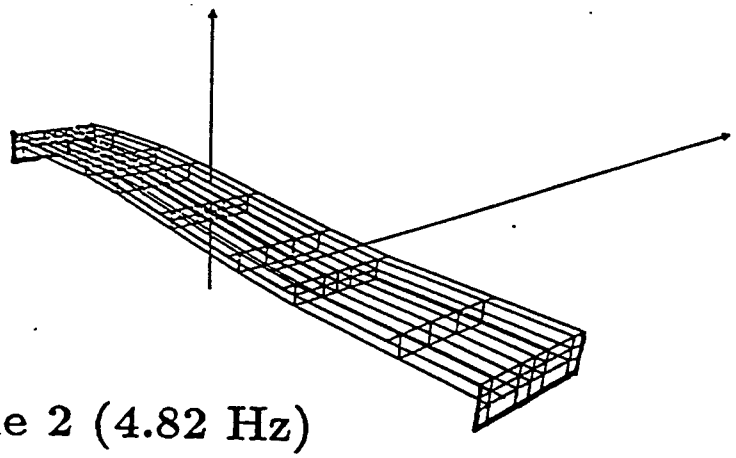

Mode 2 (4.82 Hz)

**FIGURE 4-6 FIXED Model: Fundamental Modeshapes**

abutment end walls and the pier footing were restrained. Integrated displacements supplied with the acceleration records were used as the inputs. These displacements were obtained using baseline corrections, because a very large relative displacement arises between the two abutments if uncorrected accelerations are used. This relative displacement if realized would have destroyed the bridge or foundation system and must be considered artificial. In addition, a low pass filter was applied to remove frequencies, f $\leq$ .1 Hz, from the displacements.

**TABLE 4-II Eigenvalue Analysis Results for MRO DYNAFLOW Models**

| Mode No. | Freq. f (Hz) | MPF[1] | Mode Shape Description (Deck Behavior) |
|---|---|---|---|
| FIXED | Model | | |
| 1. | 3.71 | 38.0 | Torsion + Symmetric Transverse Bending |
| 2. | 4.83 | 1.15 | Antisymmetric Vertical Bending |
| SSI | Model | | |
| 1. | 2.45 | 13.5 | Torsion + Symmetric Transverse Bending |
| 2. | 3.17 | 35.3 | Torsion + Symmetric Transverse Bending |
| 3. | 3.74 | 0.2 | Antisymmetric Vertical Bending |

[1] MPF= Modal Participation Factor

The peak response acceleration for the MRO during the IV79 occurred for record No. 7 which corresponds to the transverse translational acceleration, $\ddot{\Delta}$, at the deck level of the central pier location (see fig. 4-1). The computed time history is compared with the recorded one in figure 4-7 indicating an excellent agreement. The effect of torsional response of the deck on the actions at the top of the column can be seen by estimating the rotational acceleration, $\ddot{\theta}$, at the deck level of the central pier location. This is computed as shown in figure 4-7 using the difference of the two vertical translational accelerations on opposite sides of the deck and assuming small deformations. The computed time history is compared with the one derived from the records in figure 4-7 indicating reasonable agreement. The primary source of the remaining discrepancy is probably the lack of recorded motions at opposite sides of the abutment end wall which would permit a rotational motion to be input to the model at the abutments. Such motions would probably increase the computed ones at the central pier location and provide a better agreement.

As anticipated, the peak flexural response occurs at the base of the column of the central pier and the computed stresses in the deck elements remain very low. The computed axial force and transverse bending moment time histories for the FIXED model central pier column base are plotted in figure 4-8a. The axial force is normalized with respect to the dead load reaction, $N_0$= 5.34 MN, while the bending moment is normalized with respect to the maximum computed moment capacity, $M_u$= 10.75 MN-m. The peak flexural response

is seen to approach the flexural capacity during the period of strong motion.

The strains in the outer fibers provide indicators of peak material response. In the context of the fiber model, the key fiber responses are those of the unconfined concrete fibers at the edges of the gross section and the confined concrete and reinforcing steel fibers nearest the edges of the effective confinement zone in the direction of the maximum bending moment. In this case, the major bending occurs about the $X_3$ axis, so the key fibers lie on the $X_2$ axis. Figure 4-9 shows the computed stress-strain hysteresis of these key fibers. The concrete is seen to have undergone only one major cycle causing high compressive stresses. The material nonetheless did not develop any softening or post-peak response. The steel is seen to have undergone both compressive and tensile yielding, but the strains do not reach values likely to initiate low cycle fatigue or fracture.

Visual examinations reported by others indicate that the structure remained virtually undamaged by the IV79 event. It is clear, therefore, that major damage including significant crushing and opening of large cracks did not occur. Certainly collapse did not occur. Without actual strain measurements, it is difficult to assess precisely how accurate the computed predictions of damage are. While the computations clearly do not predict major damage, the authors cannot say whether the onset of yielding in some steel bars matches the visual observation reported by others. In summary, the authors find the calibration of mass and stiffness for moderately intense excitation to be adequate, if slightly conservative, for the prediction of nonlinear response and minor damage.

## 4.2 Soil-Structure Interaction Model

In order to predict moderate and severe damage to the MRO central pier column, the SSI model must be developed and calibrated relative to the FIXED model predictions and the CASE 2 frequencies. The approach taken in this work is to represent in an effective manner the dominant actions at the abutments which contribute significantly to the central pier column damage. Linear truss elements available in DYNAFLOW (Prevost, 1996) are used to model the lumped stiffness and Rayleigh damping at each DOF modeled except at the central pier footing where concentrated nodal stiffness elements are used for the rotational DOF. The truss elements allow for a grounding node to be defined at which acceleration time histories may be applied as inputs to the model. At the central pier recorded motions are available for the translational DOF at the top of the footing (see fig. 4-1), so truss elements are not needed. Concentrated nodal mass elements are used to model each embankment soil mass.

The behavior of the foundation system at the abutments and the interaction between the end wall, wing wall, footing, piles and the soil including the compacted fill between the wing walls and the the embankment soil is quite complex. For the purposes of this work, a simplified approach was adopted which attempted to model the effective 6-DOF actions of the foundation system about the center of rotation of the deck where it connects to the abutment end wall. The abutment end wall was assumed to interact with the large embankment mass only in the transverse translational DOF.

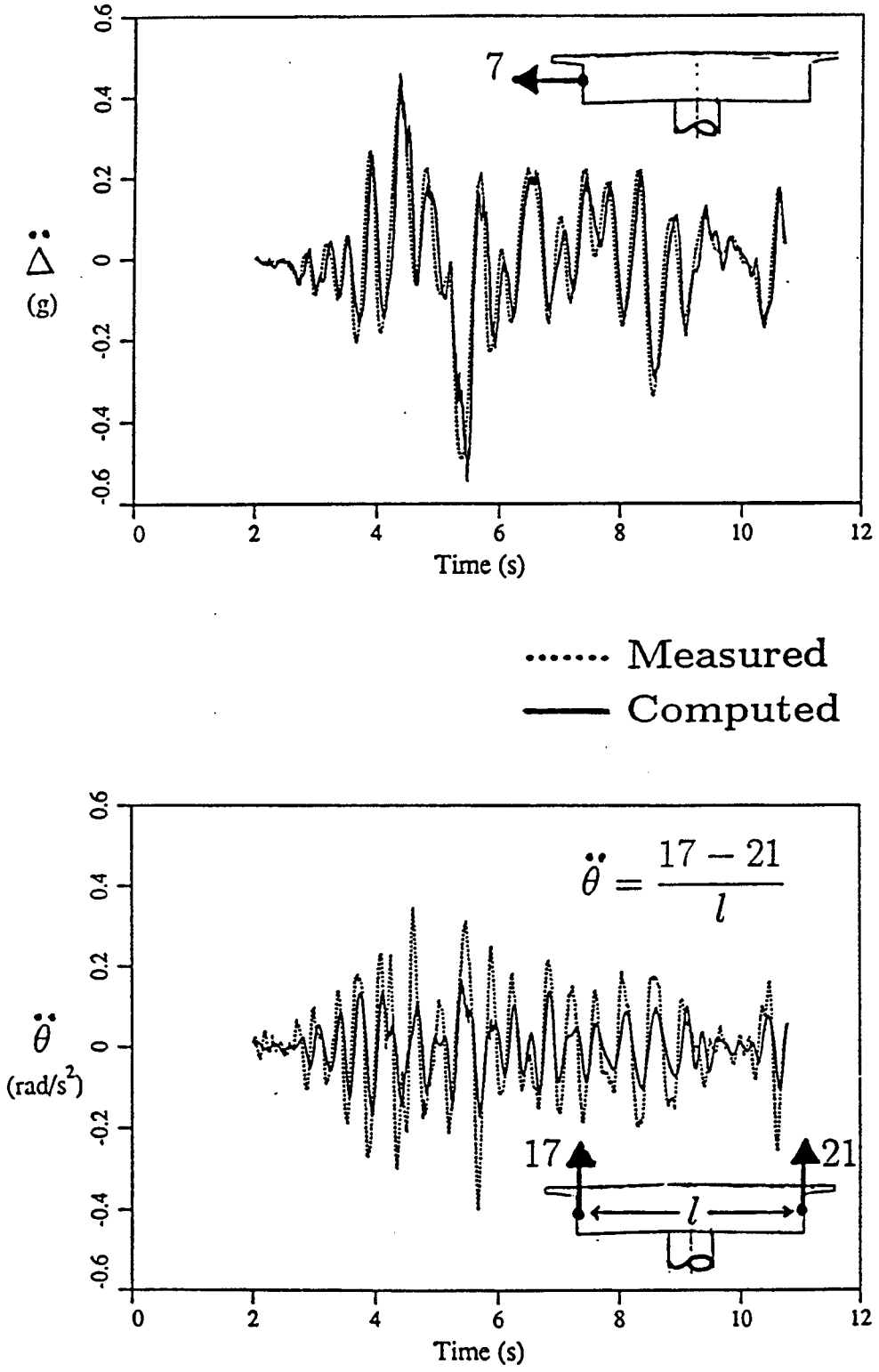


**FIGURE 4-7 FIXED Model: Deck Accelerations using IV79 Input Motions**

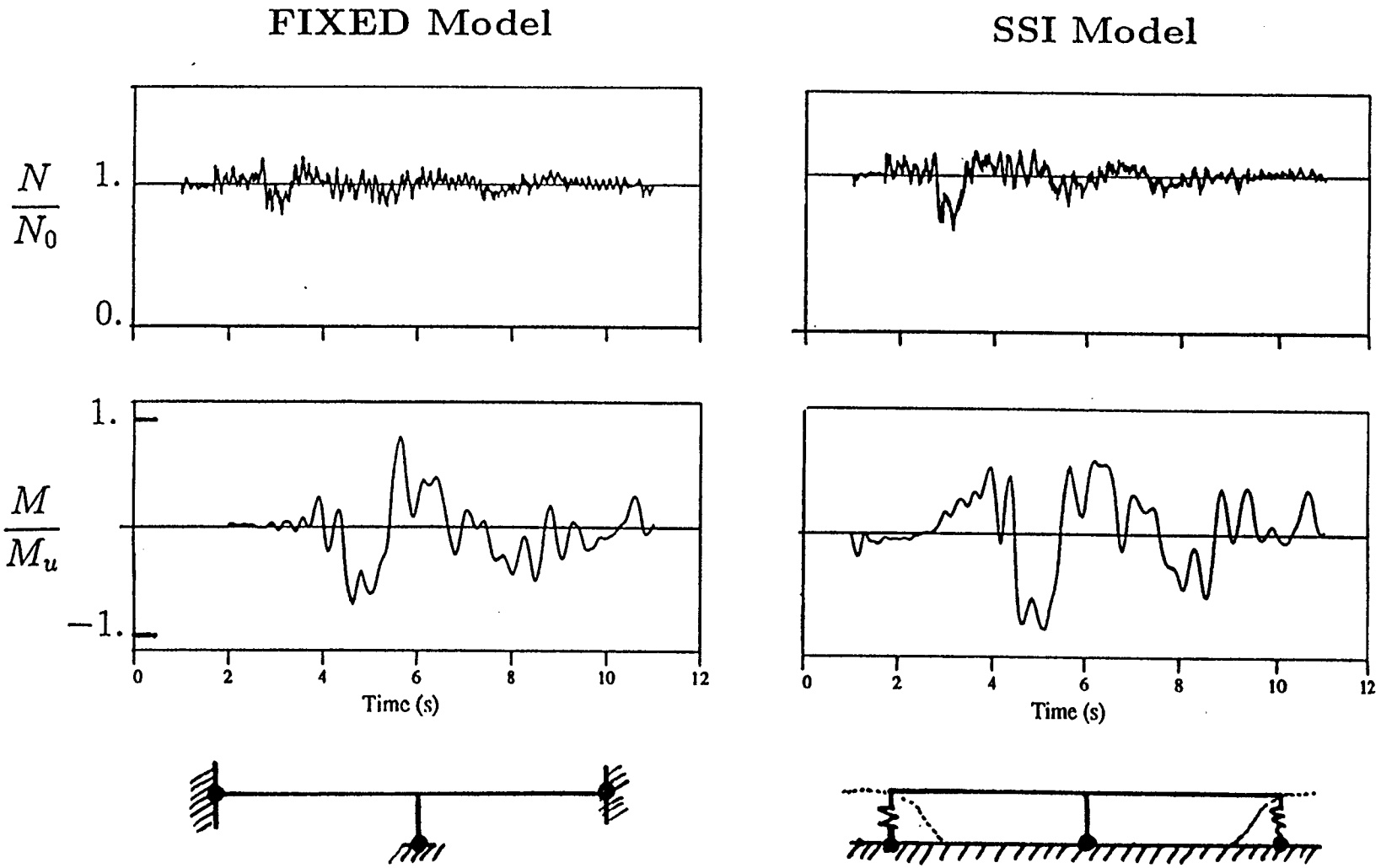


**FIGURE 4-8 Central Pier Column Base End Forces using IV79 Inputs**

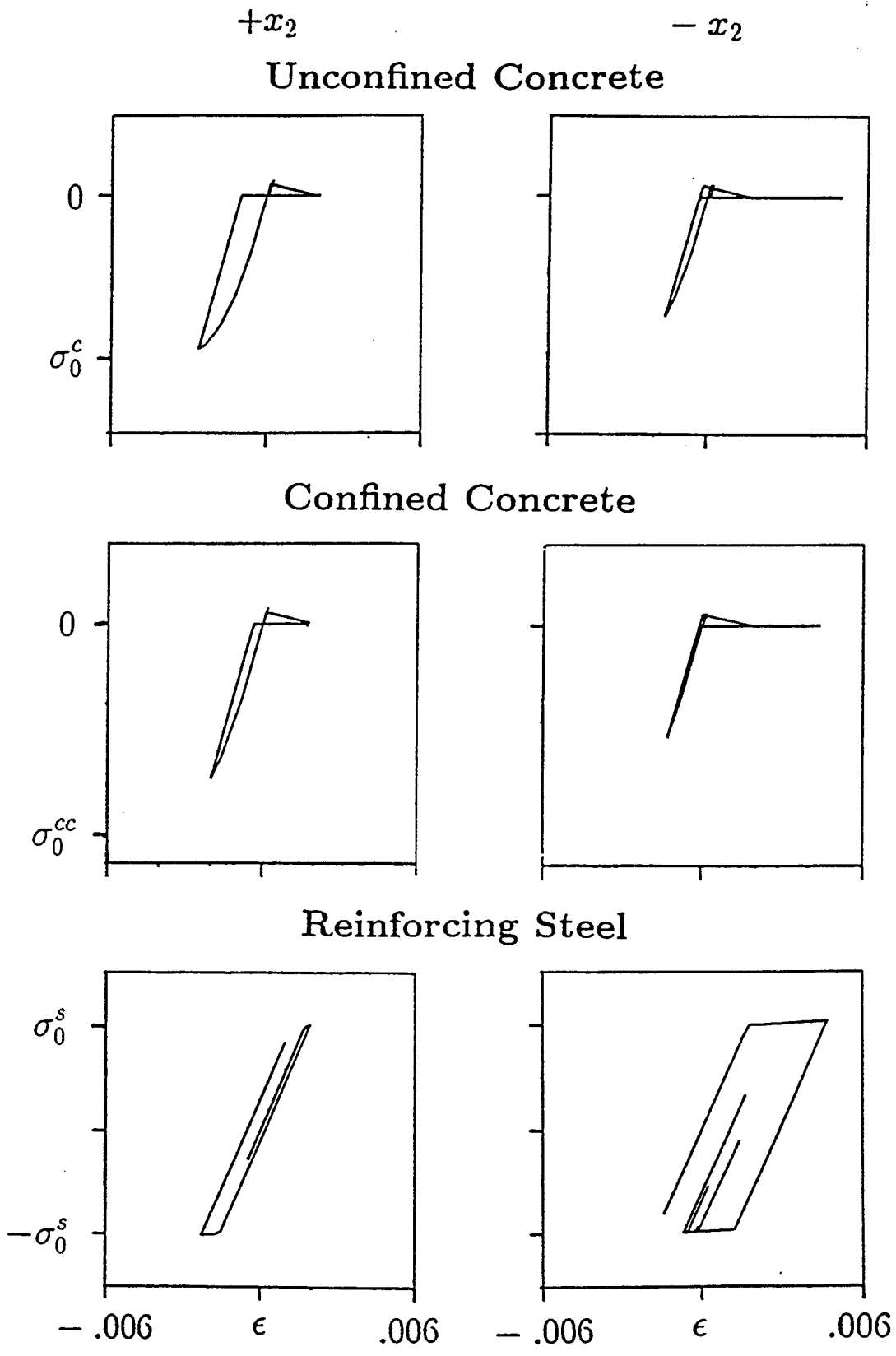


**FIGURE 4-9 FIXED Model: Extreme Fiber Material Hysteresis using IV79 Inputs**

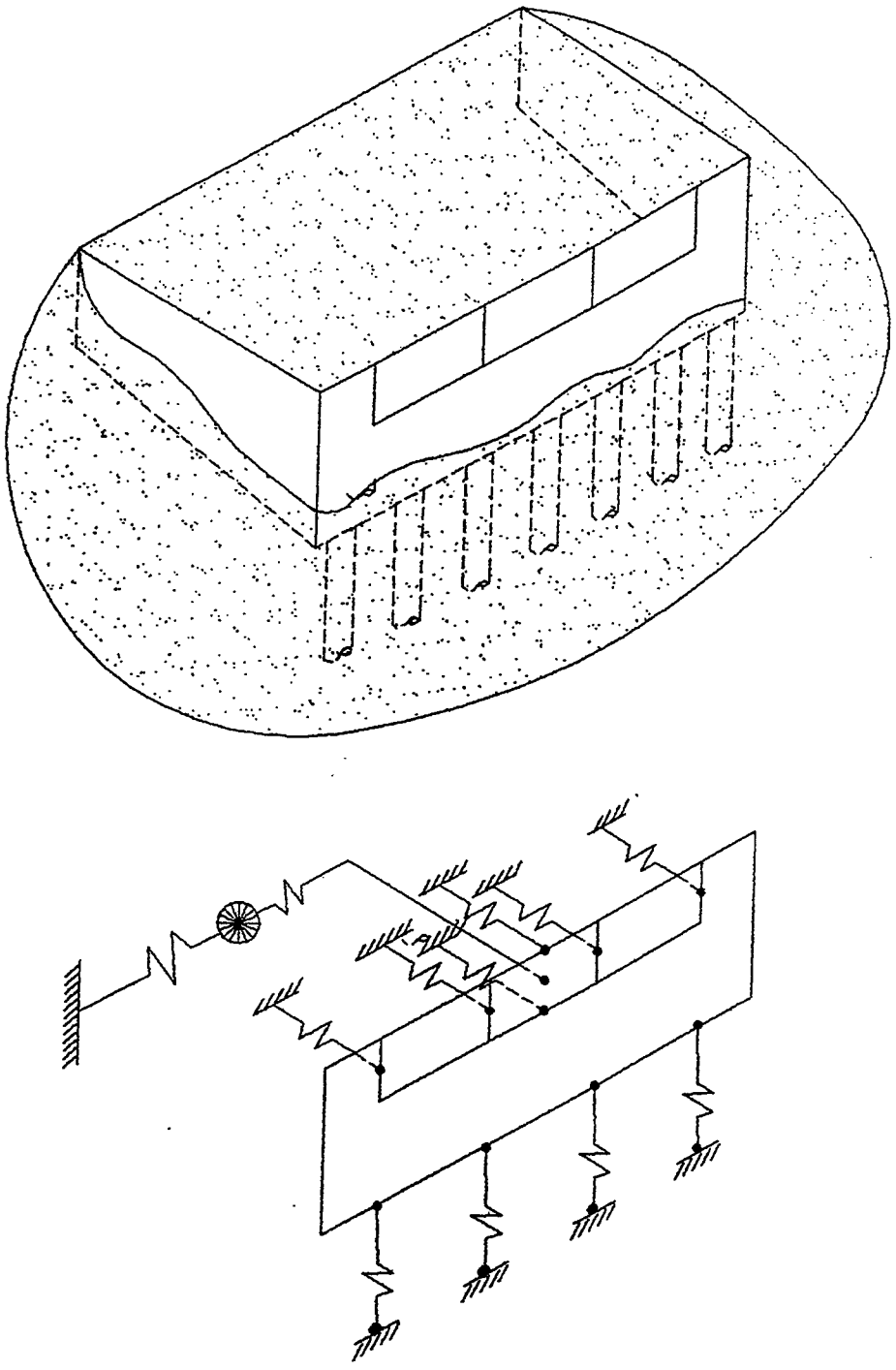

**FIGURE 4-10 SSI Model: Equivalent Spring System for Abutment Foundations**

Figure 4-10 shows the schematic idealization of the abutment end wall foundation system and the interaction with the embankment mass. The concentrated stiffnesses for the DOF at the center of rotation of the deck were distributed to the deck web positions assuming rigid body rotations. Thus, vertical stiffness and rotational stiffness associated with deck torsional motions were developed by a set of four vertical springs. Similarly, longitudinal stiffness and rotational stiffnesses associated with deck bending motions were developed by a set of six longitudinal springs. The transverse stiffness was completely lumped at the center of deck rotation and was connected in series to the large lumped embankment spring at the point of concentrated mass.

The initial properties of the lumped stiffnesses at the center of rotation were made based on two previous studies of an equivalent foundation system for the MRO. The first study (Levine and Scott, 1989) estimated rotational stiffnesses only. The second study (Werner, Crouse, Katafygiotis, and Beck, 1993) provided a wide range of rotational and transverse stiffnesses for the abutment system obtained by system identification of a beam model using the IV79 records.

The rotational stiffnesses associated with deck bending motions obtained in the Levine and Scott study were adopted for the SSI model. The rotational stiffness associated with deck torsion obtained in the Levine and Scott study was an order of magnitude less than the lower limit identified in the Werner et al. study, so the best estimate identified in the Werner et al. study was adopted. Longitudinal and vertical translational stiffness were estimated for the distributed springs using the above rotational stiffness and the assumption of rigid body rotations. The transverse translational stiffnesses of the abutment system identified in the Werner et al. study were adopted. Also adopted from the Werner et al. study were the transverse translational embankment mass and stiffness estimates which were based on a 2D representation of the embankment idealized as a trapezoidally shaped shear beam. Such an analysis approach was presented in (Wilson and Tan, 1990).

An eigenvalue analysis was performed for the SSI model with results listed in table 4-II and mode shapes plotted in figure 4-11. Excellent agreement with the Case 2 values listed in table 4-I was obtained for the transverse modes listed but an 18 percent difference was found for the vertical mode. This difference is associated with the vertical spring stiffnesses of the abutments which appear to be too soft. Tuning might be performed using these stiffnesses as free parameters, but the initial estimates were taken as being appropriate for this study.

Time history analysis was then performed using the IV79 input motions. In this case, the transverse and vertical acceleration records (Nos. 1 and 2) for the central pier top of footing were applied both to the column base and to the grounding points for the abutment springs. The vertical record was applied to the four vertical springs at each abutment end wall and the transverse record was applied to each embankment spring. For the SSI model any differential displacements at the abutments is associated with the dynamic response of the SSI model, so no preconditioning of the records was applied.

The computed axial force and transverse bending moment time histories for the SSI model central pier column base are plotted in figure 4-8b for comparison with the time

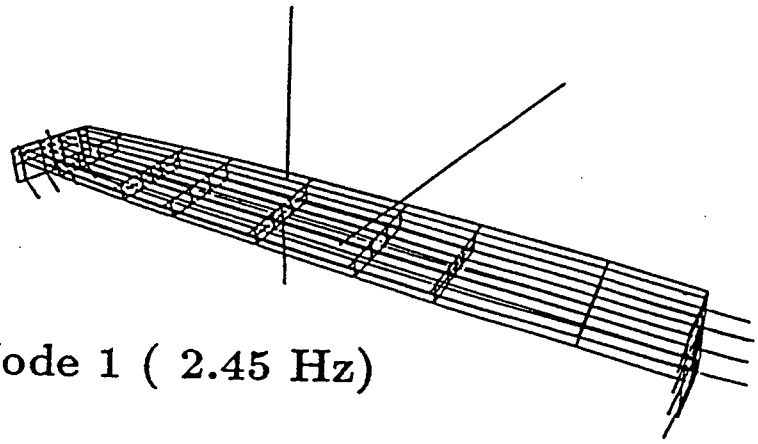

Mode 1 ( 2.45 Hz)

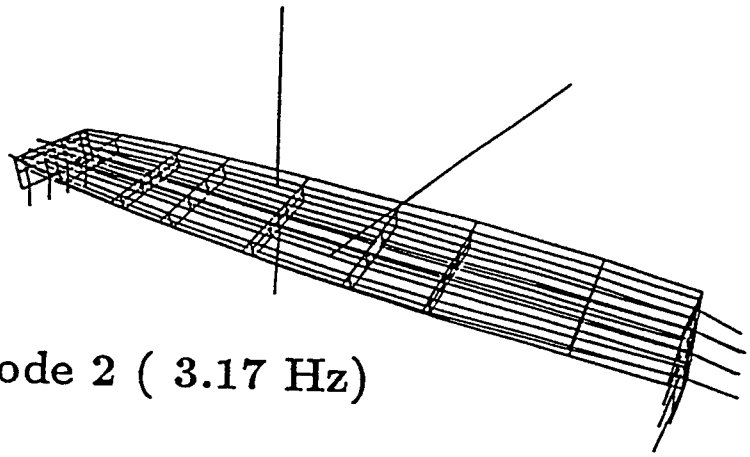

Mode 2 ( 3.17 Hz)

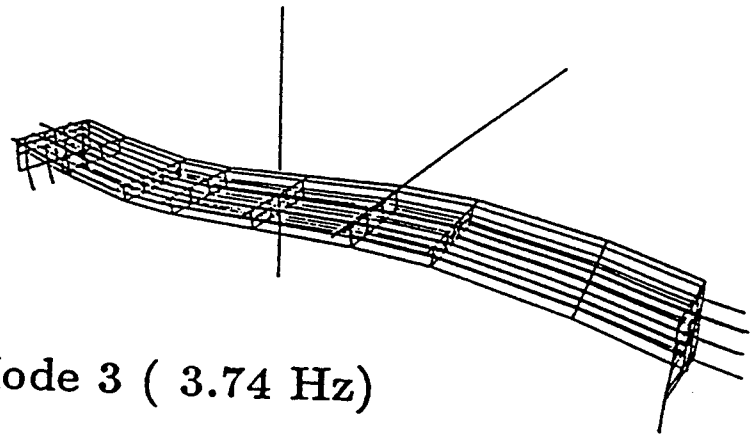

Mode 3 ( 3.74 Hz)

**FIGURE 4-11 SSI Model: Fundamental Modeshapes**

histories for the FIXED model. The basic characteristics of the response appear to have been captured adequately for the purposes of this work. In particular, the range of response during the strong motion appears to be the same magnitude. The calibration of the mass and stiffness for the SSI model is therefore considered adequate for the prediction of damage during simulated events whose motions can be applied as inputs in the same manner.

# SECTION 5
# SEISMIC FRAGILITY PREDICTIONS FOR A RC BRIDGE

The tendency of a structure to sustain damage during an intense seismic event is referred to as seismic fragility. Seismic fragility curves attempt to quantify this tendency based on classification of global system damage limit states, selection of seismic event intensity measures, and implementation of a probabilistic formulation of the relationship between damage and intensity.

The approach to fragility analysis adopted in this work is one in which the relationship between damage and intensity is obtained through numerical experiments that simulate the event motions and compute the damage responses using the nonlinear-dynamic time history analysis of the SSI model. The random nature of the relationship is considered by creating a finite number of realizations first of the system and then of the input motions. For the realizations of the system, the scaled IV79 record is used for the analysis. For the realizations of the ground motion, the calibrated SSI model is used for the analysis.

The random nature of the system is modeled by considering key parameters of the fiber model for the central pier column of the SSI model to be random variables. Multiple realizations of the system are obtained by taking random samples from simple probability distributions assigned to these variables.

The random nature of the input motions is modeled using an auto-regressive moving-average (ARMA) model to characterize an underlying stationary stochastic process. Non-stationarity is described using standard deviation and frequency envelope functions that are applied to the stationary series.

This basic approach to fragility analysis has been applied to building systems modeled as 1D hysteretic shear beams (Hwang and Jaw, 1990) and 2D hysteretic frames (Hwang and Huo, 1994; Singhal and Kiremidjian, 1995). The advantage of this approach is that, although the statistics and probabilistic description of the system must be considered a first order approximation, the damage response estimation can be made with as much detail and, presumably, accuracy as the model used in each simulation.

The authors are aware of only one attempt to construct fragility curves for a 3D highway bridge system. Ang and Kim (Ang and Kim, 1992) did so for a 3D curved bridge that collapsed during the 1971 San Fernando event. A global damage index approach is adopted and statistics of the damage index are computed analytically based on the solution of a set of nonlinear stochastic differential equations representing the dynamic response of a multi-DOF hysteretic model of assumed plastic hinge locations along the bridge. The probabilistic formulation is sufficiently advanced to provide an accurate estimation of the damage index statistics given the basic model of the system and excitation. However, the model of the structure system and nonlinear behavior is oversimplified to the point where the characterization of the damage response becomes the major uncertainty.

This study has considered two damage indices for use in fragility analysis of the 3D

MRO bridge system. The first is the maximum softening damage index (DiPasquale and Cakmak, 1990). This index was slightly redefined (DiPasquale and Cakmak, 1988) and shown to be the most reliable damage index for building structures in a comparison with other commonly proposed indices. The comparison was based on system identification analyses of both RC test frames and seismic records of actual RC buildings.

A simple method of computing this index using single input-single output (SISO) system identification of time series has been proposed by the authors (Mullen, Micaletti, and Cakmak, 1995) and was used to analyze the simulated responses. The computed indices were found to be very low and insensitive to increases in intensity. This was primarily a result of the modeling of the deck and foundation springs as elastic and nondegrading. In building structures, particularly ductile moment-resisting frames, damage tends to be distributed. The MRO model, and MRO superstructure in reality, do not permit such distributed damage.

A damage index that is more specifically related to the behavior of the column has, therefore, been considered. The index selected for consideration is similar to the one found to be the next most reliable index, the maximum (inter)story drift ratio, which is defined as the maximum relative displacement of the column ends normalized with respect to the building height. In this case there is only one "story".

This drift damage index was found to exhibit a clear relationship with intensity, and it is easy to compute using time history analysis. To delineate limit states for this measure, the peak compressive strains in the outer fibers are monitored and correlated to the nominal values of the index.

### 5.1 Random Sampling of System Random Variables

The calibration of the fiber model indicated that key variables affecting the predicted response include the set $E_c, E_s^*, \sigma_o^c, k_1, k_2, \epsilon^{cc}(.2 \cdot \sigma_o)$ which respectively govern the initial stiffness of concrete and steel, the peak strength of unconfined and confined concrete, and the post-peak strength and stiffness of the confined concrete.

For convenience, all variables were assumed to be uncorrelated. Each variable in the set $E_c, E_s^*, \sigma_o^c$ was assumed to be normally distributed with mean given by the calibration values and coefficient of variation, COV= .10. These two moments are sufficient to fully characterize the normal distribution. Negative values for the physical parameters are not permissible, so the normal distribution was truncated in the negative tail to preclude this possibility in the sample. The remaining variables, $k_1, k_2, \epsilon^{cc}(.2 \cdot \sigma_o)$ , were assumed to be uniformly distributed within a prescribed range of values. The two bounding values of each uniform variate are sufficient to fully prescribe the uniform distribution. Table 5-I summarizes the complete set of assigned distribution parameters.

A program SSI-MCRV was written to take a random sample for the basic set of random variables and the SSI model was modified to incorporate the new material curves associated with the random sample.

A random sample of size 30 was generated in this fashion. The first 10 were used

to obtain responses to the same IV79 records that were used in the SSI calibration. The second 10 were subjected to the IV79 records uniformly scaled by a factor of 2, and the third 10 were subjected to the IV79 records uniformly scaled by a factor of 3.

**TABLE 5-I Fiber Model Random Variable Parameters**

| Parameter | Units | Parameter 1 | Parameter 2 |
|---|---|---|---|
| Normal Variates | | Mean | Std. Dev. |
| $E_c$ | MPa | 28338 | 2833.8 |
| $E_s$ | MPa | 189190 | 18919. |
| $\sigma_o^c$ | MPa | 35.854 | 3.5854 |
| Uniform Variates | | Lowest | Highest |
| $k_1$ | | 1.1 | 1.5 |
| $k_2^{cc}$ | | .75 | .98 |
| $\epsilon^{cc}(.2 \cdot \sigma_o)$ | | .04 | .1 |

## 5.2 ARMA Generation of Random Seismic Ground Motion

The approach to generation of random ground motion time series adopted in this work follows the basic strategy used by Cakmak et al. (Cakmak, Sherif, and Ellis, 1985) for stabilization of a univariate nonstationary time series and the basic assumptions used by Ellis et al. (Ellis, Srinivasan, and Cakmak, 1990) for implementing a constrained ARMA simulation of a random time series given an amplitude and frequency modulating function.

This section explains the special considerations taken to ensure reasonable correspondence of simulated time series characteristics with those observed at the MRO site. Because the site is so close to a rupturing fault, the database used to establish relationships between the ARMA and envelope function parameters and physical variables relating to the earthquake intensity was felt to be unreliable for this site.

Of particular concern was the dominance of low frequency content, $.3 \leq f \leq .5$ Hz, indicated in figure 4-3. The parametric relations derived from the database in (Cakmak, Sherif, and Ellis, 1985) tend to predict a higher dominant frequency for this site. This problem has motivated the use of a more direct approach in which the modulating functions used in the simulations are taken from direct analysis of the IV79 records, specifically, the tranvserse component of motion for the instrument near the bridge (No. 24 in fig. 4-1, see also plot in fig. 4-3).

A set of 30 realizations was generated using the above procedure. Figure 5-1 shows two of the realizations of the stabilized series and the corresponding modulated nonstationary series. Each realization was applied to the SSI model used in the calibration study to obtain responses. The first 10 were used unmodified. The second 10 were uniformly scaled by a factor of 2 and the third 10 by a factor of 3.

### 5.3 Damage and Intensity Measures

A family of fragility curves may be constructed by considering a set of damage limit states. For each such limit state, i, the value of fragility, $P_f^{ij}$, is defined here as the conditional probability of exceeding the damage limit state, $\delta^i$, given an excitation of intensity, $I^j$. More formally,

$$\begin{aligned} P_f^{ij} &= P[\delta \geq \delta^i | I = I^j] \\ &= 1 - F^j(\delta^i) \end{aligned} \tag{5.1}$$

where

$F^j$ = Cumulative probability distribution for $\delta_i$ at intensity, j

For consistency with the fragility studies described earlier, PGA is adopted here as the measure of intensity.

Two measures of damage have been considered based on an evaluation (Rodriguez-Gomez and Cakmak, 1990) of several popular damage measures proposed for building structures. The evaluation was based on nonlinear-dynamic simulations performed on a lowrise RC building frame using a program similar to IDARC2D. The frame model was subjected to ground motions generated by the ARMA procedure in EQGEN (Ellis, Srinivasan, and Cakmak, 1990).

A first set of simulations was performed (DiPasquale and Cakmak, 1988) using the model subjected to a random sample of artificial input motions covering a range of PGA= .2 - 1.0 g. Each damage measure was calculated and used to classify the frame as collapsed or surviving. A second earthquake was then applied that caused collapse. The prediction made by each damage measure was evaluated in terms of whether the prediction was in fact collapse. The only measure to predict collapse without exception was the maximum softening damage index, $\delta_M$, (DiPasquale and Cakmak, 1988). The next best performance was obtained by the final softening damage index, $\delta_F$, (DiPasquale and Cakmak, 1988) and the maximum interstory drift measure (Sozen, 1981), each of which had only two false predictions. Since $\delta_F$ involves the same type of computation as $\delta_M$, it is not considered further here.

The $\delta_M$ for the SSI Model simulations was first computed using the the definition in (DiPasquale and Cakmak, 1988). The Moving Window Transfer Function (MWTF) approach (Mullen, Micaletti, and Cakmak, 1995) was applied to the computed time histories of response to estimate this index for the SSI model. The MWTF analysis showed that there is little sensitivity of $\delta_M$ to the intensity over the range applied in the simulations. This lack of sensitivity is attributed to the modeling of all elements except the column as linear. No possibility of a distribution of damage throughout the superstructure or foundation is, therefore, possible. The global response is thus essentially linear due to the relative stiffnesses of the column, deck, and foundation elements. While the linearity in the actual deck structure seems reasonable, the actual embankment stiffnesses will likely experience further softening under increasing intensities. The uncertainties in the foundation stiffnesses, however, did not warrant such refinement in this model.

The conclusion was drawn that an alternative measure of damage is appropriate in

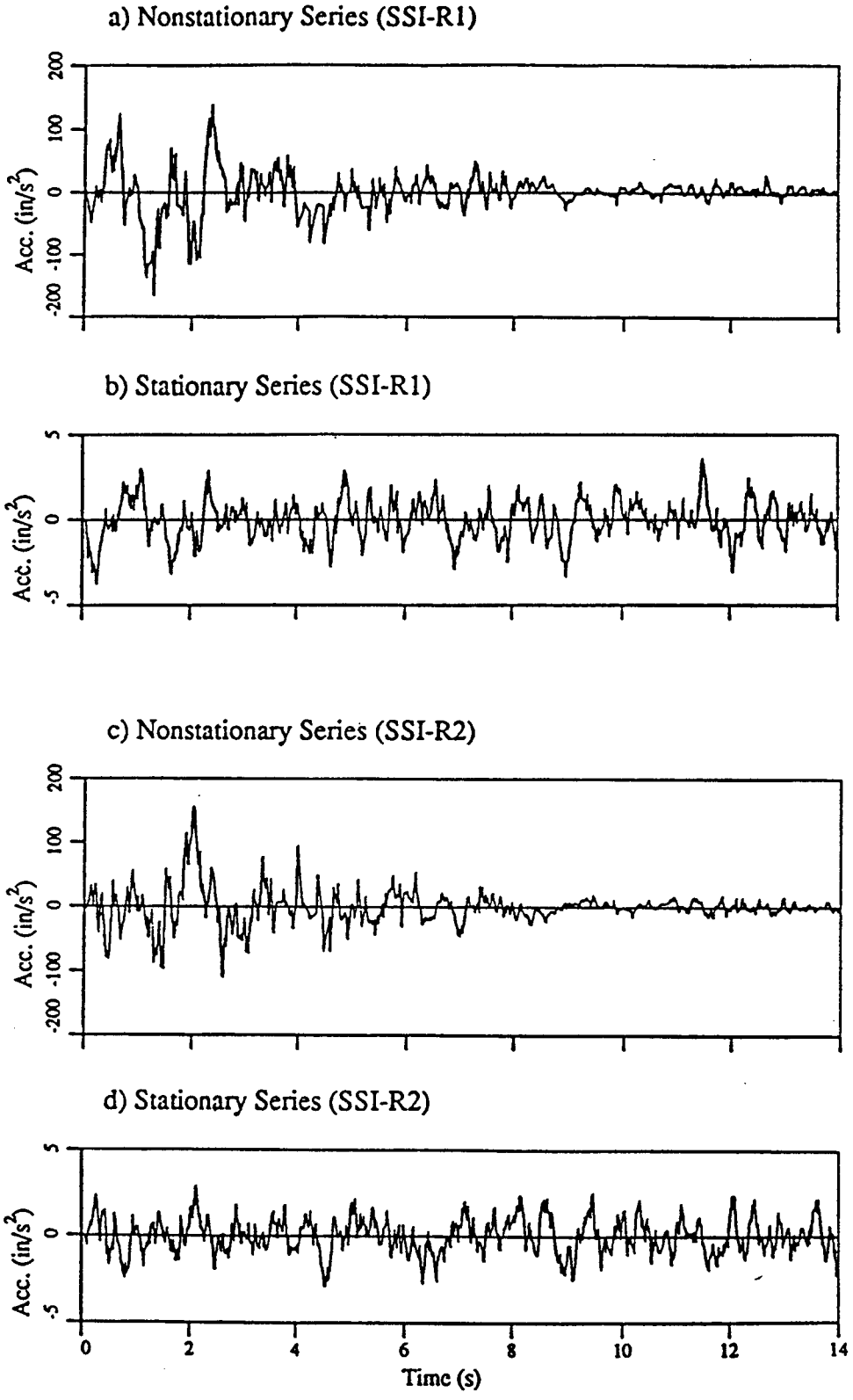


**FIGURE 5-1 Realizations of ARMA Generated Seismic Motions**

this case. The idea of the maximum interstory drift index which offerred the next best reliability in the study mentioned above has been examined for use in this analysis. Since the bridge does not have stories in the sense of a building, a comparable measure of damage is proposed.

Let $\Delta$ be the relative column end displacements in the transverse direction comparable to the $\Delta$ shown in figure 3-2 for a cantilever test specimen. A displacement damage measure comparable to maximum interstory drift is defined here by normalizing $\Delta$ with respect to the height of the column, $L$. Note in figure 3-2 that such a normalization gives an approximate rotation about the base for a cantilever or single curvature case.

The maximum interstory drift measure for buildings uses the height of the building as the normalizing parameter. The bridge here may be seen as a one story case of a building. The displacement-based or drift damage index used here is now defined more formally as:

$$\delta = \delta_\Delta = \frac{\Delta_M}{L} \tag{5.2}$$

where

$$\Delta_M = Max\{\Delta(t)\} \quad t \in \{0, \tau\}$$

This definition was applied to the simulated time histories and the computed indices were found to exhibit a clear relationship between damage and intensity. It has thus been adopted for use in this study.

The drift index, $\delta_\Delta$, is equivalent to the story drift ratio used by building design codes (International Congress of Building Officials, 1994, and Southern Building Code Congress International, Inc., 1994) to limit displacements of buildings during seismic events. The most recent recommendations (Building Seismic Safety Council, 1995) set an allowable limit for ductile systems in critical facilities with the highest seismic hazard exposure is presently a story drift of .01 or 1 percent.

## 5.4 Damage Limit States

A sample time history of the computed displacement, $\Delta(t)$, normalized with respect to the column height, $L = 6.36$ m (20.87 ft), is shown in figure 5-4. A very substantial value, $\delta_\Delta = .028$, is obtained for this case. The corresponding extreme fiber material hysteresis curves are shown in figure 5-5. These curves serve to define the severity of the damage in terms of material response.

At the top of figure 5-3, it is seen that the strength of the unconfined concrete has been completely lost on the negative $X_2$ face, implying severe spalling has taken place.

The confined concrete maintains reserve strength, but nonetheless has degraded significantly. The low strength and large compressive strain, $\epsilon^{cc} = .07$, indicates that severe crushing has probably taken place in the constituent mortar and/or aggregate phases of the concrete.

Finally, reinforcing steel has undergone several large cycles implying low cycle fatigue

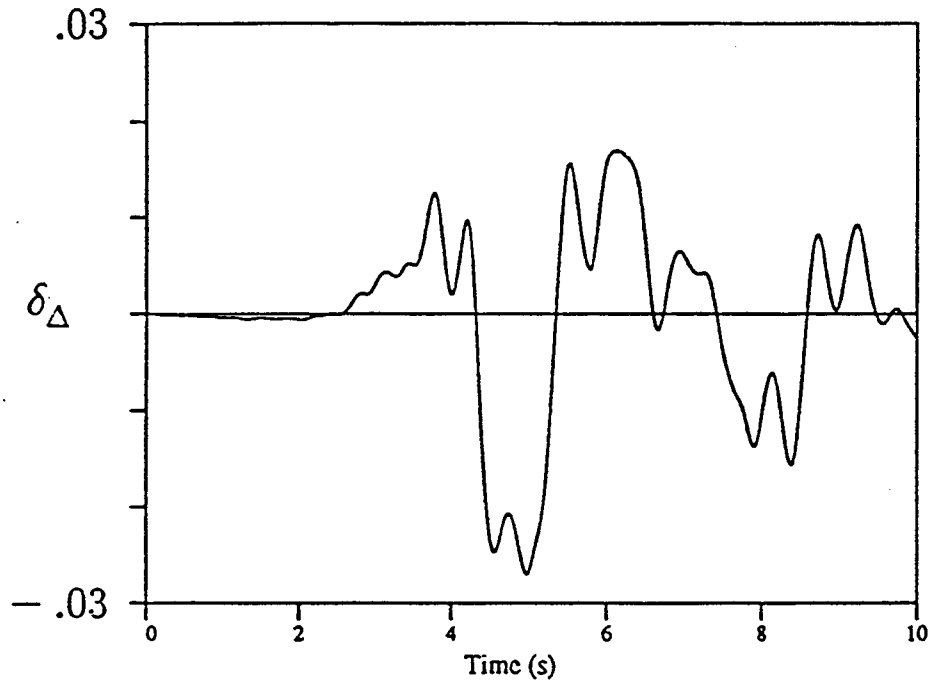


**FIGURE 5-2 SSI Model: Column Damage Time History, PGA= 1 g**

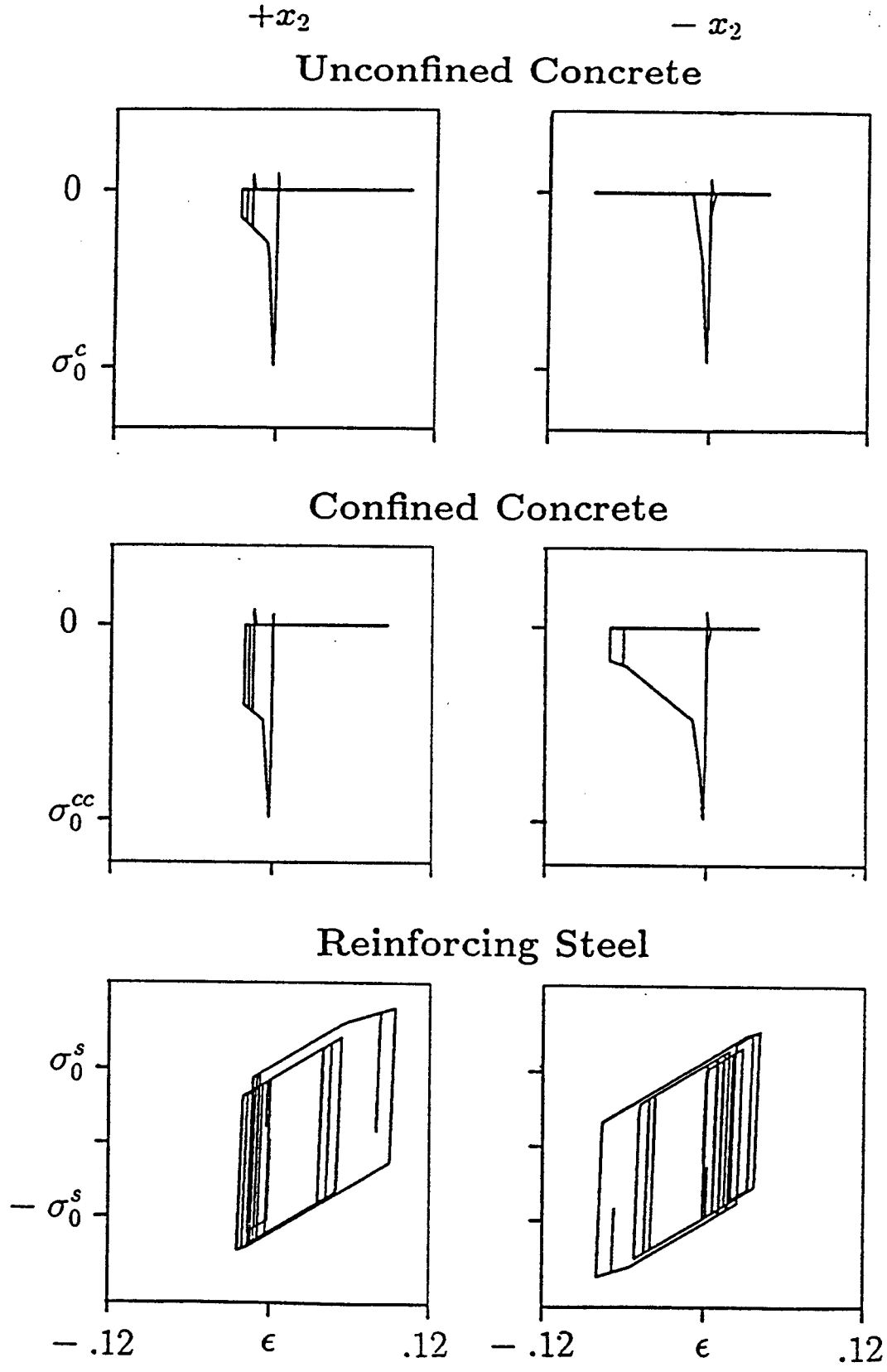


**FIGURE 5-3 SSI Model: Material Hysteresis Curves, PGA= 1 g**

may have been initiated. The near peak strength and large strain, $\epsilon^s = .1$, achieved on the positive $X_2$ face indicates that a fracture may have occurred in one of the bars.

By itself, spalling of the unconfined concrete does not pose a threat to the safety of the column and system. It nonetheless, represents damage that must be repaired, since corrosion may ensue in the reinforcing bars. Significant degradation of the confined concrete represents a potential threat to the column safety in the event of a strong aftershock or subsequent large event. This degradation probably occurs in combination with large strain cycles in the outer reinforcing bars implying the onset of low cycle fatigue. Finally, significant loss of the confined concrete strength and associated crushing phenomena as well as fracture of the reinforcing steel due to low cycle fatigue or simply overstraining could lead to collapse.

The random simulations described earlier are used to provide the necessary correlations between strain levels and displacement damage limit states for this bridge. Figure 5-4 shows the computed drift damage index, $\delta_\Delta$, as a function of PGA for the simulations. The results are plotted as solid squares for the case of the SSI model with random sampling of the fiber model variables using the measured record scaled to three different PGA values. The results are plotted as open squares for the case of the calibrated SSI model subjected to random input motion having scaled standard deviation envelopes. The variation associated with the fiber model variables is negligible in comparison to that associated with the random input motion.

A minimum least squares linear regression analysis of the random input motion results using a standard statistical program (SPLUS, 1995) provides the following relationship between drift damage and PGA intensity.

$$\delta_\Delta = -0.0026909 + 0.027328 * PGA \tag{5.3}$$

This expression is plotted in figure 5-5 along with the random input motion results.

Table 5-II summarizes the random input motion results sorted in order of increasing $\delta_\Delta$ . For reference, the corresponding values are provided for the peak compressive strains obtained in the extreme unconfined and confined fibers of the column base considering both positive and negative $X_2$ faces. Also listed are the estimated peak displacement ductilities, $\mu = \Delta_M/\Delta_Y$, based on the fiber model estimate of the first steel yield displacement of approximately, $\Delta_Y = .0254$ m (1 in). By virtue of this estimate, the numerical value of the ductility is identical to that of $\Delta_M$ when it is expressed in inches.

By considering the fiber model parameters in the third column of table 3-II and material curves plotted in figure 4-5, it possible to classify the limit states for the displacement damage according to the nominal index values listed in table 5-III. The value for severe damage of $\delta_\Delta = .016$ is close to the value of interstory drift of .02 which is considered to be a severe damage limit state for buildings.

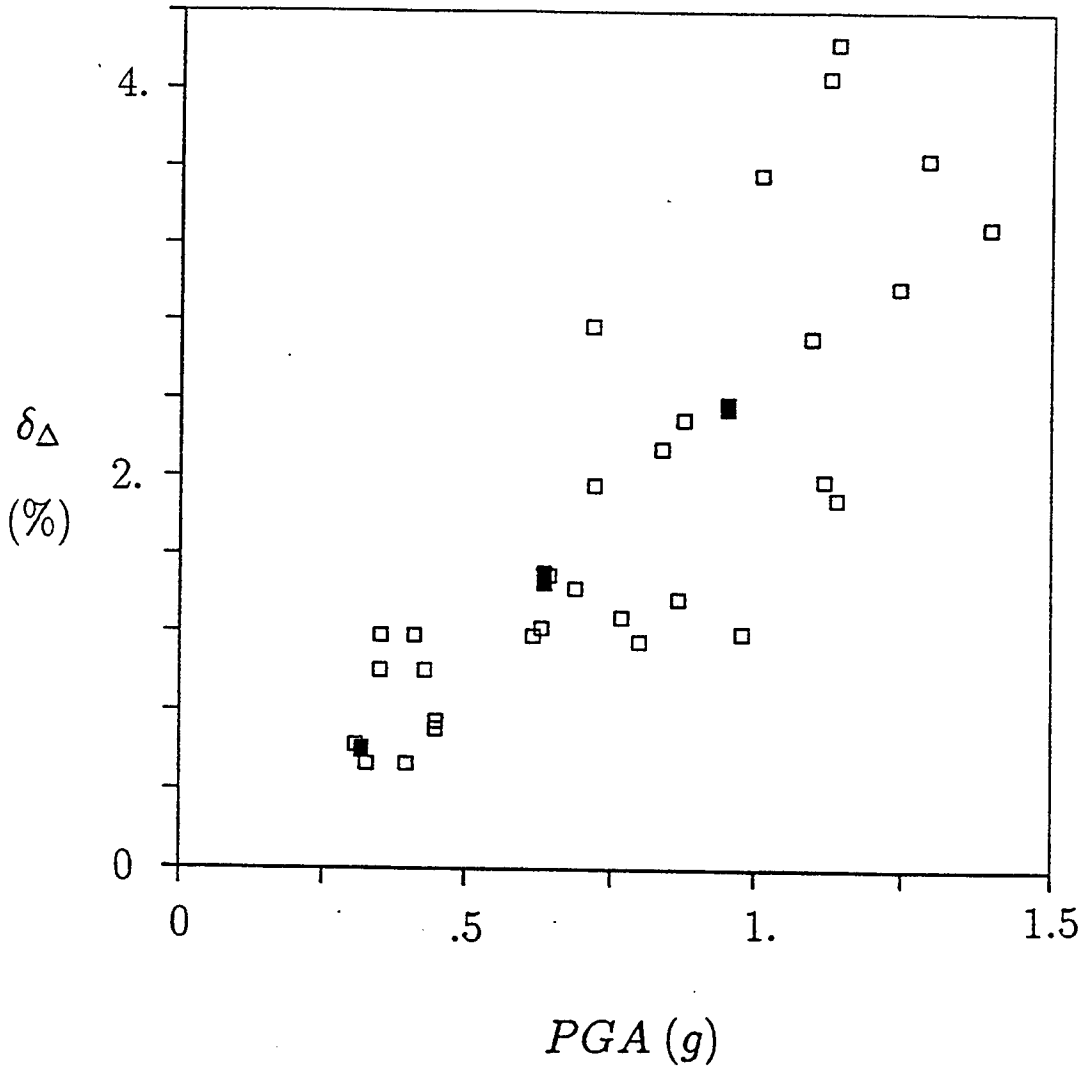


**FIGURE 5-4 SSI Model: Column Damage, Random Simulations**

**TABLE 5-II Drift Damage for Random Input Simulations**

| PGA (g) | $\mu$ | $\delta_\Delta$ (%) | $\lvert\epsilon_M^{cc}\rvert$ (%) | $\lvert\epsilon_M^{c}\rvert$ (%) |
|---|---|---|---|---|
| .397 | 1.32 | .5271 | .151 | .199 |
| .327 | 1.33 | .5311 | .157 | .202 |
| .308 | 1.56 | .6229 | .169 | .236 |
| .448 | 1.77 | .7068 | .234 | .335 |
| .449 | 1.86 | .7427 | .243 | .354 |
| .350 | 2.50 | .9982 | 1.54 | 1.89 |
| .429 | 2.52 | 1.006 | .421 | .619 |
| .799 | 2.90 | 1.158 | 2.32 | 2.81 |
| .351 | 2.95 | 1.178 | .595 | .876 |
| .410 | 2.95 | 1.178 | .650 | .928 |
| .615 | 2.95 | 1.178 | 2.21 | 2.70 |
| .978 | 2.98 | 1.214 | 2.28 | 2.77 |
| .630 | 3.04 | 1.214 | 2.41 | 2.92 |
| .767 | 3.20 | 1.278 | 2.69 | 3.25 |
| .867 | 3.42 | 1.366 | .969 | 1.34 |
| .688 | 3.58 | 1.420 | 3.43 | 4.13 |
| .642 | 3.72 | 1.485 | .952 | 1.35 |
| 1.14 | 4.71 | 1.881 | 5.07 | 6.09 |
| .721 | 4.90 | 1.957 | 2.74 | 3.29 |
| 1.12 | 4.97 | 1.985 | 15.6 | 18.4 |
| .838 | 5.38 | 2.148 | 1.58 | 2.21 |
| .875 | 5.75 | 2.296 | 5.54 | 6.64 |
| 1.10 | 6.78 | 2.707 | 1.80 | 2.53 |
| .716 | 6.91 | 2.759 | 9.33 | 11.1 |
| 1.24 | 7.42 | 2.963 | 6.27 | 7.50 |
| 1.40 | 8.22 | 3.282 | 2.72 | 3.68 |
| 1.01 | 8.89 | 3.550 | 1.83 | 2.67 |
| 1.29 | 9.09 | 3.630 | 6.40 | 7.64 |
| 1.12 | 10.2 | 4.073 | 13.7 | 16.1 |
| 1.14 | 10.6 | 4.233 | 2.57 | 3.69 |

**TABLE 5-III Nominal Damage Limit State Classifications**

| i | $\delta_\Delta$ (%) | Classification | Material Damage Behavior |
|---|---|---|---|
| 1 | .4 | Light Damage | Moderate Unconfined Concrete Degradation |
| 2 | .8 | Minor Damage | Moderate Confined Concrete Degradation |
| 3 | 1.2 | Moderate Damage | Severe Confined Concrete Degradation |
| 4 | $\geq$ 1.6 | Severe Damage | Confined Concrete Crushing; Bar Fractures |

## 5.5 Predicted Fragility Curves for the MRO

Equation (5.1) has been applied to the data in table 5-II to obtain fragility curves corresponding to the limit states defined in table 5-III. A normal distribution truncated below zero has been assigned to the damage measure, $\delta_\Delta$, based on the simulation results. The statistical package (SPLUS, 1995) was used to develop a routine for evaluating (5.1). It as been assumed that:

1. The linear regression result in (5.3) defines a mean damage versus intensity relation of the form,

$$m_\delta = A + B * m_I \tag{5.4}$$

2. The residual standard deviation, $\sigma_\delta^2$, provides a suitable estimator for the standard deviation, $\sigma_\delta(I)$, at all intensities, I, generated by the simulations, namely, $I_{PGA}$= [.3, 1.4 ]g.

The predicted fragility curves are presented in figure 5-6. Examining a single value of fragility, e. g. $P_f^{ij} = .5$, it is seen that PGA= .4, .55, .7, 1. g are required to achieve Light, Minor, Moderate, and Severe damage limit states, respectively. These fragilities are difficult to assess based on one set of simulations on one bridge, but nonetheless seem to indicate a rather sturdy construction. This observation is certainly in agreement with the bridge's performance in past seismic events.

## 5.6 Predicted Curves for Varying Span Lengths

A sensitivity analysis has been performed to study the effect of the central pier-to-abutment span length of the bridge on the fragility. In order to provide information useful to the design community, the corresponding changes in other superstructure dimensions have been considered in the modeling. In particular, the geometric dimensions recommended by California Department of Transportation (CalTrans) designers (Gates, 1996) were incorporated for:

1. Deck depth-to-span ratio, $R_d$= .055
2. Deck depth-to-column diameter, $R_c$= .95

Consideration was also given to the range of spans thought to be practical by Cal-

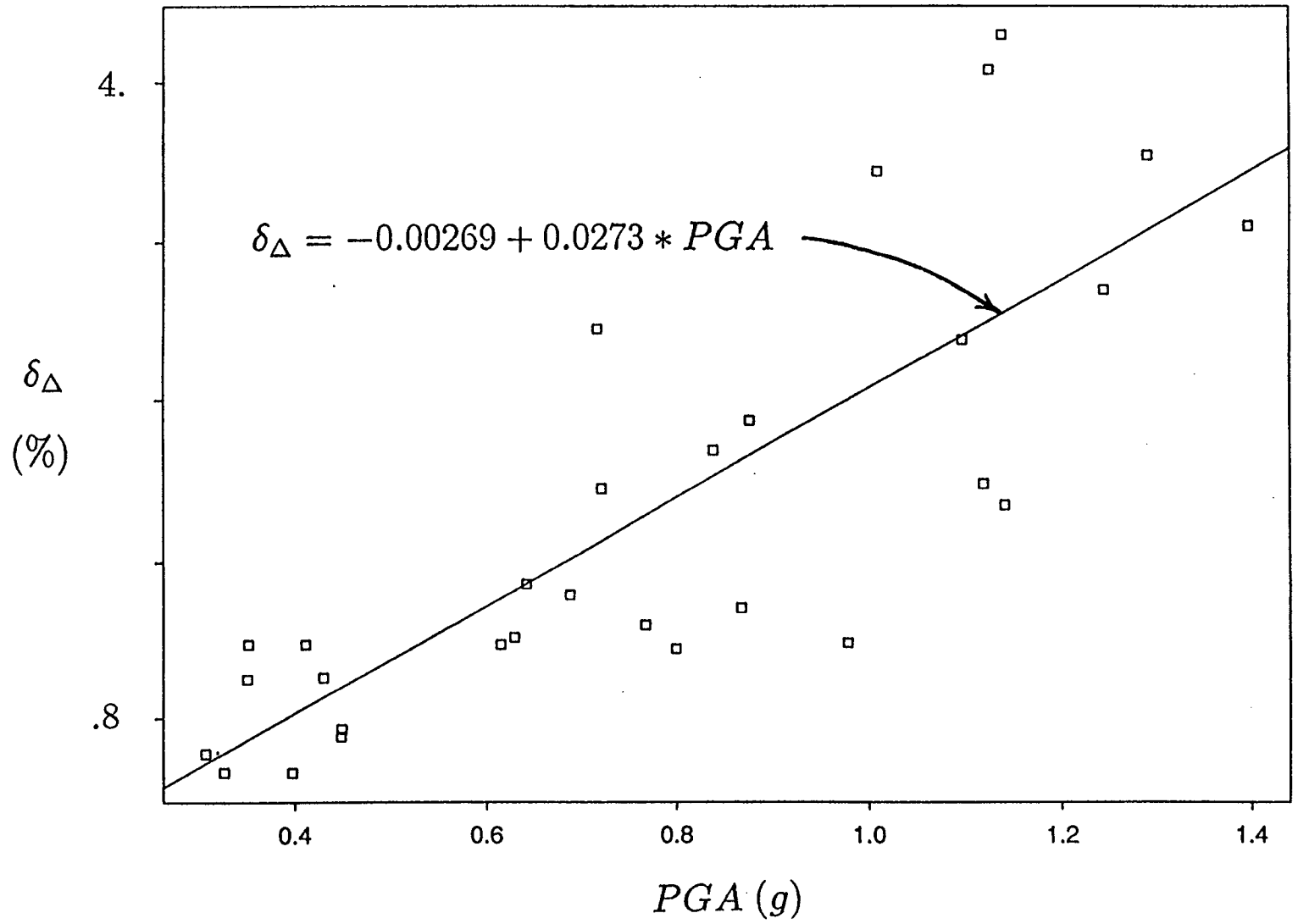


**FIGURE 5-5 SSI Model: Damage-Intensity Regression**

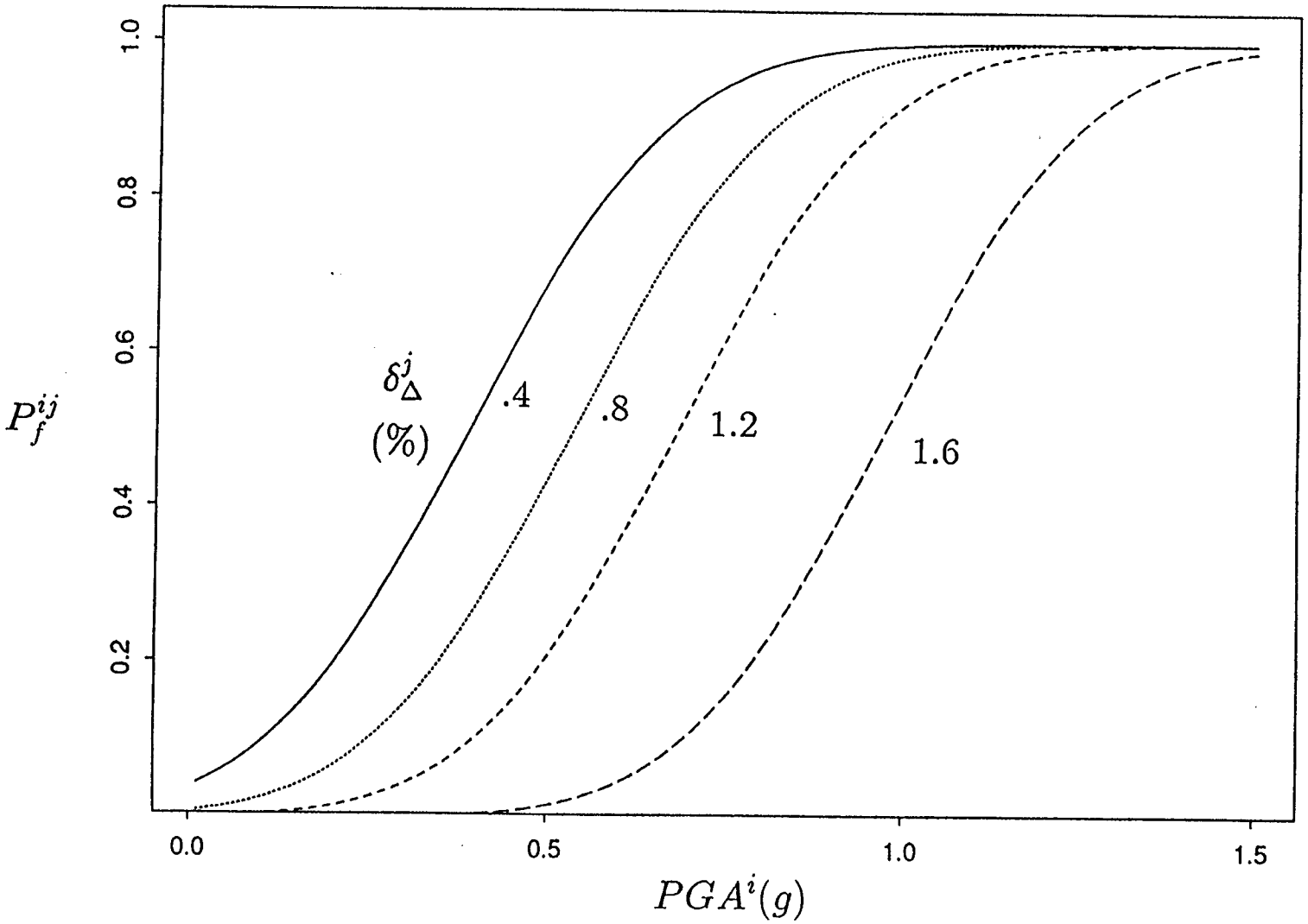


**FIGURE 5-6 SSI Model: Fragility Curves**

Trans designers for the MRO type of construction. The common range of spans for non-prestressed reinforced concrete hollow-box multi-cell decks was 50-120 ft (Gates, 1996). The nominal span for the MRO is 100 ft. To provide a convenient set of spans for the modeling, four additional DYNAFLOW models were constructed with spans of 50, 75, 125, and 150 ft, respectively.

Each of the four models was subjected to twenty (20) input time history motions. The motions were the same as in Runs 11-30 of the SSI model. The drift damage index defined in (5.2) was computed for each of the simulated response time histories. The indices are summarized in table 5-IV which lists the results in order of increasing PGA of the input motion. Regressions of the form given in (5.3) were performed based on each set of 20 simulations. A mean damage-intensity relationship of the form given in (5.4) was then obtained for each span length. The parameters of these relations are summarized in table 5-V. It should be noted that the parameters in table 5-V for the 100 ft case include only the Runs 11-30 and are therefore different than those in (5.3). Both the indices and the regression lines are plotted in figure 5-7 for each span length.

Fragility curves were calculated for the various span lengths using the procedure described in Section 5.4 above. The computed curves are plotted in figure 5-8 for each span length. Again, considering a single value, $P_f^{ij} = .5$, it is seen that PGA= 1.14, .76, .57, .53, .56 g are required to achieve a Moderate damage limit state for the spans of 50, 75, 100, 125, 150 ft, respectively.

Examining table 5-IV for a particular simulation, it is clear that the drift damage increases monotonically with increasing span with only a few exceptions. In a few cases, no solution was achieved, but the trend with span length is nonetheless clear for these instances. These cases usually involved very large drifts (in excess of 4 percent).

The trend of increasing drift with PGA is clearly not monotonic for a particular span length, i. e. model. There is significant scatter which is the justification for a probabilistic approach here. Nonetheless, the mean behavior as exhibited by the plots in figure 5-7 and the positive slope parameter, B, of the regression lines given in table 5-V. The slope parameter also confirms the trend of increasing drift with increasing span length. The variability or scatter increases as well with increasing span length as indicated by the standard deviation parameter, $\sigma_\delta^o$, in table 5-V. The coefficient of variation at a given intensity level may be estimated using:

$$V(I) = \frac{\sigma}{m_I} \approx \frac{\sigma_\delta^o}{(A + B \cdot I)} \tag{5.5}$$

This measure of variability evaluated at the value of I= .8 g, shows increases of .24, .35, .42,, .43, .55, respectively, with increasing span.

**TABLE 5-IV Drift Damage for Various Span Lengths**

| Run | PGA | Span (ft) | | | | |
|---|---|---|---|---|---|---|
| | g | 50 | 75 | 100 | 125 | 150 |
| 18 | 0.6152 | 0.5910 | 0.7786 | 1.1779 | 1.3736 | 1.3416 |
| 15 | 0.6296 | 0.6948 | 0.7587 | 1.2139 | 1.3576 | 1.3177 |
| 16 | 0.6422 | 0.7147 | 1.0382 | 1.4854 | 1.7968 | 1.9046 |
| 17 | 0.7165 | 1.0861 | 1.8168 | 2.7591 | 3.3701 | 3.9051 |
| 13 | 0.7206 | 0.8345 | 1.2378 | 1.9566 | 2.3958 | 2.6753 |
| 14 | 0.7674 | 0.7371 | 1.0062 | 1.2778 | 1.2658 | 1.1180 |
| 20 | 0.7993 | 0.6908 | 0.7627 | 1.1580 | 1.3137 | 1.2179 |
| 19 | 0.8379 | 1.0102 | 1.4415 | 2.1482 | 2.7751 | 3.2355 |
| 12 | 0.8670 | 0.6349 | 0.9623 | 1.3656 | 1.6211 | 1.7968 |
| 29 | 0.8755 | 1.0382 | 1.5054 | 2.2960 | 2.8071 | 3.1345 |
| 11 | 0.9776 | 0.6788 | 0.9503 | 1.1899 | 1.2817 | 1.2418 |
| 25 | 1.0091 | 1.1819 | 2.0604 | 3.5498 | 4.5680 | 5.2108 |
| 23 | 1.0967 | 0.9352 | 1.7341 | 2.7084 | 3.1760 | 3.3689 |
| 22 | 1.1186 | * | 2.8909 | 4.7277 | * | 7.0716 |
| 28 | 1.1245 | 1.6012 | 2.4557 | 4.0569 | * | * |
| 21 | 1.1383 | * | 2.4756 | 4.2326 | 5.8697 | 7.1075 |
| 26 | 1.1405 | 1.0741 | 1.3935 | 1.8807 | 2.3598 | 2.6234 |
| 27 | 1.2439 | 1.1979 | 1.6930 | 2.9628 | 4.0050 | * |
| 24 | 1.2908 | 1.6810 | 2.3159 | 3.6296 | 4.6718 | 5.5103 |
| 30 | 1.3968 | 1.3616 | 1.9765 | 3.2822 | 4.2246 | 5.0311 |

* Solution diverged.

**TABLE 5-V Damage-Intensity Regression Parameters**

| Span (ft) | A (%) | B (%) | $\sigma_\delta^o$ (%) |
|---|---|---|---|
| 50 | .023090 | 1.0345 | .20534 |
| 75 | -.25810 | 1.9158 | .44660 |
| 100 | -.77569 | 3.3971 | .80755 |
| 125 | -1.0145 | 4.0860 | .97722 |
| 150 | -2.0947 | 5.8004 | 1.4059 |

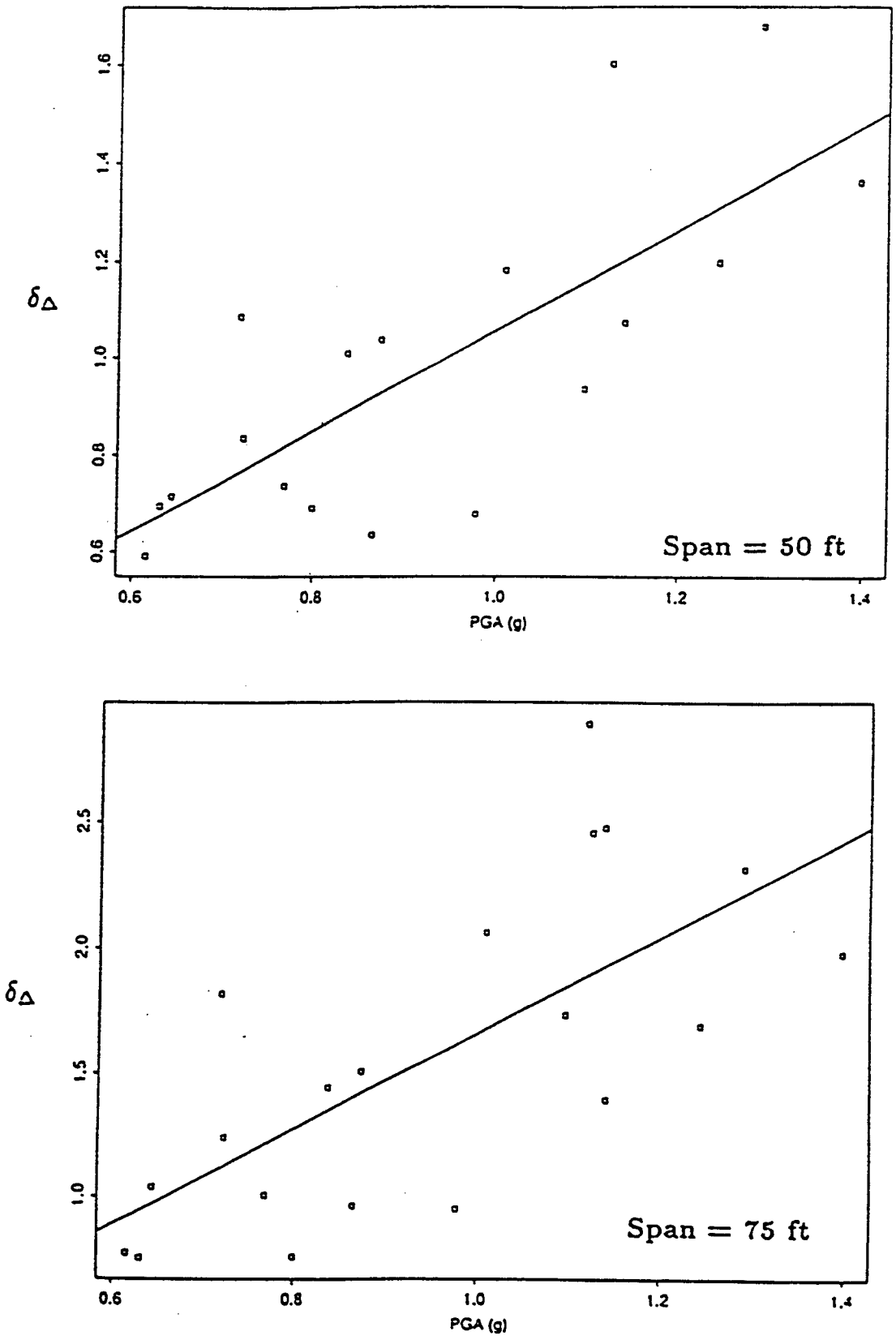


**FIGURE 5-7 Drift Damage for Various Span Lengths**

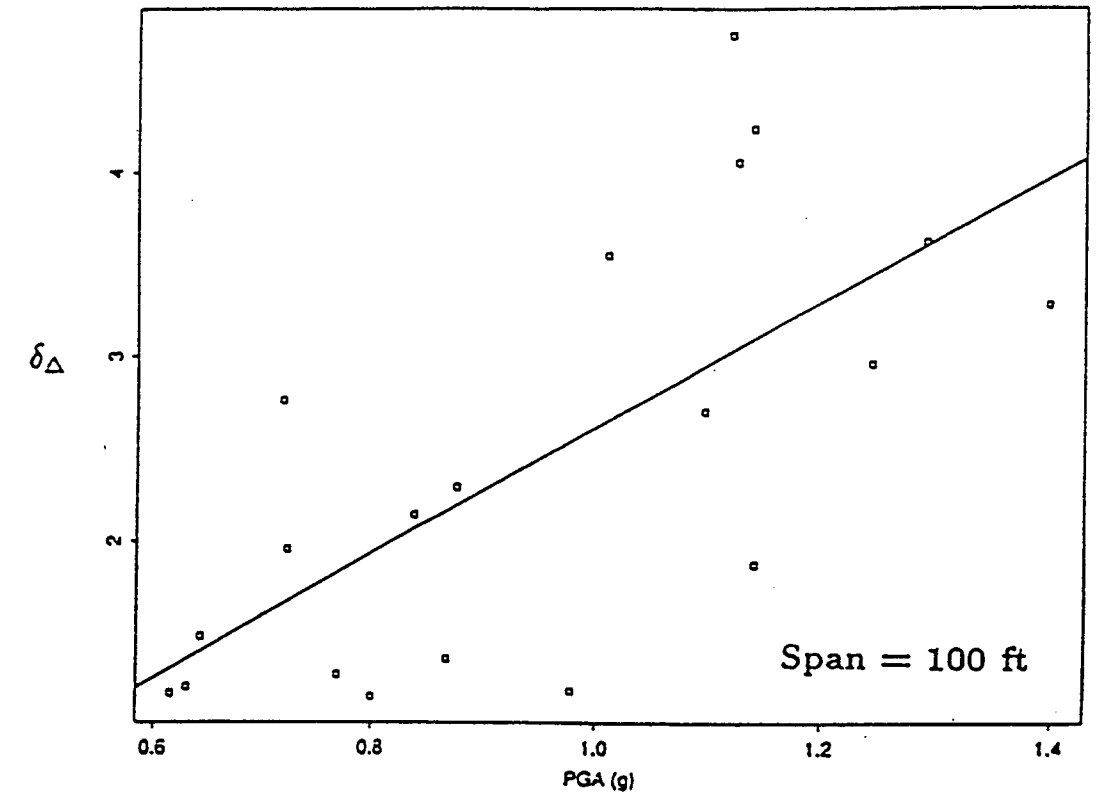


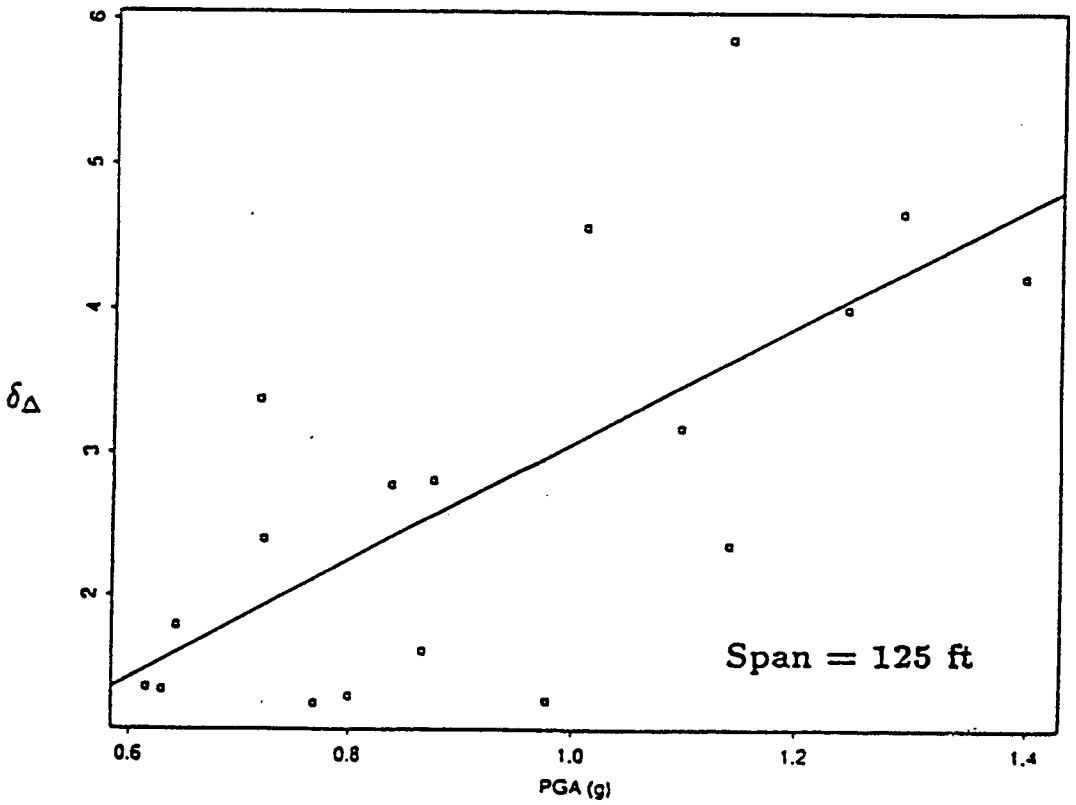


**FIGURE 5-7 Drift Damage for Various Span Lengths (Cont'd)**

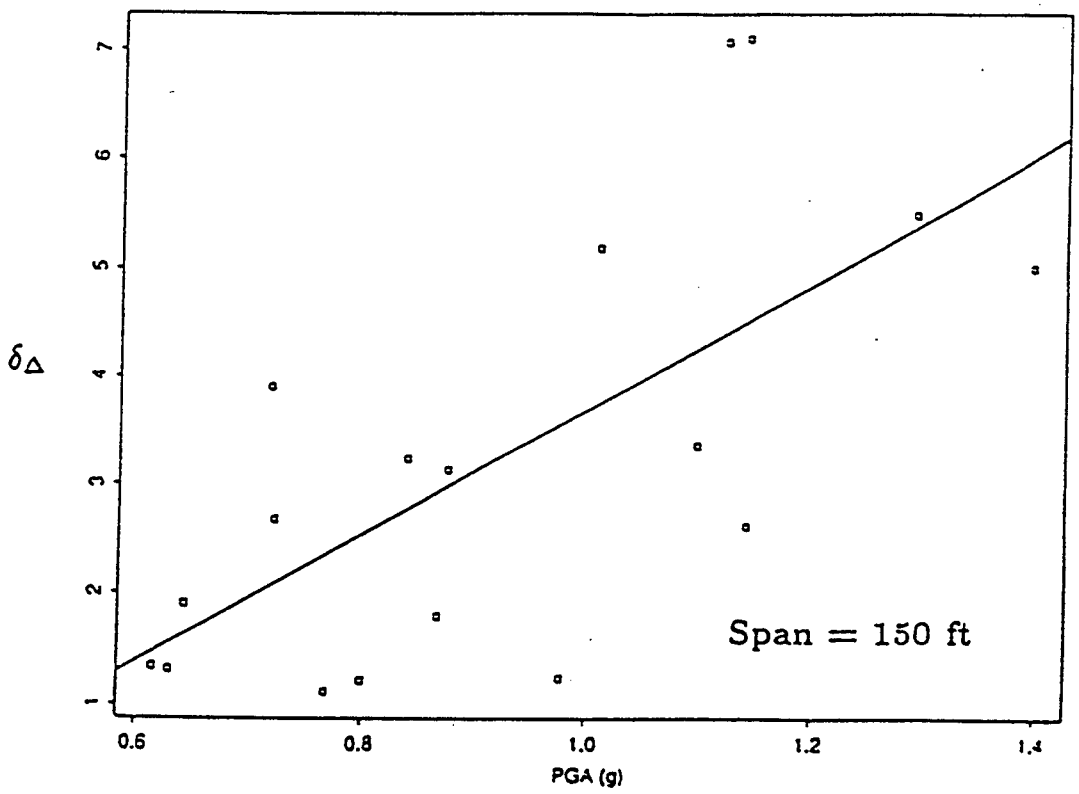


**FIGURE 5-7 Drift Damage for Various Span Lengths (Cont'd)**

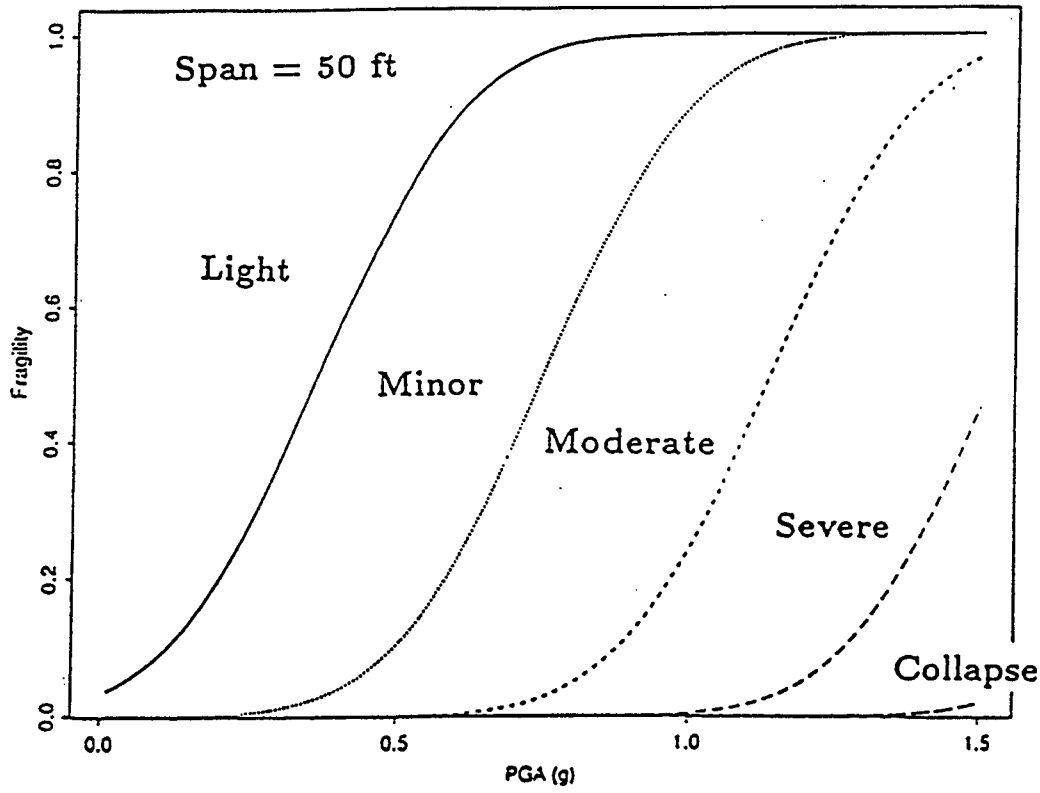


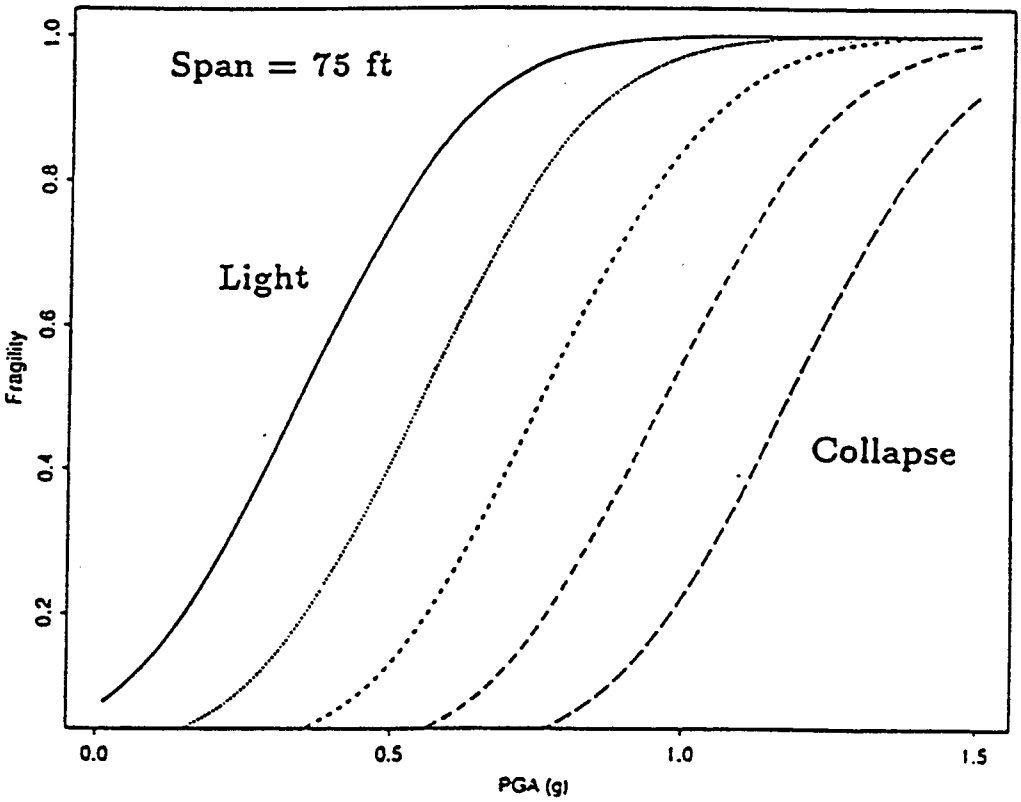


**FIGURE 5-8 Fragility Curves for Various Span Lengths**

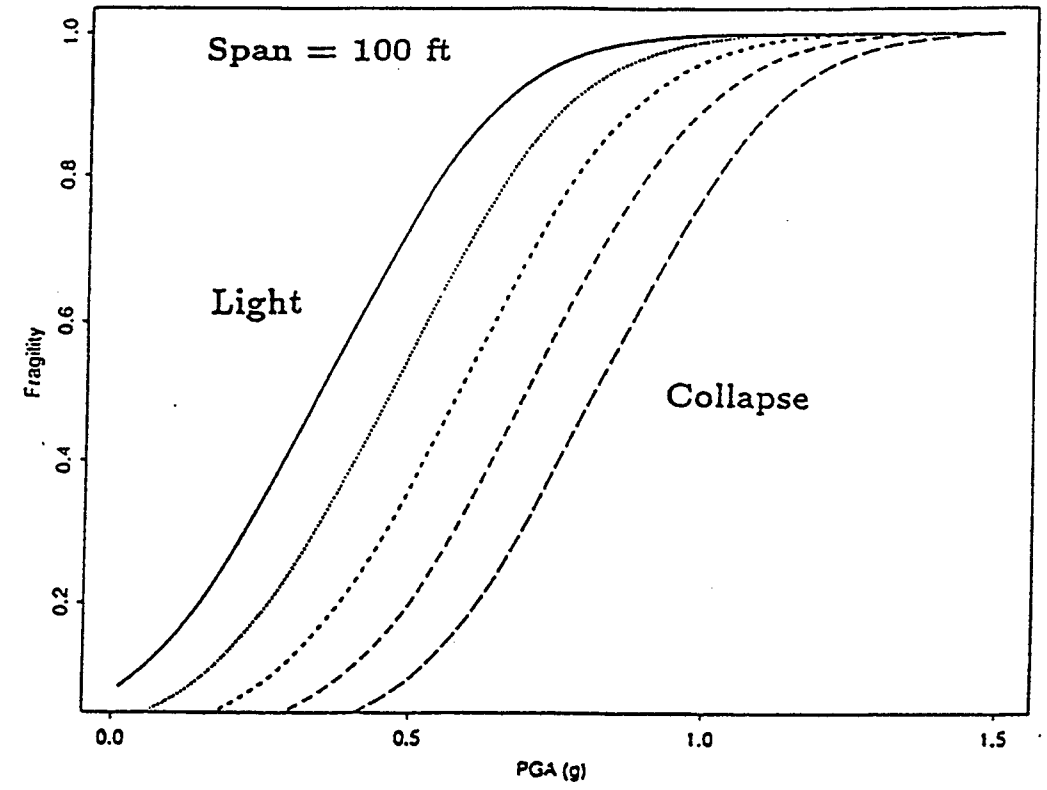


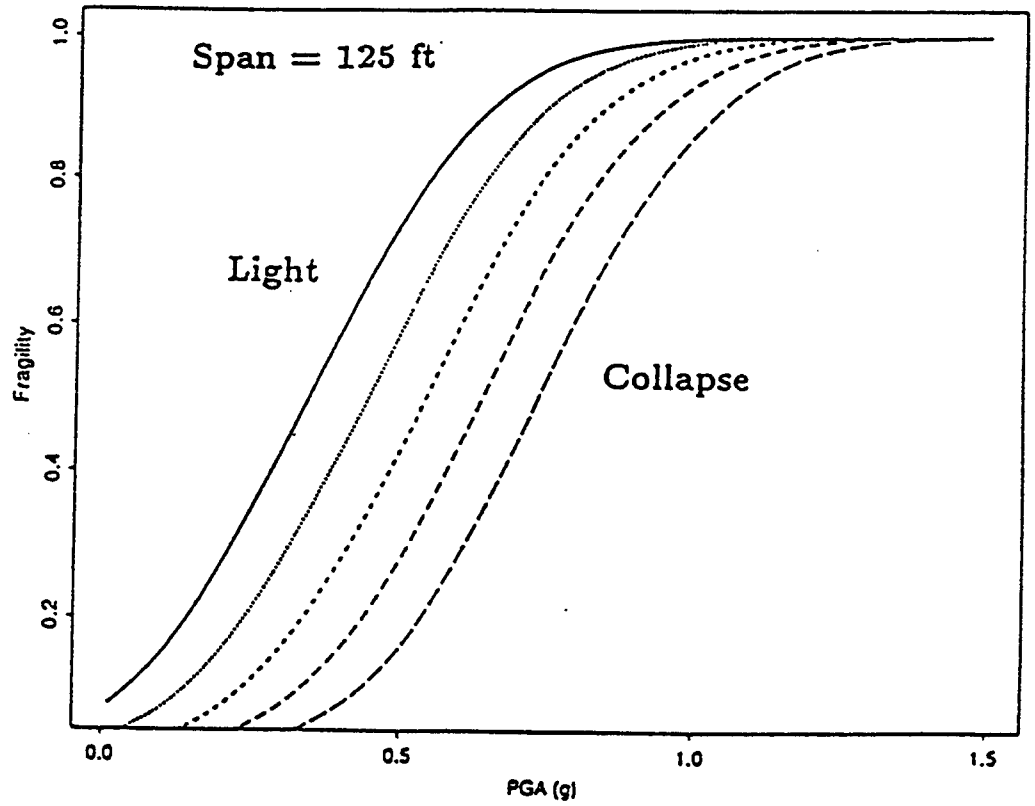


**FIGURE 5-8 Fragility Curves for Various Span Lengths (Cont'd)**

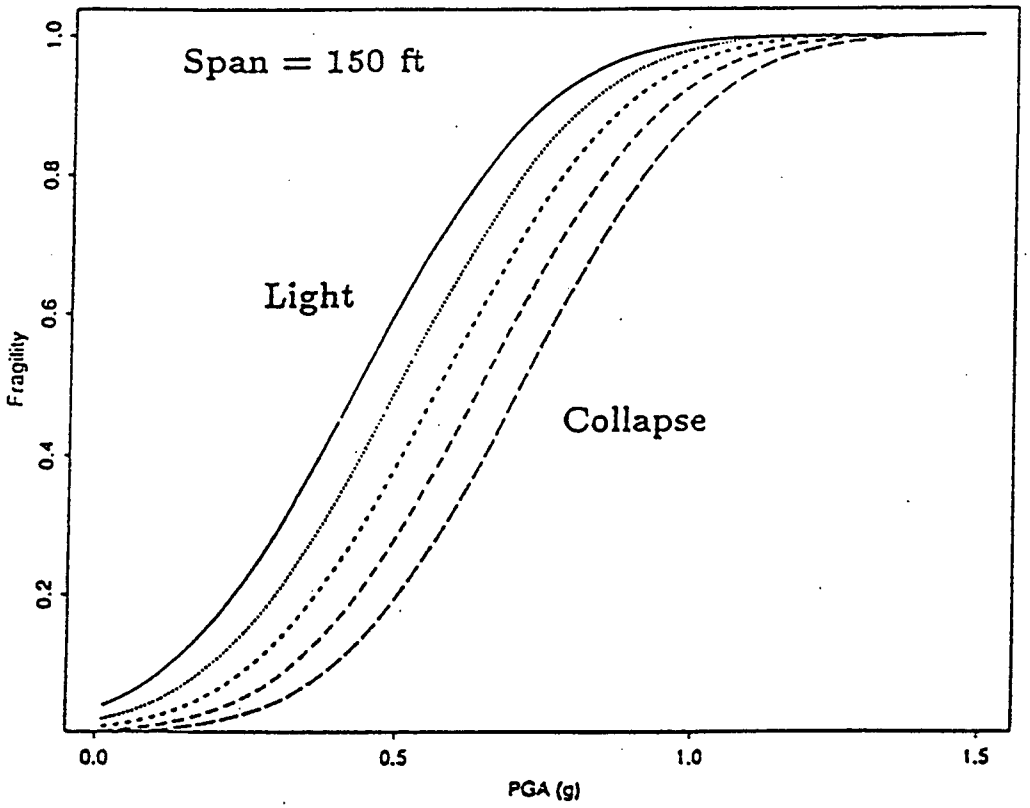


**FIGURE 5-8 Fragility Curves for Various Span Lengths (Cont'd)**

# SECTION 6
# CONCLUSIONS

The analysis of fragility of a conventional RC highway bridge has been attempted using simulated responses computed using a finite element model of the 3D bridge structural system. In the development of the model, emphasis has been placed on representing the 3D interaction of the major subsystems which include the column of the central pier, the deck superstructure, and the foundations. The principal damage mode considered was the flexural damage of the column.

A fiber model has been developed from first principles of continuum mechanics to permit the time and loadpath dependent interaction of axial force and biaxial moments on the column cross-sections. This modeling of the damage permits the computation of nonlinear-dynamic time histories of response which capture the ability of the system to redistribute forces as dictated by the damage in the column as well as the ability of the column to sustain large motions through ductile behavior.

The fiber model is shown to exhibit satisfactory performance in predicting load-deformation response of test columns using a relatively small number of simple parameters relating to the basic material constitutive laws, the geometry of the gross cross-section, and the reinforcement detailing. With these basic parameters a great deal of flexibility in modeling complex damage behaviors including cracking, crushing, spalling, and steel plasticity can be obtained. The fiber model also enables the analysis to be performed with reasonable accuracy that is not subject to any size or geometry effects that can be discerned from the experiments used to examine the sensitivity of the response to the basic parameters of the model.

When applied to a 3D bridge system and seismic response calculation, the modeling of the other subsystems introduces additional complexities. The principle complexities relate to the proper representation of the mass and stiffness distribution of the deck superstructure and the definition of the boundary conditions for interaction between the deck and foundation elements. For the conventional bridge analyzed, the interaction of embankment soil with the deck proved to be of major importance to the development of motions at the ends of the column and thus the demands on the column both in terms of force and displacement.

Despite the complexities faced in modeling the overall system and nonlinear damage in the column, a satisfactory prediction of response at the location of maximum response was obtained using relatively few free parameters and lumped properties for the foundation-deck interaction.

A probabilistic framework for fragility was considered at a basic level which is felt appropriate for the current state of knowledge of the fundamental damage and intensity measures that are applied to RC structures and highway bridges in particular. While the parameters of the fiber model were thought to be an important source of uncertainty in

the estimation of damage indices, they proved to be secondary to the variability associated with random input motions generated using stochastic time series models.

The fragility analysis has been conducted so as to take advantage of the fiber model analysis capabilities. In particular, a displacement ductility damage measure is proposed which may be readily computed using the bridge model time history analysis and fiber analysis of the isolated column. Limit states for the damage measure are readily correlated to material damage states that imply certain consequences for the overall system repairability and safety.

Finally, the computed fragility curves corresponding to these limit states seem to make intuitive sense relative to the bridge's design, construction, and performance in past seismic events.

The tools and analysis approach developed in this study are in principle applicable to a variety of RC highway bridge structures. In reality, other bridge types will introduce additional complexities and perhaps exhibit different response and fragility characteristics. In studies not restricted to a specific site, additional sources of uncertainties in the ground motion modeling will contribute to the assessment of fragility. Also, in structures involving more complex subsystems and subsystem interactions, the number of critical damage modes will increase as well. Hopefully, this study will provide a reference case and initial basis for undertaking these more complex situations.

## REFERENCES


Ang, A. H.-S. and Kim, W.-J., "Damage Assessment of Existing Bridge Structures with System Identification," Proceedings of 2nd U.S.-Asia Conference on Engineering for Mitigating Natural Hazards Damage, 1992.

As-built drawings for the Meloland Road Overcrossing, California Department of Transportation, completed July 1, 1971: Sheet 5 (Bent Details) and Sheet 6 (Typical Section and Girder Layout).

Bard, P.-Y., "Comportement Sismique d'un Passage Superieur d'Autoroute: Analysie de Donnees Experimentales," *Bulletin Liaison Laboratoire de Ponts et Chassees*, **167**, 1990, pp. 61-76.

Broderick, B. M., and Elnashai, A. S., "Analysis of the failure of Interstate 10 freeway ramp during the Northridge earthquake of 17 January 1994," *Earthquake Engineering and Structural Dynamics*, **24**, 1995, pp. 189-208.

Building Seismic Safety Council, "NEHRP Recommended Provisions for Seismic Regulations for New Buildings," Section 2.2.7, 1994 edition.

Chang, G. A., and Mander, J. B., "Seismic Energy Based Fatigue Damage Analysis of Bridge Columns: Part I- Evaluation of Seismic Capacity," *NCEER-94-0006*, National Center for Earthquake Engineering Research, State University of New York, Buffalo, 1994.

Chen, W. F. and Atsuta, T., *Theory of Beam-Columns, Volume 2: Space Behavior and Design*, McGraw-Hill, 1977.

Chen, W. F. and Han, *Plasticity for Structural Engineers*, 1988.

DiPasquale, E. and Cakmak, A. S., "Seismic Damage Assessment using Linear Models," *Soil Dynamics and Earthquake Engineering*, **9**, 4, 1990, pp. 194-215.

DiPasquale, E. and Cakmak, A. S., "Identification of the Serviceability Limit State and Detection of Seismic Structural Damage," *Technical Report NCEER-88-0022*, National Center for Earthquake Engineering Research, State University of New York at Buffalo, 1988.

Ellis, G. W. and Cakmak, A. S., "Modelling Earthquake Ground Motions in Seismically Active Regions using Parametric Time Series Methods," *Technical Report NCEER-87-0014*, National Center for Earthquake Engineering Research, State University of New York at Buffalo, 1987.

Ellis G. W., Srinivasan M., and Cakmak A. S., "A Program to Generate Site Dependent Time Histories: EQGEN," *Technical Report NCEER-90-0009*, National Center for Earthquake Engineering Research, State University of New York at Buffalo, 1990.

Fyrileiv, O., "SESAM Theory Manual: FENRIS- Finite Element Nonlinear Integrated System," Det Norske Veritas SESAM AS, Hovik, Norway, 1993.

Gates, J., Chief of Structures Division, California Department of Trasportation, personal communication, June 6, 1996.

Hughes, T. J. R., *The Finite Element Method: Linear Static and Dynamic Finite Element Analysis*, Prentice-Hall, 1987.

Hwang, H. M. H. and Jaw, J.-W., "Probabilistic Damage Analysis of Structures," *Journal of Structural Engineering*, **116**, 7, 1990, pp. 1992-2007.

Hwang, H. M. H. and Huo, J.-R. "Generation of Hazard-Consistent Fragility Curves for Seismic Loss Estimation Studies," *Soil Dynamics and Earthquake Engineering*, 1995.

"IAI-NEABS: Integrated Software Package- Linear and Nonlinear Earthquake Analysis of Bridge Systems and Post-Processor Utilities," IAI-NEABS User's Manual, Imbsen and Associates, Inc., Sacramento, California, 1993.

Imbsen, R. A. and Penzien, J., "Evaluation of Energy Absorbtion Characteristeristics of Highway Bridges under Seismic Conditions," *Report No. UCB/EERC 84-16*, to the California Department of Transportation, Earthquake Engineering Research Center, University of California at Berkeley, 1986.

International Conference of Building Officials, "Uniform Building Code, Volume 2: Structural Engineering Design Provisions," Section 1628.8, 1994.

Kawashima and Penzien, J., 1976 (see Imbsen and Penzien, 1986).

King, D. J., Priestley, M. J. N. and Park, R., "Computer Program for Concrete Column Design," Dept. of Civil Engineering Report No. 86-12, University of Canterbury, New Zealand, 1986.

Kunnath, S. K., and Reinhorn, A. M., "Inelastic Three-Dimensional Response Analysis of Reinforced Concrete Building Structures (IDARC-3D): Part I- Modeling," *NCEER-89-0011*, National Center for Earthquake Engineering Research, State University of New York, Buffalo, 1989.

Kunnath, S. K., Reinhorn, A. M., and Lobo, R. F., "IDARC Version 3.0: A Program fo the Inelastic Damage Analysis of Reinforced Concrete Structures", *NCEER-92-0022*, National Center for Earthquake Engineering Research, State University of New York, Buffalo, 1992.

Levine, M. B. and Scott, R. F., "Dynamic Response Verification of Simplified Bridge-Foundation Model," *Journal of Geotechnical Engineering*, **115**, 2, 1989, pp. 246-260.

Madas, P., and Elnashai, A. S., "A new passive confinement model for the analysis of concrete structures subjected to cyclic and transient dynamic loading," *Earthquake Engineering and Structural Dynamics*, **21**, 1992, pp. 409-431.

Mander, J. B., Priestley, M. J. N., and Park, R. "Theoretical Stress-Strain Model for Confined Concrete," *Journal of Structural Engineering*, **114**, 8, 1988, pp. 1804-1826.

Mullen, C. L., Micaletti, R. C., Jr., and Cakmak, A. S., "A Simple Method for Estimating the Maximum Softening Damage Index," *Soil Dynamics and Earthquake Engineering VII*, Cakmak, A. S. and Brebbia, C. A., eds., Computational Mechanics Publications, 1995, pp. 372-378.

Powell, G., Filippou, F., Prakash, V., Campbell, S., "Analytical Platform Development for Precast Structural Systems," Structural Engineering in Natural Hazards Mitigation, American Society of Civil Engineers, pp. 65-70.

Prevost, J.-H., "DYNAFLOW.v96 Users Manual," Department of Civil Engineering and Operations Research, Princeton University, New Jersey, 1996.

Priestley, M. J. N., Seible, F. and Uang, C. M., "The Northridge Earthquake of January 17, 1994. Damage Analysis of Selected Freeway Bridges," *Report No. SSRP 94-06*, University of California at San Diego, 1994.

Reinhorn, A. M., "3D-BASIS-TABS," *NCEER-89-0011*, National Center for Earthquake Engineering Research, State University of New York, Buffalo.

S-PLUS: Copyright (c) 1988, 1995 MathSoft, Inc., Version 3.3 Release 1 for Sun SPARC, SunOS 4.1.x : 1995.

Saenz L. P., discussion of paper entitled, "Equation for the Stress-Strain Curve of Concrete," *Journal of the American Concrete Institute*, **61**, 9, 1964, pp. 1229-1235.

Shakal, A. F., Ragsdale, J. T., and Sherburne, R. W., "CSMIP Strong-Motion Instrumentation and Records from Transportation Structures-Bridges," Proceedings of Symposium on Lifeline Earthquake Engineering: Performance, Design, and Construction, Technical Council on Lifeline Earthquake Engineering, American Society of Civil Engineering, 1984, pp. 117-132.

Singhal, A. and Kiremidjian, A. S., "Analytical Formulation of Fragilities," *Soil Dynamics and Earthquake Engineering VII*, Cakmak, A. S. and Brebbia, C. A., eds., Computational Mechanics Publications, 1995, 389-396.

Southern Building Code Congress International, Inc., "Standard Building Code," Section 1607.3.7, 1994 edition.

Sozen, M. A., "Review of Earthquake Response of Reinforced Concrete Buildings with a view to Drift Control," State of the Art in Earthquake Engineering, Turkish National Committee on Earthquake Engineering, Istanbul, Turkey, 1981.

Stone, W. C., and Cheok, G. S., "Inelastic Behavior of Full-Scale Bridge Columns Subjected to Cyclic Loading," *NIST/BSS 166*, National Institute of Standards and Technology, 1989.

Taucer, F. F., Spacone, E., and Filippou, F. C., "A Fiber Beam-Column Element for Seismic Response Analysis of Reinforced Concrete Structures," *UCB/EERC-91/17*, Earthquake Engineering Research Center, University of California, Berkeley, 1991.

Taylor, A. W., and Stone, W. C., "A Summary of Cyclic Lateral Load Tests on Spiral Reinforced Concrete Columns," *NISTIR 5285*, National Institute of Standards and Technology, 1993.

Tseng, W. S. and Penzien, J., "Analytical Investigations of the Seismic Response of Long, Multiple Span Highway Bridges," *Report No. EERC 73-12*, to the Federal Highway Administration, Earthquake Engineering Research Center, University of California at Berkeley, 1973.

Wang, C.-K., and Salmon, C. G., *Reinforced Concrete Design*, 4th ed., Harper & Row, New York, 1985.

Werner, S. D., Beck J. L. and Levine M. B., "Seismic Response Evaluation of the Meloland Road Overpass, using 1979 Imperial Valley Earthquake Records." *Earthquake Engineering and Structural Dynamics*, **15**, 1987, pp. 249-274.

Werner, S. D., Crouse C. B., Katafygiotis L. and Beck J. L., "Model Identification and Seismic Analysis of Meloland Road Overcrossing." Dames and Moore Technical Report to CalTrans, 1993.

Wilson, J. C. and Tan, B. S., "Bridge Abutments: Formulation of Simple Model for Earthquake Response Analysis," *Journal of Engineering Mechanics*, **116**, 8, 1990, pp. 1828-1837.

Zahn, F. A., Park, R., and Priestley, M. J. N., "Strength and Ductility of Square Reinforced Concrete Column Sections Subjected to Biaxial Bending," *ACI Structural Journal*, March-April, 1989, pp. 123-131.

Zeris, C. A., and Mahin, S. A., "Analysis of reinforced concrete beam-columns under uniaxial excitation," *Journal of Structural Engineering*, **114**, 4, 1988, pp. 804-820.

Zeris, C. A., and Mahin, S. A., "Behavior of reinforced concrete structures subjected to biaxial excitation," *Journal of Structural Engineering*, **117**, 9, 1991, pp. 2657-2673.

Zienkiewicz, O. C. and Taylor, R. L., *The Finite Element Method-Volume 2: Solid and Fluid Mechanics, Dynamics, and Nonlinearity*, 4th ed., McGraw-Hill, 1994.

# APPENDIX A
# 3D RC COLUMN DAMAGE ELEMENT FORMULATION

## A.1 Global System and Solution Algorithms

The strong form of the hyperbolic initial boundary value problem for dynamic behavior of the global structure treated as a continuum is summarized below following the notation of a standard finite element text (Hughes, 1987).

Let the open set, $\Omega \subset \mathcal{R}^3$, define the interior domain of the body (structure), $\Gamma$ the piecewise smooth boundary, and the closed set, $\bar{\Omega} = \Omega \cup \Gamma$. Let $\mathbf{x} \in \bar{\Omega}$ be an arbitrary point on the structure and $\mathbf{n}$ a unit outward normal to $\Gamma$. Also, let time span the closed interval, $t \in [0, T]$.

Assume the boundary surface admits the following decomposition:

$$\Gamma = \Gamma_g \cup \Gamma_h$$
$$\emptyset = \Gamma_g \cap \Gamma_h$$

Given:

| | | |
|---|---|---|
| body forces | $f_i$ : | $\Omega \times ]0,T[ \mapsto \mathcal{R}$ |
| boundary displacements | $g_i$ : | $\Gamma_g \times ]0,T[ \mapsto \mathcal{R}$ |
| boundary tractions | $h_i$ : | $\Gamma_h \times ]0,T[ \mapsto \mathcal{R}$ |
| initial displacements | $u_{0i}$ : | $\Omega \mapsto \mathcal{R}$ |
| initial velocities | $\dot{u}_{0i}$ : | $\Omega \mapsto \mathcal{R}$ |
| density | $\rho$ : | $\Omega \mapsto \mathcal{R}$ |

where i= 1,2,3

Find the unknown displacements: $u_i : \bar{\Omega} \times [0,T] \mapsto \mathcal{R}^3$

satisfying the equations of motion:

$$\sigma_{ij,j} + \rho(f_i - u_{i,tt}) = 0 \quad on \ \Omega \times ]0,T[ \tag{A.1}$$

subject to the prescribed boundary and initial conditions:

$$u_i = g_i \qquad on \ \Gamma_{g_i} \times ]0,T[$$
$$\sigma_{ij} n_j = h_i \qquad on \ \Gamma_{h_i} \times ]0,T[$$
$$u_i(\mathbf{x},0) = u_{0i}(\mathbf{x}) \qquad \mathbf{x} \in \Omega$$
$$u_{i,t}(\mathbf{x},0) = \dot{u}_{0i}(\mathbf{x}) \qquad \mathbf{x} \in \Omega$$

The strong form may be recast in weak or variational form as:

$$\int_\Omega [\sigma_{ij,i} + \rho(f_i - u_{i,tt})]\bar{u}_i \ d\Omega = 0 \tag{A.2}$$

Assuming small deformation gradients, the strain-displacement relations are:

$$\epsilon_{ij} = u_{(i,j)} = \frac{1}{2}(u_{i,j} + u_{j,i}) \tag{A.3}$$

Integrating (2.2) by parts and making use of the divergence theorem, the strain-displacement relations, and the natural boundary conditions, the weak form becomes:

$$\int_{\Omega} [\bar{u}_{(i,j)}\sigma_{ij} - \rho\bar{u}_i(f_i - u_{i,tt})] \; d\Omega - \int_{\Gamma_h} \bar{u}_i h_i \; d\Gamma = 0 \qquad (A.4)$$

The Galerkin method provides an approximate solution, $u_i^h$, to (2.1.4) by expanding the actual and variational kinematic fields using the same finite set of basis functions. Let $\eta = 1, 2, ..., nnp$ be the set of all nodes, $\eta_{g_i} \subset \eta$ the set of nodes at which $u_i^h = g_i$. Let $A \in \eta - \eta_{g_i}$ and the shape function associated with node $A$ be denoted by $N_A(\mathbf{x})$ and satisfy the relation $N_A(\mathbf{x}_B) = \delta_{AB}$ where $\mathbf{x}_B$ denotes the position vector of node $B$ and $\delta_{AB}$ the Kronecker delta. The semidiscrete formulation is obtained using:

$$u_i^h(\mathbf{x}, t) = \sum_A N_A(\mathbf{x}) \; u_{iA}^h(t) \qquad (A.5a)$$

$$\bar{u}_i^h(\mathbf{x}, t) = \sum_A N_A(\mathbf{x}) \; \bar{u}_{iA}^h(t) \qquad (A.5b)$$

Substitution of (2.5) into (2.4) leads to the matrix form of the *neq* x *neq* system of equations representing the global force balance. For known external force vector, $\mathbf{F} : ]0, T[ \mapsto \mathcal{R}^{neq}$, and unknown displacement vector, $\mathbf{d} : ]0, T[ \mapsto \mathcal{R}^{neq}$:

$$\mathbf{M} : \ddot{\mathbf{d}} + \mathbf{K} : \mathbf{d} = \mathbf{F} \qquad (A.6a)$$

$$\mathbf{d}(0) = \mathbf{d}_0 \qquad (A.6b)$$

$$\dot{\mathbf{d}}(0) = \dot{\mathbf{d}}_0 \qquad (A.6c)$$

where:

$$\mathbf{M} : \ddot{\mathbf{d}} = \int_{\Omega} \rho \; \mathbf{N}_A \otimes \mathbf{N}_B : \ddot{\mathbf{d}} \; d\Omega \qquad (A.7a)$$

$$\mathbf{K} : \mathbf{d} = \int_{\Omega} \mathbf{B}_A^T : \sigma \; d\Omega \qquad (A.7b)$$

$$\mathbf{F} = \int_{\Omega} \rho \; \mathbf{N}_A : \mathbf{f} \; d\Omega + \int_{\Gamma_h} \mathbf{N}_A : \mathbf{h} \; d\Gamma_h \qquad (A.7c)$$

In the above, $\mathbf{K}$ represents the linear or time/load-path dependent nonlinear secant stiffness matrix, $\mathbf{N}$ the nodal shape function matrix, $\mathbf{B}$ the strain versus nodal displacement matrix, $\sigma$ the stress vector, $\mathbf{f}$ the nodal body force vector, and $\mathbf{h}$ the surface traction vector.

If Rayleigh damping is assumed to occur, a damping matrix, $\mathbf{C}$, may be defined which is proportional to the mass matrix, $\mathbf{M}$, and a linear secant stiffness matrix, $\mathbf{K}^L$:

$$\mathbf{C} = a \; \mathbf{M} + b \; \mathbf{K}^L \qquad (A.8)$$

Assuming a nonlinear secant stiffness matrix, $\mathbf{K}^{NL}$, exists, the damped global force balance equations become:

$$\mathbf{R} = \mathbf{M} : (\ddot{\mathbf{d}} + a \ \dot{\mathbf{d}}) + b \ \mathbf{K}^{L} : \dot{\mathbf{d}} + \mathbf{K}^{NL} : \mathbf{d} - \mathbf{F} = \mathbf{0} \qquad (A.9)$$

The solution of (2.9) may be accomplished using step-by-step numerical integration or in cases of weak nonlinearity by approximate modal solution procedures. In this work which uses the DYNAFLOW global system level routines, the Generalized Newmark Family of direct Linear Single Step Methods is adopted, (see e.g. Hughes, 1987). Let $\mathbf{d}_n, \mathbf{v}_n, \mathbf{a}_n$ be the approximations of $\mathbf{d}(t_n), \dot{\mathbf{d}}(t_n), \ddot{\mathbf{d}}(t_n)$, respectively. Then, (2.9) is approximately satisfied by the following residual force and two-parameter finite difference formulae:

$$\mathbf{R} = \mathbf{M} : (\mathbf{a}_{n+1} + a \ \mathbf{v}_{n+1}) + b \ \mathbf{K}^{L} : \mathbf{v}_{n+1} + \mathbf{K}^{NL} : \mathbf{d}_{n+1} - \mathbf{F}_{n+1} \approx \mathbf{0} \qquad (A.10a)$$

$$\mathbf{d}_{n+1} = \mathbf{d}_n + \Delta t \ \mathbf{v}_n + \frac{1}{2}\Delta t^2[(1-2\beta)\mathbf{a}_n + 2\beta \mathbf{a}_{n+1}] \qquad (A.10b)$$

$$\mathbf{v}_{n+1} = \mathbf{v}_n + \Delta t[(1-\alpha)\mathbf{a}_n + \alpha \mathbf{a}_{n+1}] \qquad (A.10c)$$

For the material nonlinear behavior considered in this work, $\mathbf{K}^{NL}$ is dependent not only on $\mathbf{d}_{n+1}$ but also on the load or displacement history. An incremental (iterative) approach is therefore necessary. DYNAFLOW uses a predictor-multi-corrector iteration scheme (see Hughes, 1987, for a linear-dynamic example of such a scheme). Various options are provided to the user for updating the global stiffness matrix during iterations and for performing line searches to accelerate convergence. The details of these are not the focus of this work and will not be discussed here. The following discussion will assume a full Newton-Raphson iteration scheme is being used.

For the case expressed by (2.10), the residual force may be approximated through a first order Taylor expansion (see Zienkiewicz and Taylor, 1994), which for iteration i gives:

$$\mathbf{R}_{n+1}^{i+1} \approx \mathbf{R}_{n+1}^{i} + \left[\frac{\partial \mathbf{R}}{\partial \mathbf{a}}\right]_{n+1}^{i} \Delta \mathbf{a}_n^i = 0 \qquad (A.11a)$$

where

$$\left[\frac{\partial \mathbf{R}}{\partial \mathbf{a}}\right]_{n+1}^{i} = (1 + a \ \alpha \Delta t)\mathbf{M} + b \ \alpha \Delta t \mathbf{K}^{L} + \beta \Delta t^2 [\mathbf{K}^{NL}]_{n+1}^{i} \qquad (A.11b)$$

$$[\mathbf{K}^{NL}]_{n+1}^{i} = \int_{\Omega} \mathbf{B}_A^T \ \left[\frac{\partial \sigma}{\partial \mathbf{d}}\right]_{n+1}^{i} \ d\Omega \qquad (A.11c)$$

$$\mathbf{a}_{n+1}^{i+1} = \mathbf{a}_n + \Delta \mathbf{a}_n^i \qquad (A.11d)$$

The iteration proceeds from $\mathbf{a}_{n+1}^1 = \mathbf{a}_n$ to $\mathbf{a}_{n+1}^i = \mathbf{a}_{n+1}$ at which point $\mathbf{R}_{n+1}^i \approx 0$ to within a prescribed tolerance. DYNAFLOW also accepts a tolerance on the final incremental displacement for acceptance of convergence. Since the global stiffness matrix may be time-/loadpath dependent, the choice of these tolerances has some effect on the computed

results. As mentioned, alternative iteration methods may be used in DYNAFLOW which do not require updating the global tangent stiffness matrix at every iteration or even every time step. In the applications described in this work, an iterative strategy was adopted whereby a BFGS quasi-Newton-Raphson update was performed every two-four iterations and Strang line searches every iteration.

For problems with material nonlinearity, $\sigma^i_{n+1} = \sigma(\mathbf{d}^i_{n+1})$, the form of which will depend on the assumed constitutive (stress-strain) law. This aspect will be seen to be especially important for the beam-column damage element whose formulation will be described next.

## A.2 Beam-Column Element Formulation

As the bridge application in subsequent sections will demonstrate, the proposed 1D element is intended to be used in combination with other 1D, 2D, and 3D elements which may have either linear or nonlinear constitutive laws. The previous section discussed the aspects of the global formulation common to all of these elements. Basic aspects of the proposed element are similar to those of a standard linear-static 3D beam-column element (Hughes, 1987) and the 3D nonlinear-dynamic one expressed in the theory manual for the proprietary FENRIS program (Fyrileiv, 1993). A lumped mass formulation is adopted for the mass expressed in (2.7a). The stiffness expressed in (2.11c) is formulated based on the no-warping Bernoulli-Euler assumption for kinematics of a cross-section during combined axial and biaxial flexure deformation. The element stiffness matrix is derived in a manner which is consistent with the stiffness method of finite element analysis (Hughes, 1987) and the requirements of the DYNAFLOW predictor-corrector integration algorithm.

This section develops the formulation for the element stiffness matrix contribution to the global tangent stiffness expressed in (2.11c) based on a local element reference system. The development is considered general to members of any material capable of meeting the kinematic assumptions for the cross-section. Section 2.3 develops the fiber approach to integration of the element stiffness used to capture material nonlinearity and the interaction of steel and concrete in a reinforced concrete member. Section 2.4 discusses fiber constitutive relations proposed for use in modeling both the steel and reinforced concrete.

Figure 2-1 shows the 1D idealization of the 3D element domain and the kinematic assumptions implied by the Bernoulli-Euler beam theory for the interaction of axial and biaxial flexural deformations. In the notation of Section 2.2, the element domain is expressed as $\Omega^e = \{\mathbf{x} : (x_1, x_2, x_3) \in \mathcal{R}^3; x_1 \in [0, L^e]; (x_2, x_3) \in A^e\}$. Let P be an arbitrary point described by a position vector, $\mathbf{x} \in \mathbf{\Omega^e}$. The coordinate $x_1$ defines the position of P along the neutral axis. The $(x_2, x_3)$ axes are assumed to be the principal axes of the cross-section (transformed to an equivalent homogeneous isotropic material in the case of sections having more than one material state), such that:

$$0 = \int_{A_e} x_2 \cdot dA = \int_{A_e} x_3 \cdot dA = \int_{A_e} x_2 \cdot x_3 \cdot dA \qquad (A.12)$$

Strictly speaking, the location of the principal axes at each cross-section translates and

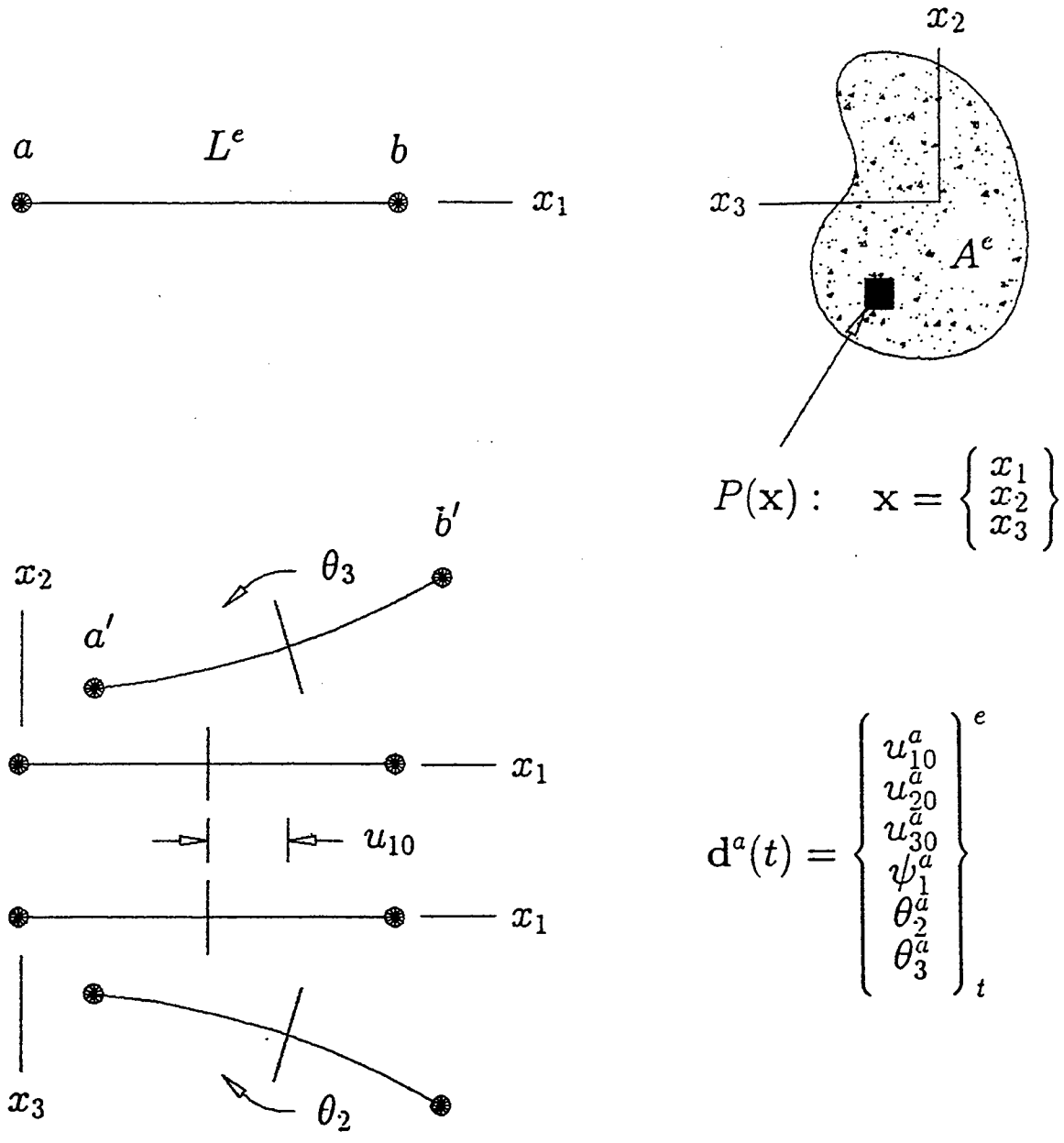


**FIGURE A-1 Beam-Column Element Domain, DOF and Kinematics**

rotates as the element experiences damage. These variations are accounted for in the procedure for integrating the element stiffness. The cross-section is presumed initially prismatic and undamaged so that each cross-section domain is identical both in material state and geometry.

For any given cross-section at time t, define the following quantities at each position on the $x_1$-axis:

| | |
|---|---|
| Axial $x_1$ deflection | $u_{10}(x_1,t) = u_1(x_1,0,0,t)$ |
| Transverse $x_2$ deflection | $u_{20}(x_1,t) = u_2(x_1,0,0,t)$ |
| Transverse $x_3$ deflection | $u_{30}(x_1,t) = u_3(x_1,0,0,t)$ |
| Twist about $x_1$ | $\psi_1(x_1,t)$ |
| Rotation about $x_2$ | $\theta_2(x_1,t) = u_{30,1}(x_1,t)$ |
| Rotation about $x_3$ | $\theta_3(x_1,t) = u_{20,1}(x_1,t)$ |
| | |
| Axial strain | $\epsilon_{10}(x_1,t) = u_{10,1}(x_1,t)$ |
| Curvature about $x_2$ | $\kappa_2(x_1,t) = \theta_{2,1}(x_1,t) = u_{30,11}(x_1,t)$ |
| Curvature about $x_3$ | $\kappa_3(x_1,t) = \theta_{3,1}(x_1,t) = u_{20,11}(x_1,t)$ |

The following relations express the Bernoulli-Euler kinematic interaction of axial and flexural deformations on the normal displacement and strain, respectively, at an arbitrary point, P:

$$\begin{aligned} u_1(\mathbf{x},t) &= u_{10}(x_1,t) - x_2 \cdot \theta_3(x_1,t) + x_3 \cdot \theta_2(x_1,t) \\ \epsilon_{11}(\mathbf{x},t) &= u_{1,1}(\mathbf{x},t) \\ &= \epsilon_{10}(x_1,t) - x_2 \cdot \kappa_3(x_1,t) + x_3 \cdot \kappa_2(x_1,t) \end{aligned} \tag{A.13}$$

It is thus assumed that the transverse deflections and twist are decoupled from the axial deflection and flexural rotations at a section. Shear strains arising from interaction of section transverse deflections and twist are not expressed here. The influence of transverse shear deformation on the transverse deflections at a section is not accounted for in the present formulation. The only transverse deflections monitored are those at the member ends which are needed for computation of flexural contributions to the normal strain.

The translations and rotations at the two member ends shown in figure 2-1 are selected as the element nodal degrees-of-freedom (DOF). For nodes, a and b, located at $\{x_1^a, x_1^b\} = \{0, L^e\}$, respectively, the displacement vector for element, e, in local coordinates becomes:

$$\begin{aligned} [\mathbf{d}^e(t)]^T &= \{[\mathbf{d}_a]^T, [\mathbf{d}_b]^T\}_t^e \\ &= \{u_{10}^a, u_{20}^a, u_{30}^a, \psi_1^a, \theta_2^a, \theta_3^a, u_{10}^b, u_{20}^b, u_{30}^b, \psi_1^b, \theta_2^b, \theta_3^b\}_t^e \end{aligned} \tag{A.14}$$

The displacement vector may be decomposed into subvectors whose DOF relate directly

to axial, twist, and biaxial flexure deformation:

$$\mathbf{d}^e_{A1}(t) = \begin{pmatrix} u^a_{10} \\ u^b_{10} \end{pmatrix}^e_t \quad \mathbf{d}^e_{T1}(t) = \begin{pmatrix} \psi^a_1 \\ \psi^b_1 \end{pmatrix}^e_t$$
$$\mathbf{d}^e_{B2}(t) = \begin{pmatrix} u^a_{30} \\ u^b_{30} \\ \theta^a_2 \\ \theta^b_2 \end{pmatrix}^e_t \quad \mathbf{d}^e_{B3}(t) = \begin{pmatrix} u^a_{20} \\ u^b_{20} \\ \theta^a_3 \\ \theta^b_3 \end{pmatrix}^e_t \tag{A.15}$$

A linear shape function is applied to the axial deflection and twist, and a cubic (Hermite polynomial) shape function to the flexural rotations. The resulting Galerkin approximation to the solution becomes:

$$\begin{aligned} u_{10}(x_1,t) &= [\mathbf{N}^L(x_1)]^T \cdot \mathbf{d}^e_{A1}(t) \quad \psi_1(x_1,t) = [\mathbf{N}^L(x_1)]^T \cdot \mathbf{d}^e_{T1}(t) \\ u_{20}(x_1,t) &= [\mathbf{N}^H(x_1)]^T \cdot \mathbf{d}^e_{B3}(t) \quad \theta_2(x_1,t) = [\mathbf{N}^H_{,1}(x_1)]^T \cdot \mathbf{d}^e_{B2}(t) \\ u_{30}(x_1,t) &= [\mathbf{N}^H(x_1)]^T \cdot \mathbf{d}^e_{B2}(t) \quad \theta_3(x_1,t) = [\mathbf{N}^H_{,1}(x_1)]^T \cdot \mathbf{d}^e_{B3}(t) \end{aligned} \tag{A.16}$$

where

$$\mathbf{N}^L(x_1) = \begin{pmatrix} N^L_1(x_1) \\ N^L_2(x_1) \end{pmatrix} = \begin{pmatrix} \frac{x^b_1 - x_1}{L^e} \\ \frac{x_1 - x^a_1}{L^e} \end{pmatrix} = \begin{pmatrix} 1 - \frac{x_1}{L^e} \\ \frac{x_1}{L^e} \end{pmatrix}$$
$$\mathbf{N}^H(x_1) = \begin{pmatrix} N^H_1(x_1) \\ N^H_2(x_1) \\ N^H_3(x_1) \\ N^H_4(x_1) \end{pmatrix} = \begin{pmatrix} [1 + 2 \cdot N^L_2(x_1)] \cdot [N^L_1(x_1)]^2 \\ [1 + 2 \cdot N^L_1(x_1)] \cdot [N^L_2(x_1)]^2 \\ L^e \cdot N^L_2(x_1) \cdot [N^L_1(x_1)]^2 \\ L^e \cdot N^L_1(x_1) \cdot [N^L_2(x_1)]^2 \end{pmatrix}$$
$$\mathbf{N}^H_{,1}(x_1) = \begin{pmatrix} N^H_{1,1}(x_1) \\ N^H_{2,1}(x_1) \\ N^H_{3,1}(x_1) \\ N^H_{4,1}(x_1) \end{pmatrix}$$

The linear shape function provides an exact solution at the element nodes for linear response of a beam segment subject to axial forces or torsional moments at the nodes only. The cubic approximation provides an exact solution at the element nodes for linear response of a beam segment having constant flexural rigidity, (see Hughes, 1987). The proposed shape functions are not necessarily optimal when the effective axial and flexural rigidities become nonlinear as has been noted by Zeris (Zeris and Mahin, 1988). The generalized strains become:

$$\begin{aligned} \epsilon_{10}(x_1,t) &= [\mathbf{N}^L_{,1}(x_1)]^T \cdot \mathbf{d}^e_{A1}(t) \quad \psi_1(x_1,t) = [\mathbf{N}^L_{,1}(x_1)]^T \cdot \mathbf{d}^e_{T1}(t) \\ \kappa_2(x_1,t) &= [\mathbf{N}^H_{,11}(x_1)]^T \cdot \mathbf{d}^e_{B2}(t) \quad \kappa_3(x_1,t) = [\mathbf{N}^H_{,11}(x_1)]^T \cdot \mathbf{d}^e_{B3}(t) \end{aligned} \tag{A.17}$$

where

$$\mathbf{N}^L_{,1}(x_1) = \begin{pmatrix} N^L_{1,1}(x_1) \\ N^L_{2,1}(x_1) \end{pmatrix}$$
$$\mathbf{N}^H_{,11}(x_1) = \begin{pmatrix} N^H_{1,11}(x_1) \\ N^H_{2,11}(x_1) \\ N^H_{3,11}(x_1) \\ N^H_{4,11}(x_1) \end{pmatrix}$$

The strain-displacement or compatibility vector then becomes:

$$\epsilon_{11}(\mathbf{x},t) = [\mathbf{N}^L_{,1}]^T \cdot \mathbf{d}^e_{A1}(t) - x_2 \cdot [\mathbf{N}^H_{,11}]^T \cdot \mathbf{d}^e_{B3}(t) + x_3 \cdot [\mathbf{N}^H_{,11}]^T \cdot \mathbf{d}^e_{B2}(t)$$

$$= \begin{pmatrix} N^L_{1,1}(x_1) \\ -x_2 \cdot N^H_{1,11}(x_1) \\ x_3 \cdot N^H_{1,11}(x_1) \\ 0 \\ x_3 \cdot N^H_{3,11}(x_1) \\ -x_2 \cdot N^H_{3,11}(x_1) \end{pmatrix}^T \cdot \begin{pmatrix} u^a_{10} \\ u^a_{20} \\ u^a_{30} \\ \psi^a_1 \\ \theta^a_2 \\ \theta^a_3 \end{pmatrix}^e_t + \begin{pmatrix} N^L_{2,1}(x_1) \\ -x_2 \cdot N^H_{2,11}(x_1) \\ x_3 \cdot N^H_{2,11}(x_1) \\ 0 \\ x_3 \cdot N^H_{4,11}(x_1) \\ -x_2 \cdot N^H_{4,11}(x_1) \end{pmatrix}^T \cdot \begin{pmatrix} u^b_{10} \\ u^b_{20} \\ u^b_{30} \\ \psi^b_1 \\ \theta^b_2 \\ \theta^b_3 \end{pmatrix}^e_t \qquad (A.18)$$

$$= \mathbf{B}_a(\mathbf{x}) \cdot \mathbf{d}_a(t) + \mathbf{B}_b(\mathbf{x}) \cdot \mathbf{d}_b(t) = \sum_{a=1}^{nen} \mathbf{B}_a \cdot \mathbf{d}_a(t)$$

$$= \mathbf{B}^e(\mathbf{x}) \cdot \mathbf{d}^e(t)$$

The forces and moments at the two member ends shown in figure 2-1 are selected as the element nodal forces, so the force vector for element, e, in local coordinates becomes:

$$\begin{aligned} [\mathbf{f}^e(t)]^T &= \{[\mathbf{f}_a]^T, [\mathbf{f}_b]^T\}^e_t \\ &= \{F^a_1, F^a_2, F^a_3, T^a_1, M^a_2, M^a_3, F^b_1, F^b_2, F^b_3, T^b_1, M^b_2, M^b_3\}^e_t \end{aligned} \qquad (A.19)$$

The tangent element stiffness is derived considering the implementation of (2.11c) in the element coordinate system and assuming an incremental constitutive relation is well defined between normal stress and strain at every point in the element. For purposes of defining the stiffness matrix components, define $n_{esd}$ = no. element spatial dimensions, $n_{ed}$ = no. element DOF per node, $n_{en}$ = no. element nodes, and $n_{en}$ = no. element equations. Then:

$$\begin{aligned} p &= n_{ed} \cdot (a-1) + i \\ q &= n_{ed} \cdot (b-1) + j \\ & 1 \le i,j \le n_{ed} (= 2 \cdot n_{esd} = 6) \\ & 1 \le a,b \le n_{en} (= 2) \\ & 1 \le p,q \le n_{ee} (= n_{ed} \cdot n_{en} = 12) \end{aligned} \qquad (A.20)$$

Let $\mathbf{e}_i = \{0, ...0, 1, 0, ..., 0\}^T$ where the 1 is in the ith position, then the element stiffness matrix, $\mathbf{k}^e_{pq}(t)$, and nodal stiffness submatrix, $\mathbf{k}^e_{ab}(t)$ may be defined:

$$\begin{aligned} \mathbf{k}^e_{pq}(t) &= \mathbf{e}^T_i \cdot \mathbf{k}^e_{ab}(t) \cdot \mathbf{e}_j \\ \mathbf{k}^e_{ab}(t) &= \int_{\Omega^e} \mathbf{B}^T_a(\mathbf{x}) \cdot D^{NL}(\mathbf{x},t) \cdot \mathbf{B}_b(\mathbf{x}) \end{aligned} \qquad (A.21)$$

where

$$D^{NL}(\mathbf{x},t) = E_T(\mathbf{x},t) = \frac{d\sigma_{11}}{d\epsilon_{11}}(\mathbf{x},t)$$

By virtue of the assumed kinematic relation and shape functions, it is natural to perform the stiffness integration first over the area domain and then over the axis length. The integration over the area permits an interpretation of a section stiffness, $\mathbf{k}_{ab}^{A^e}$, with units of (force per displacement) or (moment per rotation) per unit length along $x_1$:

$$\mathbf{k}_{ab}^{e}(t) = \int_{L^e} \mathbf{k}_{ab}^{A^e}(x_1, t) \cdot dx_1 \tag{A.22}$$

where

$$\mathbf{k}_{ab}^{A^e}(x_1, t) = \int_{A^e} E_T(\mathbf{x}, t) \cdot \mathbf{B}_a^T(\mathbf{x}) \cdot \mathbf{B}_b(\mathbf{x}) \cdot dA$$

For the general case, (2.22) must be integrated numerically, since the spatial and temporal variation of the tangent modulus, $E_T$, may not necessarily be explicitly defined. This fact has motivated the development of a fiber approach for RC members. The fiber approach and numerical integration procedure adopted in this work is described in the next section.

For ideal problems with materials that are homogeneous and isotropic, obey linear elasticity or perhaps a simple plasticity law such as an elastic, perfectly plastic stress-strain relation and are subject to monotonic loading, it is possible to integrate both the section and element stiffness in closed form.

Consider the linear case (see Hughes, 1987). The tangent modulus then reduces to Young's modulus, E, and the following applies for all x and t:

$$E_T = E = \frac{\sigma_{11}}{\epsilon_{11}} \tag{A.23}$$

The section stiffness then becomes:

$$\mathbf{k}_{ab}^{A^e}(x_1, t) = E \cdot \int_{A^e} \mathbf{B}_a^T(\mathbf{x}) \cdot \mathbf{B}_b(\mathbf{x}) \cdot dA \tag{A.24}$$

It may be noted that in the above formulation, it is not necessary to explicitly define the section forces. This is now done to provide a comparison of (2.24) with results of linear beam theory. The section axial force and biaxial moments are defined as:

$$\begin{aligned} F_1(x_1, t) &= \int_{A^e} \sigma_{11}(\mathbf{x}, t) \cdot dA \\ M_2(x_1, t) &= \int_{A^e} \sigma_{11}(\mathbf{x}, t) \cdot x_3 \cdot dA \\ M_3(x_1, t) &= \int_{A^e} \sigma_{11}(\mathbf{x}, t) \cdot x_2 \cdot dA \end{aligned} \tag{A.25}$$

The other section forces, $\{F_2, F_3, T_1\}$, require knowledge of the shear stresses and shear strain compatibility relations at an arbitrary section which have not been identified in the present formulation.

Integration of (2.25) requires knowledge of the instantaneous value of the normal stress which is not generally known explicitly.

Consider the linear case again. Substitution of (2.23) into (2.25), making use of the normal strain relation of (2.13), leads to the following section constitutive relation:

$$\begin{pmatrix} F_1^L(x_1,t) \\ M_2^L(x_1,t) \\ M_3^L(x_1,t) \end{pmatrix} = E \cdot \begin{pmatrix} A & Q_2 & -Q_3 \\ Q_2 & I_2 & I_{23} \\ -Q_3 & I_{23} & I_3 \end{pmatrix}_{A^e} \cdot \begin{pmatrix} \epsilon_{10}(x_1,t) \\ \kappa_2(x_1,t) \\ \kappa_3(x_1,t) \end{pmatrix} \qquad (A.26)$$

where

$$A = \int_{A^e} dA \qquad Q_2 = \int_{A^e} x_3 \cdot dA \qquad Q_3 = \int_{A^e} x_2 \cdot dA$$

$$I_2 = \int_{A^e} (x_3)^2 \cdot dA \quad I_3 = \int_{A^e} (x_2)^2 \cdot dA \quad I_{23} = \int_{A^e} x_2 \cdot x_3 \cdot dA$$

Noting that the shape function terms used to define the strain-nodal displacement matrix, $\mathbf{B^e}$, depend only on $x_1$, they may be taken out of the integration over the section area. Doing so allows (2.24) to reduce to (2.26), since it then involves the same integrals of section geometry as those defining the section properties in (2.26).

As expressed in (2.12), the assumption of principal axes as the choice for the $(x_2, x_3)$ element reference axes requires that the first moments of area, $\{Q_2, Q_3\}$, and the cross moment of area, $I_{23}$, vanish identically. Thus, the section stiffness becomes diagonalized for this ideal case, implying no interaction. This leads to the familiar beam theory results.

$$\begin{aligned} F_1^L(x_1,t) &= E \cdot A \cdot \epsilon_{10}(x_1,t) \\ M_2^L(x_1,t) &= E \cdot I_2 \cdot \kappa_2(x_1,t) \\ M_3^L(x_1,t) &= E \cdot I_3 \cdot \kappa_3(x_1,t) \end{aligned} \qquad (A.27)$$

In the general case where the tangent moduli are allowed to change both with x and t, the integrals in (2.25) must be integrated in time such that equilibrium is satisfied and such that the stress-strain relations are satisfied.

If the view is taken that at each instant, an equivalent linear system exists analogous to that expressed in (2.26), then it is possible to establish an analogous incremental constitutive relation between section force (generalized stress) and generalized strain increments. The section stiffness coefficients may then be interpreted as effective moduli of rigidity, namely the products of a fictitious Young's modulus, assumed constant for the section, and corresponding fictitious section properties. In this case, the effective first moments and cross moment only vanish if corresponding fictitious principle axes are computed.

Considering the complex effects which govern the spatial and temporal variation of the tangent moduli, it is not difficult to see how attempts at developing an incremental constitutive relation between section force and generalized strain increments semi-empirically are subject to severe limitations.

## A.3 Fiber Integration of Element Stiffness

In this work, a two-point Gauss integration over the length and a variable-point or fiber integration over the area domain at the two Gauss-point sections provides the basis for the integration of (2.22) in this work. This combination maximizes flexibility in modeling complex section details such as arbitrary gross concrete shape and reinforcement placement while minimizing storage requirements for each element.

The volume integral of the continuous function expressed in (2.21) is reduced to a summation over the length domain, $L^e$, under the assumption of Gaussian integration. In figure 2-2, this is seen to lead to flexibility in laying out the element mesh for a typical pier in a highway bridge to accommodate complex geometry and connectivity that exist in real situations. Let $\{x_1\}_{i=1}^{nint} = \{(1-\frac{1}{\sqrt{3}})\cdot\frac{L^e}{2}, (1+\frac{1}{\sqrt{3}})\cdot\frac{L^e}{2}\}, \{w_1\}_{i=1}^{nint} = \{1,1\}$, and $nint$= 2. Then,

$$\mathbf{k}_{ab}^{e}(t) = \sum_{i=1}^{nint} \mathbf{k}_{ab}^{A^e}(x_1^i, t)\cdot\frac{L^e}{2}\cdot w_i \qquad (A.28)$$

where

$$\mathbf{k}_{ab}^{A^e}(x_1^i, t) = \int_{A^e} E_T(\mathbf{x}^i, t)\cdot\mathbf{B}_a^T(\mathbf{x}^i)\cdot\mathbf{B}_b(\mathbf{x}^i)\cdot dA$$

Inspection of (2.18) reveals that key section stiffness terms consist of the following integral types, for example:

$$\begin{aligned}
[k_{11}^{ab}]^{A^e}(x_1,t) &= N_{1,1}^L(x_1)\cdot N_{1,1}^L(x_1)\cdot\int_{A^e} E_T(\mathbf{x},t)\cdot dA \\
[k_{22}^{ab}]^{A^e}(x_1,t) &= N_{1,11}^H(x_1)\cdot N_{2,11}^H(x_1)\cdot\int_{A^e} E_T(\mathbf{x},t)\cdot(x_2)^2\cdot dA \\
[k_{33}^{ab}]^{A^e}(x_1,t) &= N_{1,11}^H(x_1)\cdot N_{2,11}^H(x_1)\cdot\int_{A^e} E_T(\mathbf{x},t)\cdot(x_3)^2\cdot dA
\end{aligned} \qquad (A.29)$$

A fiber viewpoint is now adopted in order to discretize the section area for purposes of integration. A fiber is considered to be located at the centroid of a patch of the section area that is effective in resisting normal stress and obeys the strain compatibility assumption. Figure 2-3 shows the local domain of typical concrete and steel fibers appearing in a reinforced concrete section. The section stiffness at each Gauss-point may then be reduced to summations of integrals over the section fibers, each of which may, in principle, have

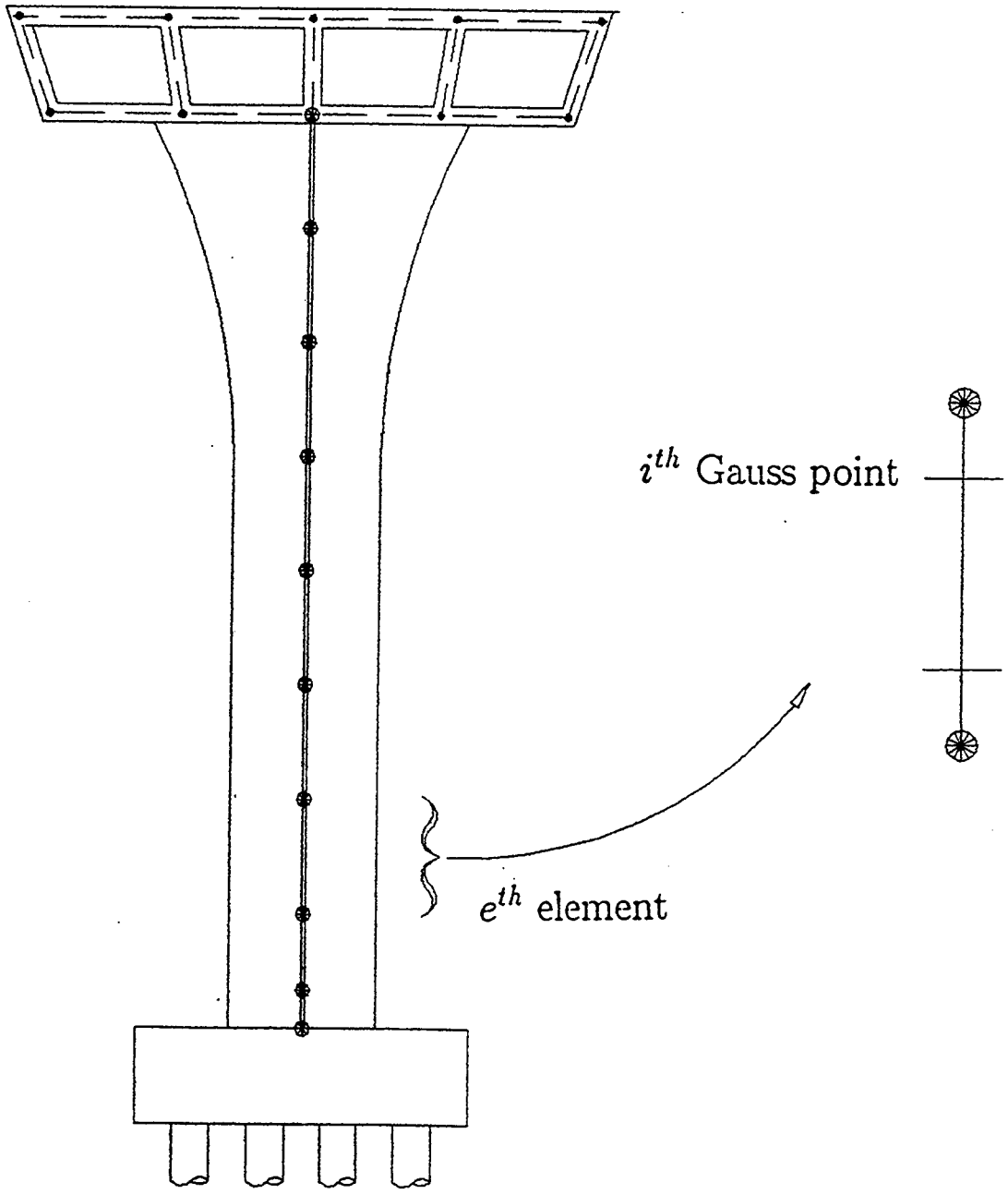


**FIGURE A-2 Gauss-Point Discretization of Element Length**

it's own shape. Thus, letting $nfib$ = no. of fibers comprising $A^e$:

$$[k_{11}^{ab}]^{A^e}(x_1^i,t) = N_{1,1}^L(x_1^i) \cdot N_{1,1}^L(x_1^i) \cdot \sum_{j=1}^{nfib} \int_{A^j} E_T(x_1^i, x_2^j, x_3^j, t) \cdot dA$$

$$[k_{22}^{ab}]^{A^e}(x_1^i,t) = N_{1,11}^H(x_1^i) \cdot N_{2,11}^H(x_1^i) \cdot \sum_{j=1}^{nfib} \int_{A^j} E_T(x_1^i, x_2^j, x_3^j, t) \cdot (x_2^j)^2 \cdot dA \qquad (A.30)$$

$$[k_{33}^{ab}]^{A^e}(x_1^i,t) = N_{1,11}^H(x_1^i) \cdot N_{2,11}^H(x_1^i) \cdot \sum_{j=1}^{nfib} \int_{A^j} E_T(x_1^i, x_2^j, x_3^j, t) \cdot (x_3^j)^2 \cdot dA$$

At this point, standard numerical integration procedures might be implemented such as Gaussian integration over a two-dimensional domain the order of which should be sufficient to accomodate the expected time-dependent variation of the tangent moduli over each fiber. This would be efficient for cases where only a small number of fibers need be considered. The need to accommodate arbitrary section geometry and various nonlinear interaction effects in the case of reinforced concrete typically demands that a large number of fibers be considered for accurate modeling of member response.

A simpler and computationally less demanding approach is taken in this work. By assuming that the tangent modulus throughout a fiber is the same as that at the fiber centroid, the integrals over the fiber domain reduce to integrals involving purely geometric terms. These geometric integrals are seen to be effective fiber properties analogous to section properties. The products of the properties and the tangent moduli are the fiber contributions to the section moduli of rigidity.

$$[k_{11}^{ab}]^{A^e}(x_1^i,t) = N_{1,1}^L(x_1^i) \cdot N_{1,1}^L(x_1^i) \cdot \sum_{j=1}^{nfib} E_T(x_1^i, x_2^j, x_3^j, t) \cdot A^j$$

$$[k_{22}^{ab}]^{A^e}(x_1^i,t) = N_{1,11}^H(x_1^i) \cdot N_{2,11}^H(x_1^i) \cdot \sum_{j=1}^{nfib} E_T(x_1^i, x_2^j, x_3^j, t) \cdot I_3^j \qquad (A.31)$$

$$[k_{33}^{ab}]^{A^e}(x_1^i,t) = N_{1,11}^H(x_1^i) \cdot N_{2,11}^H(x_1^i) \cdot \sum_{j=1}^{nfib} E_T(x_1^i, x_2^j, x_3^j, t) \cdot I_2^j$$

where

$$I_2 = A \cdot x_3^2 + I_2^0$$
$$I_3 = A \cdot x_2^2 + I_3^0$$

Since the fiber properties are assumed to be time invariant, they may be integrated exactly at the outset and stored. From (2.31), it is seen that the fiber area, centroidal position with respect to the section axes, and the centroidal second moments of area, $\{I_2^0, I_3^0\}$, are needed for each fiber. For circular sections, the exact integration of the geometric properties is accomplished with respect to a cylindrical coordinate system and then transformed to the element cartesian system.

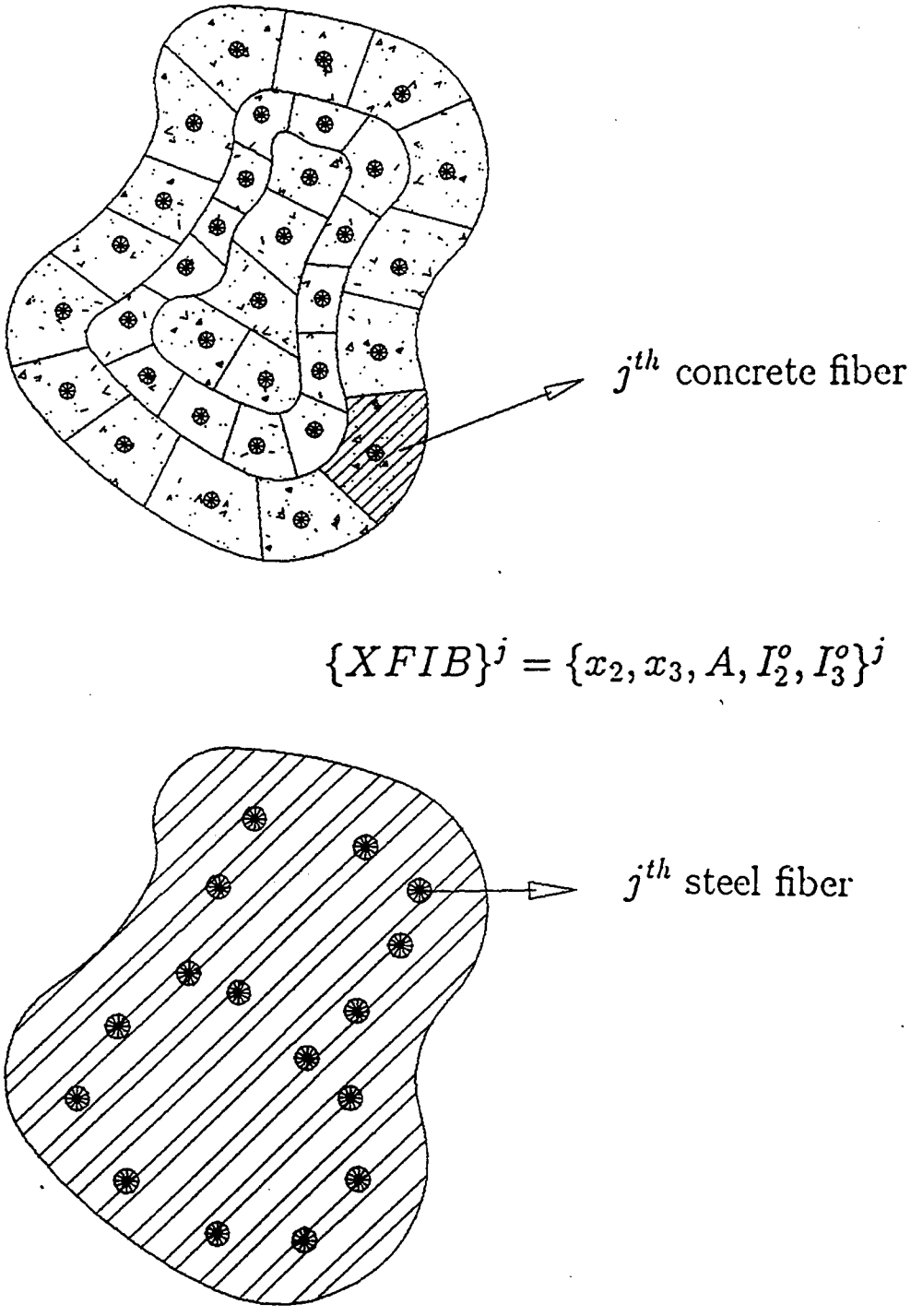


**FIGURE A-3 Fiber Discretization of Element Cross-Section**

## NATIONAL CENTER FOR EARTHQUAKE ENGINEERING RESEARCH
## LIST OF TECHNICAL REPORTS

The National Center for Earthquake Engineering Research (NCEER) publishes technical reports on a variety of subjects related to earthquake engineering written by authors funded through NCEER. These reports are available from both NCEER Publications and the National Technical Information Service (NTIS). Requests for reports should be directed to NCEER Publications, National Center for Earthquake Engineering Research, State University of New York at Buffalo, Red Jacket Quadrangle, Buffalo, New York 14261. Reports can also be requested through NTIS, 5285 Port Royal Road, Springfield, Virginia 22161. NTIS accession numbers are shown in parenthesis, if available.

NCEER-87-0001 "First-Year Program in Research, Education and Technology Transfer," 3/5/87, (PB88-134275, A04, MF-A01).

NCEER-87-0002 "Experimental Evaluation of Instantaneous Optimal Algorithms for Structural Control," by R.C. Lin, T.T. Soong and A.M. Reinhorn, 4/20/87, (PB88-134341, A04, MF-A01).

NCEER-87-0003 "Experimentation Using the Earthquake Simulation Facilities at University at Buffalo," by A.M. Reinhorn and R.L. Ketter, to be published.

NCEER-87-0004 "The System Characteristics and Performance of a Shaking Table," by J.S. Hwang, K.C. Chang and G.C. Lee, 6/1/87, (PB88-134259, A03, MF-A01). This report is available only through NTIS (see address given above).

NCEER-87-0005 "A Finite Element Formulation for Nonlinear Viscoplastic Material Using a Q Model," by O. Gyebi and G. Dasgupta, 11/2/87, (PB88-213764, A08, MF-A01).

NCEER-87-0006 "Symbolic Manipulation Program (SMP) - Algebraic Codes for Two and Three Dimensional Finite Element Formulations," by X. Lee and G. Dasgupta, 11/9/87, (PB88-218522, A05, MF-A01).

NCEER-87-0007 "Instantaneous Optimal Control Laws for Tall Buildings Under Seismic Excitations," by J.N. Yang, A. Akbarpour and P. Ghaemmaghami, 6/10/87, (PB88-134333, A06, MF-A01). This report is only available through NTIS (see address given above).

NCEER-87-0008 "IDARC: Inelastic Damage Analysis of Reinforced Concrete Frame - Shear-Wall Structures," by Y.J. Park, A.M. Reinhorn and S.K. Kunnath, 7/20/87, (PB88-134325, A09, MF-A01). This report is only available through NTIS (see address given above).

NCEER-87-0009 "Liquefaction Potential for New York State: A Preliminary Report on Sites in Manhattan and Buffalo," by M. Budhu, V. Vijayakumar, R.F. Giese and L. Baumgras, 8/31/87, (PB88-163704, A03, MF-A01). This report is available only through NTIS (see address given above).

NCEER-87-0010 "Vertical and Torsional Vibration of Foundations in Inhomogeneous Media," by A.S. Veletsos and K.W. Dotson, 6/1/87, (PB88-134291, A03, MF-A01). This report is only available through NTIS (see address given above).

NCEER-87-0011 "Seismic Probabilistic Risk Assessment and Seismic Margins Studies for Nuclear Power Plants," by Howard H.M. Hwang, 6/15/87, (PB88-134267, A03, MF-A01). This report is only available through NTIS (see address given above).

NCEER-87-0012 "Parametric Studies of Frequency Response of Secondary Systems Under Ground-Acceleration Excitations," by Y. Yong and Y.K. Lin, 6/10/87, (PB88-134309, A03, MF-A01). This report is only available through NTIS (see address given above).

NCEER-87-0013 "Frequency Response of Secondary Systems Under Seismic Excitation," by J.A. HoLung, J. Cai and Y.K. Lin, 7/31/87, (PB88-134317, A05, MF-A01). This report is only available through NTIS (see address given above).

NCEER-87-0014 "Modelling Earthquake Ground Motions in Seismically Active Regions Using Parametric Time Series Methods," by G.W. Ellis and A.S. Cakmak, 8/25/87, (PB88-134283, A08, MF-A01). This report is only available through NTIS (see address given above).

NCEER-87-0015 "Detection and Assessment of Seismic Structural Damage," by E. DiPasquale and A.S. Cakmak, 8/25/87, (PB88-163712, A05, MF-A01). This report is only available through NTIS (see address given above).

NCEER-87-0016 "Pipeline Experiment at Parkfield, California," by J. Isenberg and E. Richardson, 9/15/87, (PB88-163720, A03, MF-A01). This report is available only through NTIS (see address given above).

NCEER-87-0017 "Digital Simulation of Seismic Ground Motion," by M. Shinozuka, G. Deodatis and T. Harada, 8/31/87, (PB88-155197, A04, MF-A01). This report is available only through NTIS (see address given above).

NCEER-87-0018 "Practical Considerations for Structural Control: System Uncertainty, System Time Delay and Truncation of Small Control Forces," J.N. Yang and A. Akbarpour, 8/10/87, (PB88-163738, A08, MF-A01). This report is only available through NTIS (see address given above).

NCEER-87-0019 "Modal Analysis of Nonclassically Damped Structural Systems Using Canonical Transformation," by J.N. Yang, S. Sarkani and F.X. Long, 9/27/87, (PB88-187851, A04, MF-A01).

NCEER-87-0020 "A Nonstationary Solution in Random Vibration Theory," by J.R. Red-Horse and P.D. Spanos, 11/3/87, (PB88-163746, A03, MF-A01).

NCEER-87-0021 "Horizontal Impedances for Radially Inhomogeneous Viscoelastic Soil Layers," by A.S. Veletsos and K.W. Dotson, 10/15/87, (PB88-150859, A04, MF-A01).

NCEER-87-0022 "Seismic Damage Assessment of Reinforced Concrete Members," by Y.S. Chung, C. Meyer and M. Shinozuka, 10/9/87, (PB88-150867, A05, MF-A01). This report is available only through NTIS (see address given above).

NCEER-87-0023 "Active Structural Control in Civil Engineering," by T.T. Soong, 11/11/87, (PB88-187778, A03, MF-A01).

NCEER-87-0024 "Vertical and Torsional Impedances for Radially Inhomogeneous Viscoelastic Soil Layers," by K.W. Dotson and A.S. Veletsos, 12/87, (PB88-187786, A03, MF-A01).

NCEER-87-0025 "Proceedings from the Symposium on Seismic Hazards, Ground Motions, Soil-Liquefaction and Engineering Practice in Eastern North America," October 20-22, 1987, edited by K.H. Jacob, 12/87, (PB88-188115, A23, MF-A01).

NCEER-87-0026 "Report on the Whittier-Narrows, California, Earthquake of October 1, 1987," by J. Pantelic and A. Reinhorn, 11/87, (PB88-187752, A03, MF-A01). This report is available only through NTIS (see address given above).

NCEER-87-0027 "Design of a Modular Program for Transient Nonlinear Analysis of Large 3-D Building Structures," by S. Srivastav and J.F. Abel, 12/30/87, (PB88-187950, A05, MF-A01). This report is only available through NTIS (see address given above).

NCEER-87-0028 "Second-Year Program in Research, Education and Technology Transfer," 3/8/88, (PB88-219480, A04, MF-A01).

NCEER-88-0001 "Workshop on Seismic Computer Analysis and Design of Buildings With Interactive Graphics," by W. McGuire, J.F. Abel and C.H. Conley, 1/18/88, (PB88-187760, A03, MF-A01). This report is only available through NTIS (see address given above).

NCEER-88-0002 "Optimal Control of Nonlinear Flexible Structures," by J.N. Yang, F.X. Long and D. Wong, 1/22/88, (PB88-213772, A06, MF-A01).

NCEER-88-0003 "Substructuring Techniques in the Time Domain for Primary-Secondary Structural Systems," by G.D. Manolis and G. Juhn, 2/10/88, (PB88-213780, A04, MF-A01).

NCEER-88-0004 "Iterative Seismic Analysis of Primary-Secondary Systems," by A. Singhal, L.D. Lutes and P.D. Spanos, 2/23/88, (PB88-213798, A04, MF-A01).

NCEER-88-0005 "Stochastic Finite Element Expansion for Random Media," by P.D. Spanos and R. Ghanem, 3/14/88, (PB88-213806, A03, MF-A01).

NCEER-88-0006 "Combining Structural Optimization and Structural Control," by F.Y. Cheng and C.P. Pantelides, 1/10/88, (PB88-213814, A05, MF-A01).

NCEER-88-0007 "Seismic Performance Assessment of Code-Designed Structures," by H.H-M. Hwang, J-W. Jaw and H-J. Shau, 3/20/88, (PB88-219423, A04, MF-A01). This report is only available through NTIS (see address given above).

NCEER-88-0008 "Reliability Analysis of Code-Designed Structures Under Natural Hazards," by H.H-M. Hwang, H. Ushiba and M. Shinozuka, 2/29/88, (PB88-229471, A07, MF-A01). This report is only available through NTIS (see address given above).

NCEER-88-0009 "Seismic Fragility Analysis of Shear Wall Structures," by J-W Jaw and H.H-M. Hwang, 4/30/88, (PB89-102867, A04, MF-A01).

NCEER-88-0010 "Base Isolation of a Multi-Story Building Under a Harmonic Ground Motion - A Comparison of Performances of Various Systems," by F-G Fan, G. Ahmadi and I.G. Tadjbakhsh, 5/18/88, (PB89-122238, A06, MF-A01). This report is only available through NTIS (see address given above).

NCEER-88-0011 "Seismic Floor Response Spectra for a Combined System by Green's Functions," by F.M. Lavelle, L.A. Bergman and P.D. Spanos, 5/1/88, (PB89-102875, A03, MF-A01).

NCEER-88-0012 "A New Solution Technique for Randomly Excited Hysteretic Structures," by G.Q. Cai and Y.K. Lin, 5/16/88, (PB89-102883, A03, MF-A01).

NCEER-88-0013 "A Study of Radiation Damping and Soil-Structure Interaction Effects in the Centrifuge," by K. Weissman, supervised by J.H. Prevost, 5/24/88, (PB89-144703, A06, MF-A01).

NCEER-88-0014 "Parameter Identification and Implementation of a Kinematic Plasticity Model for Frictional Soils," by J.H. Prevost and D.V. Griffiths, to be published.

NCEER-88-0015 "Two- and Three- Dimensional Dynamic Finite Element Analyses of the Long Valley Dam," by D.V. Griffiths and J.H. Prevost, 6/17/88, (PB89-144711, A04, MF-A01).

NCEER-88-0016 "Damage Assessment of Reinforced Concrete Structures in Eastern United States," by A.M. Reinhorn, M.J. Seidel, S.K. Kunnath and Y.J. Park, 6/15/88, (PB89-122220, A04, MF-A01). This report is only available through NTIS (see address given above).

NCEER-88-0017 "Dynamic Compliance of Vertically Loaded Strip Foundations in Multilayered Viscoelastic Soils," by S. Ahmad and A.S.M. Israil, 6/17/88, (PB89-102891, A04, MF-A01).

NCEER-88-0018 "An Experimental Study of Seismic Structural Response With Added Viscoelastic Dampers," by R.C. Lin, Z. Liang, T.T. Soong and R.H. Zhang, 6/30/88, (PB89-122212, A05, MF-A01). This report is available only through NTIS (see address given above).

NCEER-88-0019 "Experimental Investigation of Primary - Secondary System Interaction," by G.D. Manolis, G. Juhn and A.M. Reinhorn, 5/27/88, (PB89-122204, A04, MF-A01).

NCEER-88-0020 "A Response Spectrum Approach For Analysis of Nonclassically Damped Structures," by J.N. Yang, S. Sarkani and F.X. Long, 4/22/88, (PB89-102909, A04, MF-A01).

NCEER-88-0021 "Seismic Interaction of Structures and Soils: Stochastic Approach," by A.S. Veletsos and A.M. Prasad, 7/21/88, (PB89-122196, A04, MF-A01). This report is only available through NTIS (see address given above).

NCEER-88-0022 "Identification of the Serviceability Limit State and Detection of Seismic Structural Damage," by E. DiPasquale and A.S. Cakmak, 6/15/88, (PB89-122188, A05, MF-A01). This report is available only through NTIS (see address given above).

NCEER-88-0023 "Multi-Hazard Risk Analysis: Case of a Simple Offshore Structure," by B.K. Bhartia and E.H. Vanmarcke, 7/21/88, (PB89-145213, A05, MF-A01).

NCEER-88-0024 "Automated Seismic Design of Reinforced Concrete Buildings," by Y.S. Chung, C. Meyer and M. Shinozuka, 7/5/88, (PB89-122170, A06, MF-A01). This report is available only through NTIS (see address given above).

NCEER-88-0025 "Experimental Study of Active Control of MDOF Structures Under Seismic Excitations," by L.L. Chung, R.C. Lin, T.T. Soong and A.M. Reinhorn, 7/10/88, (PB89-122600, A04, MF-A01).

NCEER-88-0026 "Earthquake Simulation Tests of a Low-Rise Metal Structure," by J.S. Hwang, K.C. Chang, G.C. Lee and R.L. Ketter, 8/1/88, (PB89-102917, A04, MF-A01).

NCEER-88-0027 "Systems Study of Urban Response and Reconstruction Due to Catastrophic Earthquakes," by F. Kozin and H.K. Zhou, 9/22/88, (PB90-162348, A04, MF-A01).

NCEER-88-0028 "Seismic Fragility Analysis of Plane Frame Structures," by H.H-M. Hwang and Y.K. Low, 7/31/88, (PB89-131445, A06, MF-A01).

NCEER-88-0029 "Response Analysis of Stochastic Structures," by A. Kardara, C. Bucher and M. Shinozuka, 9/22/88, (PB89-174429, A04, MF-A01).

NCEER-88-0030 "Nonnormal Accelerations Due to Yielding in a Primary Structure," by D.C.K. Chen and L.D. Lutes, 9/19/88, (PB89-131437, A04, MF-A01).

NCEER-88-0031 "Design Approaches for Soil-Structure Interaction," by A.S. Veletsos, A.M. Prasad and Y. Tang, 12/30/88, (PB89-174437, A03, MF-A01). This report is available only through NTIS (see address given above).

NCEER-88-0032 "A Re-evaluation of Design Spectra for Seismic Damage Control," by C.J. Turkstra and A.G. Tallin, 11/7/88, (PB89-145221, A05, MF-A01).

NCEER-88-0033 "The Behavior and Design of Noncontact Lap Splices Subjected to Repeated Inelastic Tensile Loading," by V.E. Sagan, P. Gergely and R.N. White, 12/8/88, (PB89-163737, A08, MF-A01).

NCEER-88-0034 "Seismic Response of Pile Foundations," by S.M. Mamoon, P.K. Banerjee and S. Ahmad, 11/1/88, (PB89-145239, A04, MF-A01).

NCEER-88-0035 "Modeling of R/C Building Structures With Flexible Floor Diaphragms (IDARC2)," by A.M. Reinhorn, S.K. Kunnath and N. Panahshahi, 9/7/88, (PB89-207153, A07, MF-A01).

NCEER-88-0036 "Solution of the Dam-Reservoir Interaction Problem Using a Combination of FEM, BEM with Particular Integrals, Modal Analysis, and Substructuring," by C-S. Tsai, G.C. Lee and R.L. Ketter, 12/31/88, (PB89-207146, A04, MF-A01).

NCEER-88-0037 "Optimal Placement of Actuators for Structural Control," by F.Y. Cheng and C.P. Pantelides, 8/15/88, (PB89-162846, A05, MF-A01).

NCEER-88-0038 "Teflon Bearings in Aseismic Base Isolation: Experimental Studies and Mathematical Modeling," by A. Mokha, M.C. Constantinou and A.M. Reinhorn, 12/5/88, (PB89-218457, A10, MF-A01). This report is available only through NTIS (see address given above).

NCEER-88-0039 "Seismic Behavior of Flat Slab High-Rise Buildings in the New York City Area," by P. Weidlinger and M. Ettouney, 10/15/88, (PB90-145681, A04, MF-A01).

NCEER-88-0040 "Evaluation of the Earthquake Resistance of Existing Buildings in New York City," by P. Weidlinger and M. Ettouney, 10/15/88, to be published.

NCEER-88-0041 "Small-Scale Modeling Techniques for Reinforced Concrete Structures Subjected to Seismic Loads," by W. Kim, A. El-Attar and R.N. White, 11/22/88, (PB89-189625, A05, MF-A01).

NCEER-88-0042 "Modeling Strong Ground Motion from Multiple Event Earthquakes," by G.W. Ellis and A.S. Cakmak, 10/15/88, (PB89-174445, A03, MF-A01).

NCEER-88-0043 "Nonstationary Models of Seismic Ground Acceleration," by M. Grigoriu, S.E. Ruiz and E. Rosenblueth, 7/15/88, (PB89-189617, A04, MF-A01).

NCEER-88-0044 "SARCF User's Guide: Seismic Analysis of Reinforced Concrete Frames," by Y.S. Chung, C. Meyer and M. Shinozuka, 11/9/88, (PB89-174452, A08, MF-A01).

NCEER-88-0045 "First Expert Panel Meeting on Disaster Research and Planning," edited by J. Pantelic and J. Stoyle, 9/15/88, (PB89-174460, A05, MF-A01). This report is only available through NTIS (see address given above).

NCEER-88-0046 "Preliminary Studies of the Effect of Degrading Infill Walls on the Nonlinear Seismic Response of Steel Frames," by C.Z. Chrysostomou, P. Gergely and J.F. Abel, 12/19/88, (PB89-208383, A05, MF-A01).

NCEER-88-0047 "Reinforced Concrete Frame Component Testing Facility - Design, Construction, Instrumentation and Operation," by S.P. Pessiki, C. Conley, T. Bond, P. Gergely and R.N. White, 12/16/88, (PB89-174478, A04, MF-A01).

NCEER-89-0001 "Effects of Protective Cushion and Soil Compliancy on the Response of Equipment Within a Seismically Excited Building," by J.A. HoLung, 2/16/89, (PB89-207179, A04, MF-A01).

NCEER-89-0002 "Statistical Evaluation of Response Modification Factors for Reinforced Concrete Structures," by H.H-M. Hwang and J-W. Jaw, 2/17/89, (PB89-207187, A05, MF-A01).

NCEER-89-0003 "Hysteretic Columns Under Random Excitation," by G-Q. Cai and Y.K. Lin, 1/9/89, (PB89-196513, A03, MF-A01).

NCEER-89-0004 "Experimental Study of `Elephant Foot Bulge' Instability of Thin-Walled Metal Tanks," by Z-H. Jia and R.L. Ketter, 2/22/89, (PB89-207195, A03, MF-A01).

NCEER-89-0005 "Experiment on Performance of Buried Pipelines Across San Andreas Fault," by J. Isenberg, E. Richardson and T.D. O'Rourke, 3/10/89, (PB89-218440, A04, MF-A01). This report is available only through NTIS (see address given above).

NCEER-89-0006 "A Knowledge-Based Approach to Structural Design of Earthquake-Resistant Buildings," by M. Subramani, P. Gergely, C.H. Conley, J.F. Abel and A.H. Zaghw, 1/15/89, (PB89-218465, A06, MF-A01).

NCEER-89-0007 "Liquefaction Hazards and Their Effects on Buried Pipelines," by T.D. O'Rourke and P.A. Lane, 2/1/89, (PB89-218481, A09, MF-A01).

NCEER-89-0008 "Fundamentals of System Identification in Structural Dynamics," by H. Imai, C-B. Yun, O. Maruyama and M. Shinozuka, 1/26/89, (PB89-207211, A04, MF-A01).

NCEER-89-0009 "Effects of the 1985 Michoacan Earthquake on Water Systems and Other Buried Lifelines in Mexico," by A.G. Ayala and M.J. O'Rourke, 3/8/89, (PB89-207229, A06, MF-A01).

NCEER-89-R010 "NCEER Bibliography of Earthquake Education Materials," by K.E.K. Ross, Second Revision, 9/1/89, (PB90-125352, A05, MF-A01). This report is replaced by NCEER-92-0018.

NCEER-89-0011 "Inelastic Three-Dimensional Response Analysis of Reinforced Concrete Building Structures (IDARC-3D), Part I - Modeling," by S.K. Kunnath and A.M. Reinhorn, 4/17/89, (PB90-114612, A07, MF-A01).

NCEER-89-0012 "Recommended Modifications to ATC-14," by C.D. Poland and J.O. Malley, 4/12/89, (PB90-108648, A15, MF-A01).

NCEER-89-0013 "Repair and Strengthening of Beam-to-Column Connections Subjected to Earthquake Loading," by M. Corazao and A.J. Durrani, 2/28/89, (PB90-109885, A06, MF-A01).

NCEER-89-0014 "Program EXKAL2 for Identification of Structural Dynamic Systems," by O. Maruyama, C-B. Yun, M. Hoshiya and M. Shinozuka, 5/19/89, (PB90-109877, A09, MF-A01).

NCEER-89-0015 "Response of Frames With Bolted Semi-Rigid Connections, Part I - Experimental Study and Analytical Predictions," by P.J. DiCorso, A.M. Reinhorn, J.R. Dickerson, J.B. Radziminski and W.L. Harper, 6/1/89, to be published.

NCEER-89-0016 "ARMA Monte Carlo Simulation in Probabilistic Structural Analysis," by P.D. Spanos and M.P. Mignolet, 7/10/89, (PB90-109893, A03, MF-A01).

NCEER-89-P017 "Preliminary Proceedings from the Conference on Disaster Preparedness - The Place of Earthquake Education in Our Schools," Edited by K.E.K. Ross, 6/23/89, (PB90-108606, A03, MF-A01).

NCEER-89-0017 "Proceedings from the Conference on Disaster Preparedness - The Place of Earthquake Education in Our Schools," Edited by K.E.K. Ross, 12/31/89, (PB90-207895, A012, MF-A02). This report is available only through NTIS (see address given above).

NCEER-89-0018 "Multidimensional Models of Hysteretic Material Behavior for Vibration Analysis of Shape Memory Energy Absorbing Devices, by E.J. Graesser and F.A. Cozzarelli, 6/7/89, (PB90-164146, A04, MF-A01).

NCEER-89-0019 "Nonlinear Dynamic Analysis of Three-Dimensional Base Isolated Structures (3D-BASIS)," by S. Nagarajaiah, A.M. Reinhorn and M.C. Constantinou, 8/3/89, (PB90-161936, A06, MF-A01). This report has been replaced by NCEER-93-0011.

NCEER-89-0020 "Structural Control Considering Time-Rate of Control Forces and Control Rate Constraints," by F.Y. Cheng and C.P. Pantelides, 8/3/89, (PB90-120445, A04, MF-A01).

NCEER-89-0021 "Subsurface Conditions of Memphis and Shelby County," by K.W. Ng, T-S. Chang and H-H.M. Hwang, 7/26/89, (PB90-120437, A03, MF-A01).

NCEER-89-0022 "Seismic Wave Propagation Effects on Straight Jointed Buried Pipelines," by K. Elhmadi and M.J. O'Rourke, 8/24/89, (PB90-162322, A10, MF-A02).

NCEER-89-0023 "Workshop on Serviceability Analysis of Water Delivery Systems," edited by M. Grigoriu, 3/6/89, (PB90-127424, A03, MF-A01).

NCEER-89-0024 "Shaking Table Study of a 1/5 Scale Steel Frame Composed of Tapered Members," by K.C. Chang, J.S. Hwang and G.C. Lee, 9/18/89, (PB90-160169, A04, MF-A01).

NCEER-89-0025 "DYNA1D: A Computer Program for Nonlinear Seismic Site Response Analysis - Technical Documentation," by Jean H. Prevost, 9/14/89, (PB90-161944, A07, MF-A01). This report is available only through NTIS (see address given above).

NCEER-89-0026 "1:4 Scale Model Studies of Active Tendon Systems and Active Mass Dampers for Aseismic Protection," by A.M. Reinhorn, T.T. Soong, R.C. Lin, Y.P. Yang, Y. Fukao, H. Abe and M. Nakai, 9/15/89, (PB90-173246, A10, MF-A02).

NCEER-89-0027 "Scattering of Waves by Inclusions in a Nonhomogeneous Elastic Half Space-Solved by Boundary Element Methods," by P.K. Hadley, A. Askar and A.S. Cakmak, 6/15/89, (PB90-145699, A07, MF-A01).

NCEER-89-0028 "Statistical Evaluation of Deflection Amplification Factors for Reinforced Concrete Structures," by H.H.M. Hwang, J-W. Jaw and A.L. Ch'ng, 8/31/89, (PB90-164633, A05, MF-A01).

NCEER-89-0029 "Bedrock Accelerations in Memphis Area Due to Large New Madrid Earthquakes," by H.H.M. Hwang, C.H.S. Chen and G. Yu, 11/7/89, (PB90-162330, A04, MF-A01).

NCEER-89-0030 "Seismic Behavior and Response Sensitivity of Secondary Structural Systems," by Y.Q. Chen and T.T. Soong, 10/23/89, (PB90-164658, A08, MF-A01).

NCEER-89-0031 "Random Vibration and Reliability Analysis of Primary-Secondary Structural Systems," by Y. Ibrahim, M. Grigoriu and T.T. Soong, 11/10/89, (PB90-161951, A04, MF-A01).

NCEER-89-0032 "Proceedings from the Second U.S. - Japan Workshop on Liquefaction, Large Ground Deformation and Their Effects on Lifelines, September 26-29, 1989," Edited by T.D. O'Rourke and M. Hamada, 12/1/89, (PB90-209388, A22, MF-A03).

NCEER-89-0033 "Deterministic Model for Seismic Damage Evaluation of Reinforced Concrete Structures," by J.M. Bracci, A.M. Reinhorn, J.B. Mander and S.K. Kunnath, 9/27/89, (PB91-108803, A06, MF-A01).

NCEER-89-0034 "On the Relation Between Local and Global Damage Indices," by E. DiPasquale and A.S. Cakmak, 8/15/89, (PB90-173865, A05, MF-A01).

NCEER-89-0035 "Cyclic Undrained Behavior of Nonplastic and Low Plasticity Silts," by A.J. Walker and H.E. Stewart, 7/26/89, (PB90-183518, A10, MF-A01).

NCEER-89-0036 "Liquefaction Potential of Surficial Deposits in the City of Buffalo, New York," by M. Budhu, R. Giese and L. Baumgrass, 1/17/89, (PB90-208455, A04, MF-A01).

NCEER-89-0037 "A Deterministic Assessment of Effects of Ground Motion Incoherence," by A.S. Veletsos and Y. Tang, 7/15/89, (PB90-164294, A03, MF-A01).

NCEER-89-0038 "Workshop on Ground Motion Parameters for Seismic Hazard Mapping," July 17-18, 1989, edited by R.V. Whitman, 12/1/89, (PB90-173923, A04, MF-A01).

NCEER-89-0039 "Seismic Effects on Elevated Transit Lines of the New York City Transit Authority," by C.J. Costantino, C.A. Miller and E. Heymsfield, 12/26/89, (PB90-207887, A06, MF-A01).

NCEER-89-0040 "Centrifugal Modeling of Dynamic Soil-Structure Interaction," by K. Weissman, Supervised by J.H. Prevost, 5/10/89, (PB90-207879, A07, MF-A01).

NCEER-89-0041 "Linearized Identification of Buildings With Cores for Seismic Vulnerability Assessment," by I-K. Ho and A.E. Aktan, 11/1/89, (PB90-251943, A07, MF-A01).

NCEER-90-0001 "Geotechnical and Lifeline Aspects of the October 17, 1989 Loma Prieta Earthquake in San Francisco," by T.D. O'Rourke, H.E. Stewart, F.T. Blackburn and T.S. Dickerman, 1/90, (PB90-208596, A05, MF-A01).

NCEER-90-0002 "Nonnormal Secondary Response Due to Yielding in a Primary Structure," by D.C.K. Chen and L.D. Lutes, 2/28/90, (PB90-251976, A07, MF-A01).

NCEER-90-0003 "Earthquake Education Materials for Grades K-12," by K.E.K. Ross, 4/16/90, (PB91-251984, A05, MF-A05). This report has been replaced by NCEER-92-0018.

NCEER-90-0004 "Catalog of Strong Motion Stations in Eastern North America," by R.W. Busby, 4/3/90, (PB90-251984, A05, MF-A01).

NCEER-90-0005 "NCEER Strong-Motion Data Base: A User Manual for the GeoBase Release (Version 1.0 for the Sun3)," by P. Friberg and K. Jacob, 3/31/90 (PB90-258062, A04, MF-A01).

NCEER-90-0006 "Seismic Hazard Along a Crude Oil Pipeline in the Event of an 1811-1812 Type New Madrid Earthquake," by H.H.M. Hwang and C-H.S. Chen, 4/16/90, (PB90-258054, A04, MF-A01).

NCEER-90-0007 "Site-Specific Response Spectra for Memphis Sheahan Pumping Station," by H.H.M. Hwang and C.S. Lee, 5/15/90, (PB91-108811, A05, MF-A01).

NCEER-90-0008 "Pilot Study on Seismic Vulnerability of Crude Oil Transmission Systems," by T. Ariman, R. Dobry, M. Grigoriu, F. Kozin, M. O'Rourke, T. O'Rourke and M. Shinozuka, 5/25/90, (PB91-108837, A06, MF-A01).

NCEER-90-0009 "A Program to Generate Site Dependent Time Histories: EQGEN," by G.W. Ellis, M. Srinivasan and A.S. Cakmak, 1/30/90, (PB91-108829, A04, MF-A01).

NCEER-90-0010 "Active Isolation for Seismic Protection of Operating Rooms," by M.E. Talbott, Supervised by M. Shinozuka, 6/8/9, (PB91-110205, A05, MF-A01).

NCEER-90-0011 "Program LINEARID for Identification of Linear Structural Dynamic Systems," by C-B. Yun and M. Shinozuka, 6/25/90, (PB91-110312, A08, MF-A01).

NCEER-90-0012 "Two-Dimensional Two-Phase Elasto-Plastic Seismic Response of Earth Dams," by A.N. Yiagos, Supervised by J.H. Prevost, 6/20/90, (PB91-110197, A13, MF-A02).

NCEER-90-0013 "Secondary Systems in Base-Isolated Structures: Experimental Investigation, Stochastic Response and Stochastic Sensitivity," by G.D. Manolis, G. Juhn, M.C. Constantinou and A.M. Reinhorn, 7/1/90, (PB91-110320, A08, MF-A01).

NCEER-90-0014 "Seismic Behavior of Lightly-Reinforced Concrete Column and Beam-Column Joint Details," by S.P. Pessiki, C.H. Conley, P. Gergely and R.N. White, 8/22/90, (PB91-108795, A11, MF-A02).

NCEER-90-0015 "Two Hybrid Control Systems for Building Structures Under Strong Earthquakes," by J.N. Yang and A. Danielians, 6/29/90, (PB91-125393, A04, MF-A01).

NCEER-90-0016 "Instantaneous Optimal Control with Acceleration and Velocity Feedback," by J.N. Yang and Z. Li, 6/29/90, (PB91-125401, A03, MF-A01).

NCEER-90-0017 "Reconnaissance Report on the Northern Iran Earthquake of June 21, 1990," by M. Mehrain, 10/4/90, (PB91-125377, A03, MF-A01).

NCEER-90-0018 "Evaluation of Liquefaction Potential in Memphis and Shelby County," by T.S. Chang, P.S. Tang, C.S. Lee and H. Hwang, 8/10/90, (PB91-125427, A09, MF-A01).

NCEER-90-0019 "Experimental and Analytical Study of a Combined Sliding Disc Bearing and Helical Steel Spring Isolation System," by M.C. Constantinou, A.S. Mokha and A.M. Reinhorn, 10/4/90, (PB91-125385, A06, MF-A01). This report is available only through NTIS (see address given above).

NCEER-90-0020 "Experimental Study and Analytical Prediction of Earthquake Response of a Sliding Isolation System with a Spherical Surface," by A.S. Mokha, M.C. Constantinou and A.M. Reinhorn, 10/11/90, (PB91-125419, A05, MF-A01).

NCEER-90-0021 "Dynamic Interaction Factors for Floating Pile Groups," by G. Gazetas, K. Fan, A. Kaynia and E. Kausel, 9/10/90, (PB91-170381, A05, MF-A01).

NCEER-90-0022 "Evaluation of Seismic Damage Indices for Reinforced Concrete Structures," by S. Rodriguez-Gomez and A.S. Cakmak, 9/30/90, PB91-171322, A06, MF-A01).

NCEER-90-0023 "Study of Site Response at a Selected Memphis Site," by H. Desai, S. Ahmad, E.S. Gazetas and M.R. Oh, 10/11/90, (PB91-196857, A03, MF-A01).

NCEER-90-0024 "A User's Guide to Strongmo: Version 1.0 of NCEER's Strong-Motion Data Access Tool for PCs and Terminals," by P.A. Friberg and C.A.T. Susch, 11/15/90, (PB91-171272, A03, MF-A01).

NCEER-90-0025 "A Three-Dimensional Analytical Study of Spatial Variability of Seismic Ground Motions," by L-L. Hong and A.H.-S. Ang, 10/30/90, (PB91-170399, A09, MF-A01).

NCEER-90-0026 "MUMOID User's Guide - A Program for the Identification of Modal Parameters," by S. Rodriguez-Gomez and E. DiPasquale, 9/30/90, (PB91-171298, A04, MF-A01).

NCEER-90-0027 "SARCF-II User's Guide - Seismic Analysis of Reinforced Concrete Frames," by S. Rodriguez-Gomez, Y.S. Chung and C. Meyer, 9/30/90, (PB91-171280, A05, MF-A01).

NCEER-90-0028 "Viscous Dampers: Testing, Modeling and Application in Vibration and Seismic Isolation," by N. Makris and M.C. Constantinou, 12/20/90 (PB91-190561, A06, MF-A01).

NCEER-90-0029 "Soil Effects on Earthquake Ground Motions in the Memphis Area," by H. Hwang, C.S. Lee, K.W. Ng and T.S. Chang, 8/2/90, (PB91-190751, A05, MF-A01).

NCEER-91-0001 "Proceedings from the Third Japan-U.S. Workshop on Earthquake Resistant Design of Lifeline Facilities and Countermeasures for Soil Liquefaction, December 17-19, 1990," edited by T.D. O'Rourke and M. Hamada, 2/1/91, (PB91-179259, A99, MF-A04).

NCEER-91-0002 "Physical Space Solutions of Non-Proportionally Damped Systems," by M. Tong, Z. Liang and G.C. Lee, 1/15/91, (PB91-179242, A04, MF-A01).

NCEER-91-0003 "Seismic Response of Single Piles and Pile Groups," by K. Fan and G. Gazetas, 1/10/91, (PB92-174994, A04, MF-A01).

NCEER-91-0004 "Damping of Structures: Part 1 - Theory of Complex Damping," by Z. Liang and G. Lee, 10/10/91, (PB92-197235, A12, MF-A03).

NCEER-91-0005 "3D-BASIS - Nonlinear Dynamic Analysis of Three Dimensional Base Isolated Structures: Part II," by S. Nagarajaiah, A.M. Reinhorn and M.C. Constantinou, 2/28/91, (PB91-190553, A07, MF-A01). This report has been replaced by NCEER-93-0011.

NCEER-91-0006 "A Multidimensional Hysteretic Model for Plasticity Deforming Metals in Energy Absorbing Devices," by E.J. Graesser and F.A. Cozzarelli, 4/9/91, (PB92-108364, A04, MF-A01).

NCEER-91-0007 "A Framework for Customizable Knowledge-Based Expert Systems with an Application to a KBES for Evaluating the Seismic Resistance of Existing Buildings," by E.G. Ibarra-Anaya and S.J. Fenves, 4/9/91, (PB91-210930, A08, MF-A01).

NCEER-91-0008 "Nonlinear Analysis of Steel Frames with Semi-Rigid Connections Using the Capacity Spectrum Method," by G.G. Deierlein, S-H. Hsieh, Y-J. Shen and J.F. Abel, 7/2/91, (PB92-113828, A05, MF-A01).

NCEER-91-0009 "Earthquake Education Materials for Grades K-12," by K.E.K. Ross, 4/30/91, (PB91-212142, A06, MF-A01). This report has been replaced by NCEER-92-0018.

NCEER-91-0010 "Phase Wave Velocities and Displacement Phase Differences in a Harmonically Oscillating Pile," by N. Makris and G. Gazetas, 7/8/91, (PB92-108356, A04, MF-A01).

NCEER-91-0011 "Dynamic Characteristics of a Full-Size Five-Story Steel Structure and a 2/5 Scale Model," by K.C. Chang, G.C. Yao, G.C. Lee, D.S. Hao and Y.C. Yeh," 7/2/91, (PB93-116648, A06, MF-A02).

NCEER-91-0012 "Seismic Response of a 2/5 Scale Steel Structure with Added Viscoelastic Dampers," by K.C. Chang, T.T. Soong, S-T. Oh and M.L. Lai, 5/17/91, (PB92-110816, A05, MF-A01).

NCEER-91-0013 "Earthquake Response of Retaining Walls; Full-Scale Testing and Computational Modeling," by S. Alampalli and A-W.M. Elgamal, 6/20/91, to be published.

NCEER-91-0014 "3D-BASIS-M: Nonlinear Dynamic Analysis of Multiple Building Base Isolated Structures," by P.C. Tsopelas, S. Nagarajaiah, M.C. Constantinou and A.M. Reinhorn, 5/28/91, (PB92-113885, A09, MF-A02).

NCEER-91-0015 "Evaluation of SEAOC Design Requirements for Sliding Isolated Structures," by D. Theodossiou and M.C. Constantinou, 6/10/91, (PB92-114602, A11, MF-A03).

NCEER-91-0016 "Closed-Loop Modal Testing of a 27-Story Reinforced Concrete Flat Plate-Core Building," by H.R. Somaprasad, T. Toksoy, H. Yoshiyuki and A.E. Aktan, 7/15/91, (PB92-129980, A07, MF-A02).

NCEER-91-0017 "Shake Table Test of a 1/6 Scale Two-Story Lightly Reinforced Concrete Building," by A.G. El-Attar, R.N. White and P. Gergely, 2/28/91, (PB92-222447, A06, MF-A02).

NCEER-91-0018 "Shake Table Test of a 1/8 Scale Three-Story Lightly Reinforced Concrete Building," by A.G. El-Attar, R.N. White and P. Gergely, 2/28/91, (PB93-116630, A08, MF-A02).

NCEER-91-0019 "Transfer Functions for Rigid Rectangular Foundations," by A.S. Veletsos, A.M. Prasad and W.H. Wu, 7/31/91, to be published.

NCEER-91-0020 "Hybrid Control of Seismic-Excited Nonlinear and Inelastic Structural Systems," by J.N. Yang, Z. Li and A. Danielians, 8/1/91, (PB92-143171, A06, MF-A02).

NCEER-91-0021 "The NCEER-91 Earthquake Catalog: Improved Intensity-Based Magnitudes and Recurrence Relations for U.S. Earthquakes East of New Madrid," by L. Seeber and J.G. Armbruster, 8/28/91, (PB92-176742, A06, MF-A02).

NCEER-91-0022 "Proceedings from the Implementation of Earthquake Planning and Education in Schools: The Need for Change - The Roles of the Changemakers," by K.E.K. Ross and F. Winslow, 7/23/91, (PB92-129998, A12, MF-A03).

NCEER-91-0023 "A Study of Reliability-Based Criteria for Seismic Design of Reinforced Concrete Frame Buildings," by H.H.M. Hwang and H-M. Hsu, 8/10/91, (PB92-140235, A09, MF-A02).

NCEER-91-0024 "Experimental Verification of a Number of Structural System Identification Algorithms," by R.G. Ghanem, H. Gavin and M. Shinozuka, 9/18/91, (PB92-176577, A18, MF-A04).

NCEER-91-0025 "Probabilistic Evaluation of Liquefaction Potential," by H.H.M. Hwang and C.S. Lee," 11/25/91, (PB92-143429, A05, MF-A01).

NCEER-91-0026 "Instantaneous Optimal Control for Linear, Nonlinear and Hysteretic Structures - Stable Controllers," by J.N. Yang and Z. Li, 11/15/91, (PB92-163807, A04, MF-A01).

NCEER-91-0027 "Experimental and Theoretical Study of a Sliding Isolation System for Bridges," by M.C. Constantinou, A. Kartoum, A.M. Reinhorn and P. Bradford, 11/15/91, (PB92-176973, A10, MF-A03).

NCEER-92-0001 "Case Studies of Liquefaction and Lifeline Performance During Past Earthquakes, Volume 1: Japanese Case Studies," Edited by M. Hamada and T. O'Rourke, 2/17/92, (PB92-197243, A18, MF-A04).

NCEER-92-0002 "Case Studies of Liquefaction and Lifeline Performance During Past Earthquakes, Volume 2: United States Case Studies," Edited by T. O'Rourke and M. Hamada, 2/17/92, (PB92-197250, A20, MF-A04).

NCEER-92-0003 "Issues in Earthquake Education," Edited by K. Ross, 2/3/92, (PB92-222389, A07, MF-A02).

NCEER-92-0004 "Proceedings from the First U.S. - Japan Workshop on Earthquake Protective Systems for Bridges," Edited by I.G. Buckle, 2/4/92, (PB94-142239, A99, MF-A06).

NCEER-92-0005 "Seismic Ground Motion from a Haskell-Type Source in a Multiple-Layered Half-Space," A.P. Theoharis, G. Deodatis and M. Shinozuka, 1/2/92, to be published.

NCEER-92-0006 "Proceedings from the Site Effects Workshop," Edited by R. Whitman, 2/29/92, (PB92-197201, A04, MF-A01).

NCEER-92-0007 "Engineering Evaluation of Permanent Ground Deformations Due to Seismically-Induced Liquefaction," by M.H. Baziar, R. Dobry and A-W.M. Elgamal, 3/24/92, (PB92-222421, A13, MF-A03).

NCEER-92-0008 "A Procedure for the Seismic Evaluation of Buildings in the Central and Eastern United States," by C.D. Poland and J.O. Malley, 4/2/92, (PB92-222439, A20, MF-A04).

NCEER-92-0009 "Experimental and Analytical Study of a Hybrid Isolation System Using Friction Controllable Sliding Bearings," by M.Q. Feng, S. Fujii and M. Shinozuka, 5/15/92, (PB93-150282, A06, MF-A02).

NCEER-92-0010 "Seismic Resistance of Slab-Column Connections in Existing Non-Ductile Flat-Plate Buildings," by A.J. Durrani and Y. Du, 5/18/92, (PB93-116812, A06, MF-A02).

NCEER-92-0011 "The Hysteretic and Dynamic Behavior of Brick Masonry Walls Upgraded by Ferrocement Coatings Under Cyclic Loading and Strong Simulated Ground Motion," by H. Lee and S.P. Prawel, 5/11/92, to be published.

NCEER-92-0012 "Study of Wire Rope Systems for Seismic Protection of Equipment in Buildings," by G.F. Demetriades, M.C. Constantinou and A.M. Reinhorn, 5/20/92, (PB93-116655, A08, MF-A02).

NCEER-92-0013 "Shape Memory Structural Dampers: Material Properties, Design and Seismic Testing," by P.R. Witting and F.A. Cozzarelli, 5/26/92, (PB93-116663, A05, MF-A01).

NCEER-92-0014 "Longitudinal Permanent Ground Deformation Effects on Buried Continuous Pipelines," by M.J. O'Rourke, and C. Nordberg, 6/15/92, (PB93-116671, A08, MF-A02).

NCEER-92-0015 "A Simulation Method for Stationary Gaussian Random Functions Based on the Sampling Theorem," by M. Grigoriu and S. Balopoulou, 6/11/92, (PB93-127496, A05, MF-A01).

NCEER-92-0016 "Gravity-Load-Designed Reinforced Concrete Buildings: Seismic Evaluation of Existing Construction and Detailing Strategies for Improved Seismic Resistance," by G.W. Hoffmann, S.K. Kunnath, A.M. Reinhorn and J.B. Mander, 7/15/92, (PB94-142007, A08, MF-A02).

NCEER-92-0017 "Observations on Water System and Pipeline Performance in the Limón Area of Costa Rica Due to the April 22, 1991 Earthquake," by M. O'Rourke and D. Ballantyne, 6/30/92, (PB93-126811, A06, MF-A02).

NCEER-92-0018 "Fourth Edition of Earthquake Education Materials for Grades K-12," Edited by K.E.K. Ross, 8/10/92, (PB93-114023, A07, MF-A02).

NCEER-92-0019 "Proceedings from the Fourth Japan-U.S. Workshop on Earthquake Resistant Design of Lifeline Facilities and Countermeasures for Soil Liquefaction," Edited by M. Hamada and T.D. O'Rourke, 8/12/92, (PB93-163939, A99, MF-E11).

NCEER-92-0020 "Active Bracing System: A Full Scale Implementation of Active Control," by A.M. Reinhorn, T.T. Soong, R.C. Lin, M.A. Riley, Y.P. Wang, S. Aizawa and M. Higashino, 8/14/92, (PB93-127512, A06, MF-A02).

NCEER-92-0021 "Empirical Analysis of Horizontal Ground Displacement Generated by Liquefaction-Induced Lateral Spreads," by S.F. Bartlett and T.L. Youd, 8/17/92, (PB93-188241, A06, MF-A02).

NCEER-92-0022 "IDARC Version 3.0: Inelastic Damage Analysis of Reinforced Concrete Structures," by S.K. Kunnath, A.M. Reinhorn and R.F. Lobo, 8/31/92, (PB93-227502, A07, MF-A02).

NCEER-92-0023 "A Semi-Empirical Analysis of Strong-Motion Peaks in Terms of Seismic Source, Propagation Path and Local Site Conditions, by M. Kamiyama, M.J. O'Rourke and R. Flores-Berrones, 9/9/92, (PB93-150266, A08, MF-A02).

NCEER-92-0024 "Seismic Behavior of Reinforced Concrete Frame Structures with Nonductile Details, Part I: Summary of Experimental Findings of Full Scale Beam-Column Joint Tests," by A. Beres, R.N. White and P. Gergely, 9/30/92, (PB93-227783, A05, MF-A01).

NCEER-92-0025 "Experimental Results of Repaired and Retrofitted Beam-Column Joint Tests in Lightly Reinforced Concrete Frame Buildings," by A. Beres, S. El-Borgi, R.N. White and P. Gergely, 10/29/92, (PB93-227791, A05, MF-A01).

NCEER-92-0026 "A Generalization of Optimal Control Theory: Linear and Nonlinear Structures," by J.N. Yang, Z. Li and S. Vongchavalitkul, 11/2/92, (PB93-188621, A05, MF-A01).

NCEER-92-0027 "Seismic Resistance of Reinforced Concrete Frame Structures Designed Only for Gravity Loads: Part I - Design and Properties of a One-Third Scale Model Structure," by J.M. Bracci, A.M. Reinhorn and J.B. Mander, 12/1/92, (PB94-104502, A08, MF-A02).

NCEER-92-0028 "Seismic Resistance of Reinforced Concrete Frame Structures Designed Only for Gravity Loads: Part II - Experimental Performance of Subassemblages," by L.E. Aycardi, J.B. Mander and A.M. Reinhorn, 12/1/92, (PB94-104510, A08, MF-A02).

NCEER-92-0029 "Seismic Resistance of Reinforced Concrete Frame Structures Designed Only for Gravity Loads: Part III - Experimental Performance and Analytical Study of a Structural Model," by J.M. Bracci, A.M. Reinhorn and J.B. Mander, 12/1/92, (PB93-227528, A09, MF-A01).

NCEER-92-0030 "Evaluation of Seismic Retrofit of Reinforced Concrete Frame Structures: Part I - Experimental Performance of Retrofitted Subassemblages," by D. Choudhuri, J.B. Mander and A.M. Reinhorn, 12/8/92, (PB93-198307, A07, MF-A02).

NCEER-92-0031 "Evaluation of Seismic Retrofit of Reinforced Concrete Frame Structures: Part II - Experimental Performance and Analytical Study of a Retrofitted Structural Model," by J.M. Bracci, A.M. Reinhorn and J.B. Mander, 12/8/92, (PB93-198315, A09, MF-A03).

NCEER-92-0032 "Experimental and Analytical Investigation of Seismic Response of Structures with Supplemental Fluid Viscous Dampers," by M.C. Constantinou and M.D. Symans, 12/21/92, (PB93-191435, A10, MF-A03).

NCEER-92-0033 "Reconnaissance Report on the Cairo, Egypt Earthquake of October 12, 1992," by M. Khater, 12/23/92, (PB93-188621, A03, MF-A01).

NCEER-92-0034 "Low-Level Dynamic Characteristics of Four Tall Flat-Plate Buildings in New York City," by H. Gavin, S. Yuan, J. Grossman, E. Pekelis and K. Jacob, 12/28/92, (PB93-188217, A07, MF-A02).

NCEER-93-0001 "An Experimental Study on the Seismic Performance of Brick-Infilled Steel Frames With and Without Retrofit," by J.B. Mander, B. Nair, K. Wojtkowski and J. Ma, 1/29/93, (PB93-227510, A07, MF-A02).

NCEER-93-0002 "Social Accounting for Disaster Preparedness and Recovery Planning," by S. Cole, E. Pantoja and V. Razak, 2/22/93, (PB94-142114, A12, MF-A03).

NCEER-93-0003 "Assessment of 1991 NEHRP Provisions for Nonstructural Components and Recommended Revisions," by T.T. Soong, G. Chen, Z. Wu, R-H. Zhang and M. Grigoriu, 3/1/93, (PB93-188639, A06, MF-A02).

NCEER-93-0004 "Evaluation of Static and Response Spectrum Analysis Procedures of SEAOC/UBC for Seismic Isolated Structures," by C.W. Winters and M.C. Constantinou, 3/23/93, (PB93-198299, A10, MF-A03).

NCEER-93-0005 "Earthquakes in the Northeast - Are We Ignoring the Hazard? A Workshop on Earthquake Science and Safety for Educators," edited by K.E.K. Ross, 4/2/93, (PB94-103066, A09, MF-A02).

NCEER-93-0006 "Inelastic Response of Reinforced Concrete Structures with Viscoelastic Braces," by R.F. Lobo, J.M. Bracci, K.L. Shen, A.M. Reinhorn and T.T. Soong, 4/5/93, (PB93-227486, A05, MF-A02).

NCEER-93-0007 "Seismic Testing of Installation Methods for Computers and Data Processing Equipment," by K. Kosar, T.T. Soong, K.L. Shen, J.A. HoLung and Y.K. Lin, 4/12/93, (PB93-198299, A07, MF-A02).

NCEER-93-0008 "Retrofit of Reinforced Concrete Frames Using Added Dampers," by A. Reinhorn, M. Constantinou and C. Li, to be published.

NCEER-93-0009 "Seismic Behavior and Design Guidelines for Steel Frame Structures with Added Viscoelastic Dampers," by K.C. Chang, M.L. Lai, T.T. Soong, D.S. Hao and Y.C. Yeh, 5/1/93, (PB94-141959, A07, MF-A02).

NCEER-93-0010 "Seismic Performance of Shear-Critical Reinforced Concrete Bridge Piers," by J.B. Mander, S.M. Waheed, M.T.A. Chaudhary and S.S. Chen, 5/12/93, (PB93-227494, A08, MF-A02).

NCEER-93-0011 "3D-BASIS-TABS: Computer Program for Nonlinear Dynamic Analysis of Three Dimensional Base Isolated Structures," by S. Nagarajaiah, C. Li, A.M. Reinhorn and M.C. Constantinou, 8/2/93, (PB94-141819, A09, MF-A02).

NCEER-93-0012 "Effects of Hydrocarbon Spills from an Oil Pipeline Break on Ground Water," by O.J. Helweg and H.H.M. Hwang, 8/3/93, (PB94-141942, A06, MF-A02).

NCEER-93-0013 "Simplified Procedures for Seismic Design of Nonstructural Components and Assessment of Current Code Provisions," by M.P. Singh, L.E. Suarez, E.E. Matheu and G.O. Maldonado, 8/4/93, (PB94-141827, A09, MF-A02).

NCEER-93-0014 "An Energy Approach to Seismic Analysis and Design of Secondary Systems," by G. Chen and T.T. Soong, 8/6/93, (PB94-142767, A11, MF-A03).

NCEER-93-0015 "Proceedings from School Sites: Becoming Prepared for Earthquakes - Commemorating the Third Anniversary of the Loma Prieta Earthquake," Edited by F.E. Winslow and K.E.K. Ross, 8/16/93, (PB94-154275, A16, MF-A02).

NCEER-93-0016 "Reconnaissance Report of Damage to Historic Monuments in Cairo, Egypt Following the October 12, 1992 Dahshur Earthquake," by D. Sykora, D. Look, G. Croci, E. Karaesmen and E. Karaesmen, 8/19/93, (PB94-142221, A08, MF-A02).

NCEER-93-0017 "The Island of Guam Earthquake of August 8, 1993," by S.W. Swan and S.K. Harris, 9/30/93, (PB94-141843, A04, MF-A01).

NCEER-93-0018 "Engineering Aspects of the October 12, 1992 Egyptian Earthquake," by A.W. Elgamal, M. Amer, K. Adalier and A. Abul-Fadl, 10/7/93, (PB94-141983, A05, MF-A01).

NCEER-93-0019 "Development of an Earthquake Motion Simulator and its Application in Dynamic Centrifuge Testing," by I. Krstelj, Supervised by J.H. Prevost, 10/23/93, (PB94-181773, A-10, MF-A03).

NCEER-93-0020 "NCEER-Taisei Corporation Research Program on Sliding Seismic Isolation Systems for Bridges: Experimental and Analytical Study of a Friction Pendulum System (FPS)," by M.C. Constantinou, P. Tsopelas, Y-S. Kim and S. Okamoto, 11/1/93, (PB94-142775, A08, MF-A02).

NCEER-93-0021 "Finite Element Modeling of Elastomeric Seismic Isolation Bearings," by L.J. Billings, Supervised by R. Shepherd, 11/8/93, to be published.

NCEER-93-0022 "Seismic Vulnerability of Equipment in Critical Facilities: Life-Safety and Operational Consequences," by K. Porter, G.S. Johnson, M.M. Zadeh, C. Scawthorn and S. Eder, 11/24/93, (PB94-181765, A16, MF-A03).

NCEER-93-0023 "Hokkaido Nansei-oki, Japan Earthquake of July 12, 1993, by P.I. Yanev and C.R. Scawthorn, 12/23/93, (PB94-181500, A07, MF-A01).

NCEER-94-0001 "An Evaluation of Seismic Serviceability of Water Supply Networks with Application to the San Francisco Auxiliary Water Supply System," by I. Markov, Supervised by M. Grigoriu and T. O'Rourke, 1/21/94, (PB94-204013, A07, MF-A02).

NCEER-94-0002 "NCEER-Taisei Corporation Research Program on Sliding Seismic Isolation Systems for Bridges: Experimental and Analytical Study of Systems Consisting of Sliding Bearings, Rubber Restoring Force Devices and Fluid Dampers," Volumes I and II, by P. Tsopelas, S. Okamoto, M.C. Constantinou, D. Ozaki and S. Fujii, 2/4/94, (PB94-181740, A09, MF-A02 and PB94-181757, A12, MF-A03).

NCEER-94-0003 "A Markov Model for Local and Global Damage Indices in Seismic Analysis," by S. Rahman and M. Grigoriu, 2/18/94, (PB94-206000, A12, MF-A03).

NCEER-94-0004 "Proceedings from the NCEER Workshop on Seismic Response of Masonry Infills," edited by D.P. Abrams, 3/1/94, (PB94-180783, A07, MF-A02).

NCEER-94-0005 "The Northridge, California Earthquake of January 17, 1994: General Reconnaissance Report," edited by J.D. Goltz, 3/11/94, (PB193943, A10, MF-A03).

NCEER-94-0006 "Seismic Energy Based Fatigue Damage Analysis of Bridge Columns: Part I - Evaluation of Seismic Capacity," by G.A. Chang and J.B. Mander, 3/14/94, (PB94-219185, A11, MF-A03).

NCEER-94-0007 "Seismic Isolation of Multi-Story Frame Structures Using Spherical Sliding Isolation Systems," by T.M. Al-Hussaini, V.A. Zayas and M.C. Constantinou, 3/17/94, (PB193745, A09, MF-A02).

NCEER-94-0008 "The Northridge, California Earthquake of January 17, 1994: Performance of Highway Bridges," edited by I.G. Buckle, 3/24/94, (PB94-193851, A06, MF-A02).

NCEER-94-0009 "Proceedings of the Third U.S.-Japan Workshop on Earthquake Protective Systems for Bridges," edited by I.G. Buckle and I. Friedland, 3/31/94, (PB94-195815, A99, MF-A06).

NCEER-94-0010 "3D-BASIS-ME: Computer Program for Nonlinear Dynamic Analysis of Seismically Isolated Single and Multiple Structures and Liquid Storage Tanks," by P.C. Tsopelas, M.C. Constantinou and A.M. Reinhorn, 4/12/94, (PB94-204922, A09, MF-A02).

NCEER-94-0011 "The Northridge, California Earthquake of January 17, 1994: Performance of Gas Transmission Pipelines," by T.D. O'Rourke and M.C. Palmer, 5/16/94, (PB94-204989, A05, MF-A01).

NCEER-94-0012 "Feasibility Study of Replacement Procedures and Earthquake Performance Related to Gas Transmission Pipelines," by T.D. O'Rourke and M.C. Palmer, 5/25/94, (PB94-206638, A09, MF-A02).

NCEER-94-0013 "Seismic Energy Based Fatigue Damage Analysis of Bridge Columns: Part II - Evaluation of Seismic Demand," by G.A. Chang and J.B. Mander, 6/1/94, (PB95-18106, A08, MF-A02).

NCEER-94-0014 "NCEER-Taisei Corporation Research Program on Sliding Seismic Isolation Systems for Bridges: Experimental and Analytical Study of a System Consisting of Sliding Bearings and Fluid Restoring Force/Damping Devices," by P. Tsopelas and M.C. Constantinou, 6/13/94, (PB94-219144, A10, MF-A03).

NCEER-94-0015 "Generation of Hazard-Consistent Fragility Curves for Seismic Loss Estimation Studies," by H. Hwang and J-R. Huo, 6/14/94, (PB95-181996, A09, MF-A02).

NCEER-94-0016 "Seismic Study of Building Frames with Added Energy-Absorbing Devices," by W.S. Pong, C.S. Tsai and G.C. Lee, 6/20/94, (PB94-219136, A10, A03).

NCEER-94-0017 "Sliding Mode Control for Seismic-Excited Linear and Nonlinear Civil Engineering Structures," by J. Yang, J. Wu, A. Agrawal and Z. Li, 6/21/94, (PB95-138483, A06, MF-A02).

NCEER-94-0018 "3D-BASIS-TABS Version 2.0: Computer Program for Nonlinear Dynamic Analysis of Three Dimensional Base Isolated Structures," by A.M. Reinhorn, S. Nagarajaiah, M.C. Constantinou, P. Tsopelas and R. Li, 6/22/94, (PB95-182176, A08, MF-A02).

NCEER-94-0019 "Proceedings of the International Workshop on Civil Infrastructure Systems: Application of Intelligent Systems and Advanced Materials on Bridge Systems," Edited by G.C. Lee and K.C. Chang, 7/18/94, (PB95-252474, A20, MF-A04).

NCEER-94-0020 "Study of Seismic Isolation Systems for Computer Floors," by V. Lambrou and M.C. Constantinou, 7/19/94, (PB95-138533, A10, MF-A03).

NCEER-94-0021 "Proceedings of the U.S.-Italian Workshop on Guidelines for Seismic Evaluation and Rehabilitation of Unreinforced Masonry Buildings," Edited by D.P. Abrams and G.M. Calvi, 7/20/94, (PB95-138749, A13, MF-A03).

NCEER-94-0022 "NCEER-Taisei Corporation Research Program on Sliding Seismic Isolation Systems for Bridges: Experimental and Analytical Study of a System Consisting of Lubricated PTFE Sliding Bearings and Mild Steel Dampers," by P. Tsopelas and M.C. Constantinou, 7/22/94, (PB95-182184, A08, MF-A02).

NCEER-94-0023 "Development of Reliability-Based Design Criteria for Buildings Under Seismic Load," by Y.K. Wen, H. Hwang and M. Shinozuka, 8/1/94, (PB95-211934, A08, MF-A02).

NCEER-94-0024 "Experimental Verification of Acceleration Feedback Control Strategies for an Active Tendon System," by S.J. Dyke, B.F. Spencer, Jr., P. Quast, M.K. Sain, D.C. Kaspari, Jr. and T.T. Soong, 8/29/94, (PB95-212320, A05, MF-A01).

NCEER-94-0025 "Seismic Retrofitting Manual for Highway Bridges," Edited by I.G. Buckle and I.F. Friedland, published by the Federal Highway Administration (PB95-212676, A15, MF-A03).

NCEER-94-0026 "Proceedings from the Fifth U.S.-Japan Workshop on Earthquake Resistant Design of Lifeline Facilities and Countermeasures Against Soil Liquefaction," Edited by T.D. O'Rourke and M. Hamada, 11/7/94, (PB95-220802, A99, MF-E08).

NCEER-95-0001 "Experimental and Analytical Investigation of Seismic Retrofit of Structures with Supplemental Damping: Part 1 - Fluid Viscous Damping Devices," by A.M. Reinhorn, C. Li and M.C. Constantinou, 1/3/95, (PB95-266599, A09, MF-A02).

NCEER-95-0002 "Experimental and Analytical Study of Low-Cycle Fatigue Behavior of Semi-Rigid Top-And-Seat Angle Connections," by G. Pekcan, J.B. Mander and S.S. Chen, 1/5/95, (PB95-220042, A07, MF-A02).

NCEER-95-0003 "NCEER-ATC Joint Study on Fragility of Buildings," by T. Anagnos, C. Rojahn and A.S. Kiremidjian, 1/20/95, (PB95-220026, A06, MF-A02).

NCEER-95-0004 "Nonlinear Control Algorithms for Peak Response Reduction," by Z. Wu, T.T. Soong, V. Gattulli and R.C. Lin, 2/16/95, (PB95-220349, A05, MF-A01).

NCEER-95-0005 "Pipeline Replacement Feasibility Study: A Methodology for Minimizing Seismic and Corrosion Risks to Underground Natural Gas Pipelines," by R.T. Eguchi, H.A. Seligson and D.G. Honegger, 3/2/95, (PB95-252326, A06, MF-A02).

NCEER-95-0006 "Evaluation of Seismic Performance of an 11-Story Frame Building During the 1994 Northridge Earthquake," by F. Naeim, R. DiSulio, K. Benuska, A. Reinhorn and C. Li, to be published.

NCEER-95-0007 "Prioritization of Bridges for Seismic Retrofitting," by N. Basöz and A.S. Kiremidjian, 4/24/95, (PB95-252300, A08, MF-A02).

NCEER-95-0008 "Method for Developing Motion Damage Relationships for Reinforced Concrete Frames," by A. Singhal and A.S. Kiremidjian, 5/11/95, (PB95-266607, A06, MF-A02).

NCEER-95-0009 "Experimental and Analytical Investigation of Seismic Retrofit of Structures with Supplemental Damping: Part II - Friction Devices," by C. Li and A.M. Reinhorn, 7/6/95, (PB96-128087, A11, MF-A03).

NCEER-95-0010 "Experimental Performance and Analytical Study of a Non-Ductile Reinforced Concrete Frame Structure Retrofitted with Elastomeric Spring Dampers," by G. Pekcan, J.B. Mander and S.S. Chen, 7/14/95, (PB96-137161, A08, MF-A02).

NCEER-95-0011 "Development and Experimental Study of Semi-Active Fluid Damping Devices for Seismic Protection of Structures," by M.D. Symans and M.C. Constantinou, 8/3/95, (PB96-136940, A23, MF-A04).

NCEER-95-0012 "Real-Time Structural Parameter Modification (RSPM): Development of Innervated Structures," by Z. Liang, M. Tong and G.C. Lee, 4/11/95, (PB96-137153, A06, MF-A01).

NCEER-95-0013 "Experimental and Analytical Investigation of Seismic Retrofit of Structures with Supplemental Damping: Part III - Viscous Damping Walls," by A.M. Reinhorn and C. Li, 10/1/95, (PB96-176409, A11, MF-A03).

NCEER-95-0014 "Seismic Fragility Analysis of Equipment and Structures in a Memphis Electric Substation," by J-R. Huo and H.H.M. Hwang, (PB96-128087, A09, MF-A02), 8/10/95.

NCEER-95-0015 "The Hanshin-Awaji Earthquake of January 17, 1995: Performance of Lifelines," Edited by M. Shinozuka, 11/3/95, (PB96-176383, A15, MF-A03).

NCEER-95-0016 "Highway Culvert Performance During Earthquakes," by T.L. Youd and C.J. Beckman, available as NCEER-96-0015.

NCEER-95-0017 "The Hanshin-Awaji Earthquake of January 17, 1995: Performance of Highway Bridges," Edited by I.G. Buckle, 12/1/95, to be published.

NCEER-95-0018 "Modeling of Masonry Infill Panels for Structural Analysis," by A.M. Reinhorn, A. Madan, R.E. Valles, Y. Reichmann and J.B. Mander, 12/8/95.

NCEER-95-0019 "Optimal Polynomial Control for Linear and Nonlinear Structures," by A.K. Agrawal and J.N. Yang, 12/11/95, (PB96-168737, A07, MF-A02).

NCEER-95-0020 "Retrofit of Non-Ductile Reinforced Concrete Frames Using Friction Dampers," by R.S. Rao, P. Gergely and R.N. White, 12/22/95, (PB97-133508, A10, MF-A02).

NCEER-95-0021 "Parametric Results for Seismic Response of Pile-Supported Bridge Bents," by G. Mylonakis, A. Nikolaou and G. Gazetas, 12/22/95, (PB97-100242, A12, MF-A03).

NCEER-95-0022 "Kinematic Bending Moments in Seismically Stressed Piles," by A. Nikolaou, G. Mylonakis and G. Gazetas, 12/23/95.

NCEER-96-0001 "Dynamic Response of Unreinforced Masonry Buildings with Flexible Diaphragms," by A.C. Costley and D.P. Abrams," 10/10/96.

NCEER-96-0002 "State of the Art Review: Foundations and Retaining Structures," by I. Po Lam, to be published.

NCEER-96-0003 "Ductility of Rectangular Reinforced Concrete Bridge Columns with Moderate Confinement," by N. Wehbe, M. Saiidi, D. Sanders and B. Douglas, 11/7/96, (PB97-133557, A06, MF-A02).

NCEER-96-0004 "Proceedings of the Long-Span Bridge Seismic Research Workshop," edited by I.G. Buckle and I.M. Friedland, to be published.

NCEER-96-0005 "Establish Representative Pier Types for Comprehensive Study: Eastern United States," by J. Kulicki and Z. Prucz, 5/28/96.

NCEER-96-0006 "Establish Representative Pier Types for Comprehensive Study: Western United States," by R. Imbsen, R.A. Schamber and T.A. Osterkamp, 5/28/96.

NCEER-96-0007 "Nonlinear Control Techniques for Dynamical Systems with Uncertain Parameters," by R.G. Ghanem and M.I. Bujakov, 5/27/96, (PB97-100259, A17, MF-A03).

NCEER-96-0008 "Seismic Evaluation of a 30-Year Old Non-Ductile Highway Bridge Pier and Its Retrofit," by J.B. Mander, B. Mahmoodzadegan, S. Bhadra and S.S. Chen, 5/31/96.

NCEER-96-0009 "Seismic Performance of a Model Reinforced Concrete Bridge Pier Before and After Retrofit," by J.B. Mander, J.H. Kim and C.A. Ligozio, 5/31/96.

NCEER-96-0010 "IDARC2D Version 4.0: A Computer Program for the Inelastic Damage Analysis of Buildings," by R.E. Valles, A.M. Reinhorn, S.K. Kunnath, C. Li and A. Madan, 6/3/96, (PB97-100234, A17, MF-A03).

NCEER-96-0011 "Estimation of the Economic Impact of Multiple Lifeline Disruption: Memphis Light, Gas and Water Division Case Study," by S.E. Chang, H.A. Seligson and R.T. Eguchi, 8/16/96, (PB97-133490, A11, MF-A03).

NCEER-96-0012 "Proceedings from the Sixth Japan-U.S. Workshop on Earthquake Resistant Design of Lifeline Facilities and Countermeasures Against Soil Liquefaction, Edited by M. Hamada and T. O'Rourke, 9/11/96, (PB97-133581, A99, MF-A06).

NCEER-96-0013 "Chemical Hazards, Mitigation and Preparedness in Areas of High Seismic Risk: A Methodology for Estimating the Risk of Post-Earthquake Hazardous Materials Release," by H.A. Seligson, R.T. Eguchi, K.J. Tierney and K. Richmond, 11/7/96.

NCEER-96-0014 "Response of Steel Bridge Bearings to Reversed Cyclic Loading," by J.B. Mander, D-K. Kim, S.S. Chen and G.J. Premus, 11/13/96, (PB97-140735, A12, MF-A03).

NCEER-96-0015 "Highway Culvert Performance During Past Earthquakes," by T.L. Youd and C.J. Beckman, 11/25/96, (PB97-133532, A06, MF-A01).

NCEER-97-0001 "Evaluation, Prevention and Mitigation of Pounding Effects in Building Structures," by R.E. Valles and A.M. Reinhorn, 2/20/97, (PB97-159552, A14, MF-A03).

NCEER-97-0002 "Seismic Design Criteria for Bridges and Other Highway Structures," by C. Rojahn, R. Mayes, D.G. Anderson, J. Clark, J.H. Hom, R.V. Nutt and M.J. O'Rourke, 4/30/97, (PB97-194658, A06, MF-A03).

NCEER-97-0003 "Proceedings of the U.S.-Italian Workshop on Seismic Evaluation and Retrofit," Edited by D.P. Abrams and G.M. Calvi, 3/19/97, (PB97-194666, A13, MF-A03).

NCEER-97-0004 "Investigation of Seismic Response of Buildings with Linear and Nonlinear Fluid Viscous Dampers," by A.A. Seleemah and M.C. Constantinou, 5/21/97, (PB98-109002, A15, MF-A03).

NCEER-97-0005 "Proceedings of the Workshop on Earthquake Engineering Frontiers in Transportation Facilities," edited by G.C. Lee and I.M. Friedland, 8/29/97.

NCEER-97-0006 "Cumulative Seismic Damage of Reinforced Concrete Bridge Piers," by S.K. Kunnath, A. El-Bahy, A. Taylor and W. Stone, 9/2/97, (PB98-108814, A11, MF-A03).

NCEER-97-0007 "Structural Details to Accommodate Seismic Movements of Highway Bridges and Retaining Walls," by R.A. Imbsen, R.A. Schamber, E. Thorkildsen, A. Kartoum, B.T. Martin, T.N. Rosser and J.M. Kulicki, 9/3/97.

NCEER-97-0008 "A Method for Earthquake Motion-Damage Relationships with Application to Reinforced Concrete Frames," by A. Singhal and A.S. Kiremidjian, 9/10/97, (PB98-108988, A13, MF-A03).

NCEER-97-0009 "Seismic Analysis and Design of Bridge Abutments Considering Sliding and Rotation," by K. Fishman and R. Richards, Jr., 9/15/97, (PB98-108897, A06, MF-A02).

NCEER-97-0010 "Proceedings of the FHWA/NCEER Workshop on the National Representation of Seismic Ground Motion for New and Existing Highway Facilities," edited by I.M. Friedland, M.S. Power and R.L. Mayes, 9/22/97.

NCEER-97-0011 "Seismic Analysis for Design or Retrofit of Gravity Bridge Abutments," by K.L. Fishman, R. Richards, Jr. and R.C. Divito, 10/2/97.

NCEER-97-0012 "Evaluation of Simplified Methods of Analysis for Yielding Structures," by P. Tsopelas, M.C. Constantinou, C.A. Kircher and A.S. Whittaker, 10/31/97.

NCEER-97-0013 "Seismic Design of Bridge Columns Based on Control and Repairability of Damage," by C-T. Cheng and J.B. Mander, 12/8/97.

NCEER-97-0014 "Seismic Resistance of Bridge Piers Based on Damage Avoidance Design," by J.B. Mander and C-T. Cheng, 12/10/97.

NCEER-97-0015 "Seismic Response of Nominally Symmetric Systems with Strength Uncertainty," by S. Balopoulou and M. Grigoriu, 12/23/97.

NCEER-97-0016 "Evaluation of Seismic Retrofit Methods for Reinforced Concrete Bridge Columns," by T.J. Wipf, F.W. Klaiber and F.M. Russo, 12/28/97.

NCEER-97-0017 "Seismic Fragility of Existing Conventional Reinforced Concrete Highway Bridges," by C.L. Mullen and A.S. Cakmak, 12/30/97.